

POLITECNICO DI TORINO

**Master Degree in Energy Engineering:
Renewable Energy Resources**

Master Thesis

**Performance of a bidirectional V2G charger under Extreme
Temperature Conditions**



Supervisor

prof. Enrico Pons

Company Tutor:

Dott. Paolo Tosco

Candidate

Alessandro Vero

Anno Accademico 2021-2022

A mio padre

†A mio nonno

Abstract

In recent years, the potential scarcity of conventional energy vectors like fossil fuels and the increasing environmental challenges motivated the widespread study on electric vehicles (EV) seen as a possibility to reduce emissions in the transports sector.

With the advent of smart charging technologies, the charging and storage capabilities of EVs could make them valuable assets to electricity networks, helping enhance grid stability and lower electricity prices. The innovation introduced by the new vehicle-to-grid (V2G) systems lies in the possibility of bidirectional energy flow, allowing the storage system to exchange energy from and to the grid.

For this new way of looking at these assets to be profitable the performances of the bidirectional chargers need to be extensively studied in all the possible operating conditions. Furthermore, it is not only important to study the technology behind the foreseen exploitation of V2G bidirectional chargers, but also the environment in which they will be inserted in.

The great variability in the registered temperatures across Europe (ranging frequently between -30°C and 45°C) [33] poses serious questions on the profitable extensive adoption of these systems; as a matter of fact, studying the market potential of a new technology is closely linked to how it behaves when it is exposed to the external environment. A complete discussion is available on the effects that external conditions can have on batteries and conventional fast chargers. However, the impact on the grid of the performances of V2G chargers without the influence of the battery requires analysis as it will affect both the infrastructure's dimensioning and design.

In this thesis work a V2G bidirectional charger supplied by the Officine Edison Laboratory has been analyzed under three significant temperature regimes (-20°C , 20°C and $+40^{\circ}\text{C}$) using a thermostatic chamber. The conversion efficiency, current total harmonic distortion, power factor and standby power were registered in these conditions. The obtained results highlighted a strong dependence of the conversion capabilities of the device with the temperature; moreover, no negative effects emerged at low temperatures proving how at these regimes the bottleneck of the performances is represented by the battery pack itself which, during our tests, wasn't thermally conditioned together with the converter.

A second test phase followed to investigate another interesting topic, namely the working temperature range of the unit. Based on the working range given in the data sheet of the WB, an analysis of the unit's ability to work outside this range was carried out. The power derating strategy, the corresponding curves and the logic overview were registered exploring the WB behavior at the extreme temperature of 55°C . Then the operating range at the opposite extreme (-25°C) was analyzed.

The final objective of this discussion led to an extensive characterization of the effects of temperatures on the performances of the device. The peculiarity of having thermally conditioned only the bidirectional converter has finally made it possible to physically isolate our results from the effect of the temperature's effect over battery storage system.

Ringraziamenti

Un ringraziamento a tutto lo staff Edison per l'accoglienza. In particolare a Paolo per avermi guidato in questo percorso, a Remì per il suo costante interesse e a Marco per il sostegno.

Un ringraziamento al professore Enrico Pons per avermi accompagnato in questo percorso.

Contents

Contents.....	8
List of figures.....	10
List of tables	12
Relevant Acronyms.....	13
1 Introduction	1
1.1 Challenges of climate change.....	2
1.2 EV development	3
1.3 The new electric paradigm: smart grids and smart charging.....	5
1.4 V2G and bidirectional chargers.....	6
1.5 V2G services	8
2 Temperature effect on EVs.....	13
2.1 Effect of Temperature on batteries	13
2.2 Thesis objective and test selection.....	16
3 Standard selection and description	19
3.1 Environmental testing	19
3.1.1 Environmental testing - Test A: Dry Cold & Test B: Dry heat.....	21
3.2 Performance tests (NREL procedure and standards).....	21
3.2.1 Conversion efficiency test.....	22
3.3 Power quality tests.....	24
3.3.1 Power factor	24
3.3.2 Current harmonics.....	25
4 Experimental layout.....	29
4.1 Physical components.....	31
4.1.1 Safety devices: Protection box and Emergency Power-Off button.....	32
4.1.2 Power source: the Power Amplifier Spherea Puissance Plus PA-3x7000-AC-DC-400V-54A-4G.....	33
4.1.3 The thermostatic chamber	34
4.1.4 The wallbox: il DUT	39
4.1.5 Electrical quantities measurement: general layout	43
4.1.6 Double load configuration: additional dissipator	46
4.1.7 Data Aquisition System: HBM- GEN7tA.....	48
4.2 Temperature measuring devices	49
4.2.1 Thermocouple Type K	49

4.2.2	RTDs	50
5	Test Preparation	52
5.1	Thermocouple calibration's procedure -80BK-A	52
5.2	Thermal conditioning procedure.....	56
5.3	Communication procedure through API	58
5.4	Operative limits of the DUT: choice of the decision variables	63
5.5	Data aquisition and processing	65
5.6	Test execution procedure	68
5.7	Error analysis.....	70
6	Tests results and processing	73
6.1	Performance tests: conversion efficiency.....	73
6.1.1	Conversion efficiency at extreme Temperature's regimes.....	75
6.1.2	Power setpoint effect on the conversion efficiency (G2V and V2G).....	83
6.1.3	Voltage supply effect on the conversion efficiency (G2V and V2G).....	86
6.1.4	Heat maps of WallBox Performances.....	90
6.2	Derating.....	94
6.2.1	Derating curve	95
6.2.2	Derating's control strategy identification.....	98
6.2.3	Safe Operating Area.....	100
6.3	Power quality tests.....	101
6.3.1	Power factor	102
6.3.2	Currents harmonics THD	105
6.3.3	Stand by power consumption	113
7	Conclusions	117
8	Bibliography and Webography.....	118

List of figures

<i>Figure 0-1 V2G as a transition enabler [4]</i>	3
<i>Figure 0-2 bidirectional smart charging standards [12]</i>	6
<i>Figure 0-3 V2X bidirectionality framework [14]</i>	7
<i>Figure 0-4 bidirectional power flow architectures</i>	9
<i>Figure 0-5 V2G ancillary services aggregator management</i>	10
<i>Figure 0-6 ancillary services summary, focus on Temperature effects on optimisation constraints</i>	11
<i>Figure 0-7 temperature effect over battery's storage capacity</i>	15
<i>Figure 0-8 battery characteristic curves according to temperature</i>	16
<i>Figure 0-9 power factor visualization</i>	24
<i>Figure 0-10 harmonic's measurment allowable errors</i>	27
<i>Figure 0-11 individual harmonics limits V2G</i>	28
<i>Figure 0-12 CHAdeMO plug and Nissan's socket</i>	30
<i>Figure 0-13 Experimental layout summary</i>	31
<i>Figure 0-14 protection box (left) emergency button (right)</i>	32
<i>Figure 0-15 Power Amplifier (left) and display (right)</i>	33
<i>Figure 0-16 Discovery chamber by Angelantoni</i>	35
<i>Figure 0-17 refrigerant liquid's cycle</i>	37
<i>Figure 0-18 Chaber's PT100s for temperature control</i>	37
<i>Figure 0-19 DUT architecture layout</i>	39
<i>Figure 0-20 electrical quantities measurements general layout</i>	43
<i>Figure 0-21 Junction boxes for voltage signals</i>	44
<i>Figure 0-22: CHAdeMO supply conductors with polarities</i>	45
<i>Figure 0-23 Hioki 3274 DC current clamp</i>	45
<i>Figure 0-24 AC current images signals</i>	46
<i>Figure 0-25 Parallelo load configuration</i>	47
<i>Figure 0-26 HBM - GEN7tA</i>	48
<i>Figure 0-27 Thermocouple type K used for testing</i>	50
<i>Figure 0-28 thermocouple calibration</i>	53

Figure 0-29 calibration curve fitting.....	54
Figure 0-30 thermocouple's calibration curves.....	55
Figure 0-31 temperature control white: control RTDs red: thermocouple.....	56
Figure 5-5 thermal conditioning time.....	57
Figure 0-32 LabVIEW setpoint panel	61
Figure 0-33 LabVIEW STATUS panel (left) DELETE (right).....	63
Figure 0-34 Perception software panel.....	66
Figure 0-35 PICO TA 189 clamp on probe.....	71
Figure 0-36 conversion efficiency power flow.....	74
Figure 0-37 efficiency varying ambient Temperature SoC=50%	75
Figure 0-38 Dissipated power vs heat sink's temperature.....	76
Figure 0-39 Temperature effect on conduction resistance in MOSFET.....	79
Figure 0-40 Temperature effect on MOSFET's power losses [37].....	80
Figure 0-41 Efficiency vs ambient temperature SoC=80%	81
Figure 0-42 additional graphs on temperature effect over conversion efficiency.....	82
Figure 0-8 G2V power setpoint effect over conversion efficiency.....	84
Figure 0-43 V2G power setpoint effect over conversion efficiency.....	84
Figure 0-44 power setpoint effect over efficiency varying all decision variables.....	85
Figure 0-45 G2V AC voltage effect over conversion efficiency SoC=80%.....	86
Figure 0-46 G2V AC voltages effect over conversion efficiency SoC=50%.....	87
Figure 0-47 V2G Temperature effect on conversion efficiencies,voltage comparison SoC=80%...	88
Figure 0-48 V2G temperature effect over conversion efficiency different voltages SoC=50%.....	88
Figure 0-49 V2G real voltage generator scheme.....	89
Figure 0-50 Heatmaps, WB conversion efficiency at different temperatures and setpoints.....	91
Figure 0-51 Heatmaps of efficiency varying AC voltage and power setpoint.....	92
Figure 0-52 Power dissipated in G2V according to power setpoint.....	93
Figure 0-53 heat dissipation scheme (left) and temperature profile (right)	94
Figure 0-54 Heat sink's temperature signal approximation procedure	96
Figure 0-55 10kW derating behaviour	97
Figure 0-56 heat sink's temperature, 10kW derating	97

<i>Figure 0-57 derating control strategy</i>	99
<i>Figure 0-58 Safe Operating Area</i>	100
<i>Figure 0-59 G2V power factor varying temperature (up), AC voltages (middle), SoC (down)</i> ...	103
<i>Figure 0-60 V2G power factor varying temperature (up), AC voltage (middle), SoC (down)</i>	104
<i>Figure 0-61 voltages from amplifier (left) currents absorbed by WB (right)</i>	107
<i>Figure 0-62 G2V 10kW frequency spectrum (fft) logarithmic scale</i>	108
<i>Figure 0-63 V2G 10kW frequency spectrum (fft) logarithmic scale</i>	108
<i>Figure 0-64 SoC effect over 23rd harmonic values</i>	111
<i>Figure 0-65 harmonics relative value at different temperatures</i>	112
<i>Figure 0-66 Standby power at different temperatures for different AC voltages</i>	115

List of tables

<i>Table 0-1 individual harmonics limits G2V</i>	27
<i>Table 0-2 thermostatic chamber specifications</i>	36
<i>Table 0-3 WB's general installation specifics</i>	41
<i>Table 0-4 WB's working specifics</i>	42
<i>Table 0-5 thermal conditioning time at different power setpoints</i>	58
<i>Table 0-6 visual LED signal's taxonomy</i>	59
<i>Table 0-7 communication time table</i>	62
<i>Table 0-8 WB temperature specifications from datasheet</i>	64
<i>Table 0-9 list of decision variables</i>	65
<i>Table 0-10 Single Sweep relevant formulas</i>	68
<i>Table 0-11 errors</i>	71
<i>Table 0-12 average conversion efficiencies</i>	83
<i>Table 0-13 peak conversion efficiencies</i>	83
<i>Table 0-14 V2G 10kW currents harmonics relative to fundamental</i>	110
<i>Table 0-15 23rd harmonics, test 2</i>	111
<i>Table 0-16 G2V (up) and V2G (down) THDs</i>	112

Relevant Acronyms

API - Application Programming Interface

AC - Alternate Current

BEV - Battery Electric Vehicle

DAQ - Data Acquisition system

DC - Direct Current

DSO - Distribution System Operator

DUT - Device Under Test

EV - Electric Vehicle

EVSE - Electric Vehicle Supply Equipment

G2V - Grid to Vehicle

PA - Power Amplifier

PHEV - Plug-In Hybrid Electric Vehicle

RCD - Residual Current Device

SoC - State of Charge

THD - Total Harmonic Distorsion

V2G - Vehicle to Grid

V2H - Vehicle to Home

V2B - Vehicle to Building

WB - WallBox

1 Introduction

In recent years, the problem of greenhouse gas emissions has led to an increased push in the electric vehicle business.

In this context, vehicle-to-grid (V2G) technology has become more and more relevant, representing a profitable market opportunity for both the electricity grid and electric vehicle owners.

The new electricity market opened up to the possibility of having prosumers (consumers and producers) also in the electric mobility market. The potentiality of the bidirectional power flow between the EVs and the grid could be used to balance the variable and intermittent output of renewable power generation, provide grid services such as voltage and frequency control, and supply emergency backup power. These so-called ancillary services aim at assuring the reliability of the power system, enhancing the power quality.

Edison S.p.A. and the Politecnico di Torino have teamed up to both deepen research on the subject and experimentally test the viability of the technology in market scenarios of interest to the company.

This paper presents one side of the project, which focuses on the experimental side. It is to be included in the broader framework of the activities born from this collaboration which range from simulation activities of the electricity market giving a better understanding of the economic potential of the project, to Real Time simulations of the effects of these systems on the distribution infrastructure in which they fit.

A bidirectional charging station was provided by Edison S.p.A. to test its validity for wider V2G deployment.

1.1 Challenges of climate change

The preservation of planet Earth, taking into account climatic changes, is an issue of increasing importance today. Our society, which has to deal with the problems of the future, is increasingly being led to a drastic revolution in its activities having to diverge from its "business as usual" approach.

On 12 June 1992, 154 nations signed the UNFCCC (United Nations Framework Convention on Climate Change) [1] in Rio de Janeiro, which, once ratified, required governments to pursue a "soft target" to reduce atmospheric concentrations of greenhouse gases with the aim of "preventing disruptive anthropogenic adverse effects on the Earth's climate system"[1]. These actions were primarily directed at industrialised countries with the intention of stabilising their greenhouse gas emissions. These are also defined as climate-altering gases, as the correlations between them and the effects of global warming and ocean acidification that are occurring are now evident.

The signatory states agreed on a "common but differentiated responsibility", with the responsibility for the short-term reduction of greenhouse gas emissions lying with the industrialised countries.

Under the terms of the UNFCCC, the treaty entered into force on March 21, 1994. Since that time, the parties have met annually in the Conference of the Parties (COP) to review progress in addressing the phenomenon of climate change. The 2°C limit imposed by COP-21 was then found to be insufficient and reduced to 1.5°C above pre-industrial levels. It is therefore necessary to reduce CO₂ emissions in the atmosphere by 45% by 2030, then this share must increase to net zero emissions by 2050.

The energy sector is one of the main culprits for the excessive production of climate-changing gases, being one of the biggest carbon intensive sectors in our system. The transport sector, on the other hand, remains one of the most reluctant to reject fossil fuels abandoning ICEs (internal combustion engines).

Today's economy makes extensive use of fossil fuels (coal, oil and natural gas), i.e. underground energy sources that were created millions of years ago by the transformation of animal and plant organisms in the absence of oxygen. These are non-renewable resources that are unevenly distributed across the planet and are the main actors in producing greenhouse gasses and mass soil pollution.

Most countries use fossil fuels (oil, gas and coal) to meet their own energy needs. Burning these fuels releases heat that can be converted into energy. During this process, the carbon contained in the fuel reacts with oxygen to produce CO₂, which is released into the atmosphere.

However, renewables are rapidly growing. Photovoltaic business were the main source of new installed capacity in 2010, while gas and wind were second and third respectively.

We are trying as a society to promote energy saving, increase energy efficiency and develop all forms of alternative energy: Wind, solar, geothermal, tidal and biomass.

Among the major drivers that will lead to the emergence of this new energy system there is the revolution of the electrical system by uniting the power grids of the five continents into an inter-network coupled with the conversion of public and private transport to hybrid electric and fuel cell vehicles for the purchase and sale of energy [2].

1.2 EV development

The gap between the greenhouse gas emissions projected in the 2016 EU Reference Scenario and the level of emissions needed to limit global warming to less than 2°C or even to 1.5°C (Paris Agreement) is massive.

The EU has already adopted a Low Emission Mobility Strategy to promote the decarbonisation of the transport sector. Closing the gap between the EU's climate targets and actual CO₂ emissions will require a mix of new technologies and policies [3]. These two are expected to evolve as new and improved technologies will enter the market changing the passengers and shipping's transport demand.

Electric Vehicles are identified as one of 3 Technology contributors and enablers to invigorate the Energy Transition by Gartner, coexistence with hydrogen development and new storage technologies [4].

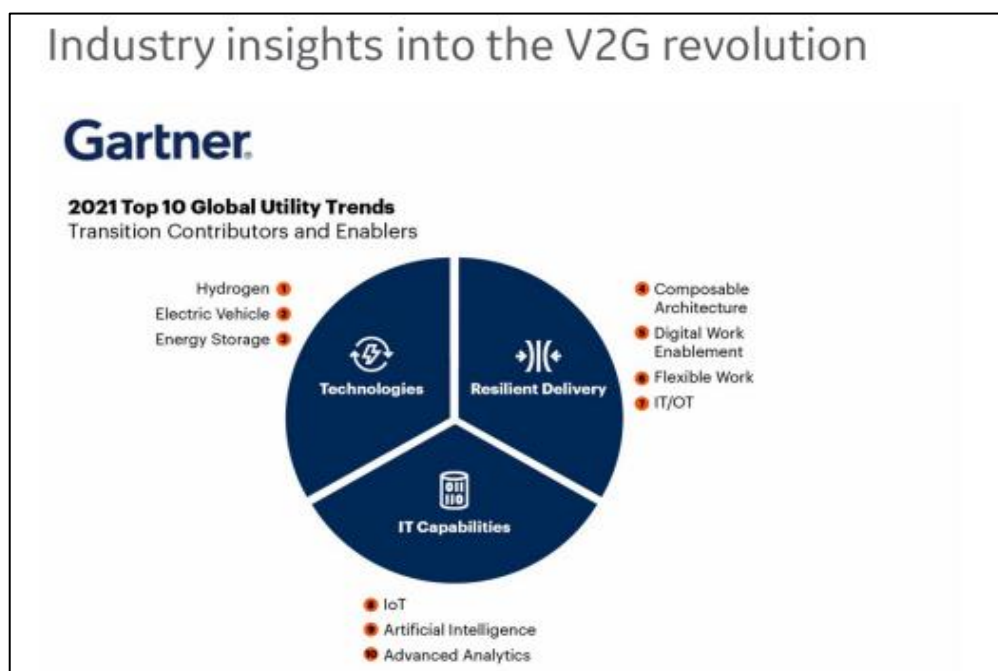


Figure 1-1 V2G as a transition enabler [4]

The spread of clean-fuel electric vehicles brings undeniable benefits in terms of improving both local and global air quality and reducing noise pollution in urban areas.

At the European level, numerous initiatives have been implemented. The first milestone has been posed by the European Roadmap "Electrification of Road Transport": a to-do list for a competitive transport sector with ambitious sustainability targets such as a 60% reduction in CO₂ emissions from transport and the predominant presence of clean vehicles in European cities [5].

The main obstacles to the large-scale diffusion of purely electric cars appear to be the recharging times, the guaranteed autonomy given by battery-powered traction systems and how these are perceived by the consumer [5].

In this framework, the development of an efficient and sufficiently distributed charging infrastructure is recognised as one of the key elements for the successful introduction of electric solutions. The existence of such a network seems to be of crucial relevance for the adoption of electric mobility by users.

However, given the significant amount of electricity they require to charge, EVs are also causing concern for utilities responsible for supplying power to the country's aging electricity grid [6].

The most serious concern for the distribution system operators (DSO) is controlling when EV charging stations will charge the vehicles. A high percentage of consumers will instinctively charge their EVs when they are at home [7], likely having a serious impact on peak demand on the grid as a single EV can double an average home's peak load (average charging power of 7kW [7] is considered in this balance).

The Smart Grid paradigm could be the breakthrough to smart charging and management of electric vehicles. The Smart Grid provides the control needed to mitigate peak load impacts and protect distribution grid components from being overloaded through a distributed network management approach.

With a Smart Grid, utilities can control when and how e-vehicles are charged while accommodating their customers' preferences and shifting or managing the loads during the day. This architecture could allow a more efficient use of the generating capacity installed. Furthermore, in this new paradigm, V2G would find application possibilities, making it possible to develop an efficient bidirectional exchange between vehicles and the network itself.

1.3 The new electric paradigm: smart grids and smart charging

This revolution of the electricity system is inscribed in a landscape in which different issues need a resolution. These solutions cannot be postponed, to successfully integrate the new technologies which do not rely on fossil fuels.

The grid has no storage capacity and electricity imbalances could lead to inefficiencies in service due to network congestions or frequency deviations. Renewable energy generation is largely non-programmable, site-dependent and geographically scattered. Therefore, the grid is subject to significant stress, either when a large amount of energy is generated from renewable sources and demand is lower or when the generation does not keep track of the demand.

The power grid must be strengthened. Increasing electricity generation from non-programmable renewable sources goes hand in hand with improving the grid and installing energy storage systems that allow the grid itself to be protected.

On the other hand, however, the conception of a new structure of the electrical system can lead to the deferral of huge investments in transmission and distribution structures. In particular, a new paradigm of conception of the network has been conceived: the paradigm of Smart Grids

A Smart Grid is a modernized electricity network that uses analogue or digital ICTs (Information and Communication Technologies) to collect and process information in an automated way to improve the efficiency, reliability, cost-effectiveness and sustainability of electricity generation and distribution [8].

One of the main issues with smart grids is balancing power generation and consumption due to the spreading of renewable intermittent power generation units and the increasing share of flexible loads (e.g. EVs).

Smart Grid is predominantly proposed as the next big thing in harnessing ICTs to enhance grid reliability enabling the integration of various appliances such as renewable energy, demand response, electric storage and electric transportation [9]. The development of ICT has brought technology up to date by supporting dynamic real-time two-way energy and information flow, facilitating the integration of renewable energy sources into the power grid, and providing consumers with tools to optimize their energy consumption by introducing Advance Metering Infrastructures (AMI), Virtual Power Plants (VPP) and other implementations [10].

With the Smart Grid, utility's back offices will be able to support, integrate and optimize the management of electric cars as part of an integrated demand side management (DSM). This approach requires systems that not only manage the charging of EV (smart charging), but also optimize it with respect to other demand response (DR) programs [11].

The traditional charging methods in plug-in electric vehicles (PEVs) market, which include plug-in hybrid electric vehicles and battery electric vehicles, are either fast charging or slow charging. Both slow and fast charging operate regardless of the status of the utility grid. They are additional loads to the grid, they cannot exchange data with the grid.

Smart charging - also called managed charging - is the proposed intelligent charging of EVs, where charging can be shifted based on grid load and in accordance with the needs of the vehicle owner.

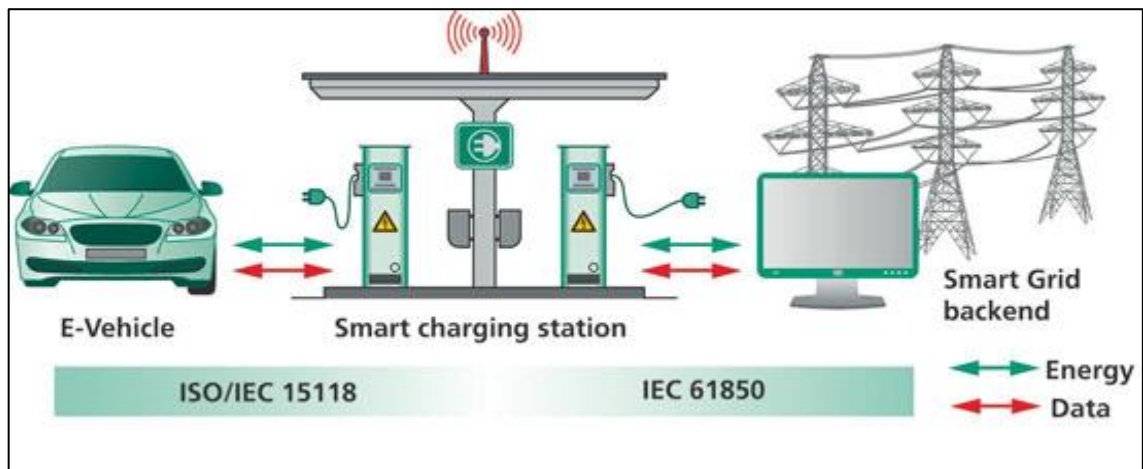


Figure 1-2 bidirectional smart charging standards [12]

It would mainly be used to meet peaks in demand (e.g. when everyone comes home from work and plugs in their electric vehicle), but could also be used to respond to market's needs. As an incentive, utilities can offer monetary and/or non-monetary benefits to EV owners who sign up for a program that allows controlled charging at times when the power grid needs capacity to throttle back.

This form of communication between the grid and the vehicle itself is known as vehicle to grid approach (V2G). Different forms of vehicle-to grid integration smart charging implementation are possible. In a broad sense, the smart charging of electric vehicles can then be divided into five forms: Uncontrolled smart charging, Basic control, V1G Unidirectional control and V2G Vehicle to Grid bidirectional charging [13].

1.4 V2G and bidirectional chargers

Vehicle-to-grid (V2G) is one step further inside the framework of the smart charging environment. Controlling their demand for electricity (V1G) and using the bidirectional (dis-)charging providing energy and power to the grid (V2G) or self-consumption (V2/H/B/X), the electric vehicles could be equipped to provide electricity to the grid [13].

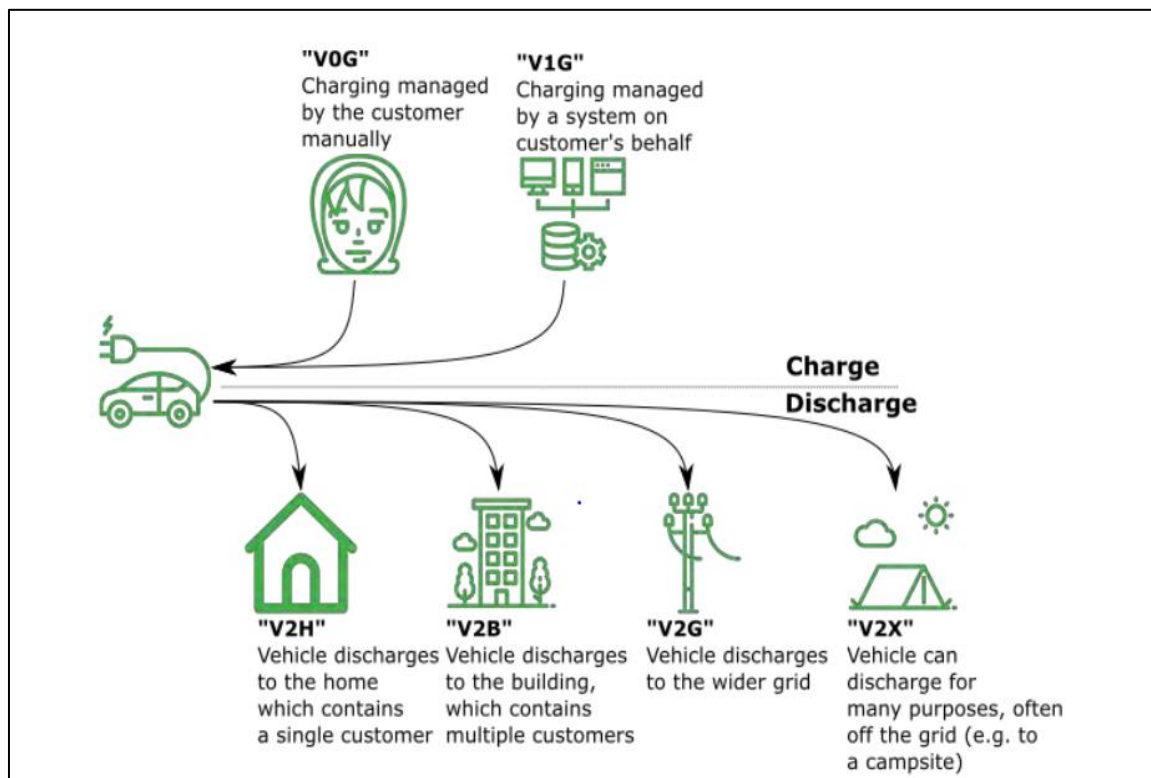


Figure 1-3 V2X bidirectionality framework [14]

The V2G employment can actively smooth the load curve providing peak power, afford backup capacity for the future, improve the reliability of the power system, while offering a revenue to the EV owner which effectively sells power to the grid [14]. The specific services that could be implemented will be discussed in the next chapter.

The idea behind the Vehicle-to-Grid (V2G) is the fact that cars spend most of their day in the parking lot. V2G is then the concept of discharging an EV battery in order to serve a secondary purpose.

Beyond the electricity system, V2G can benefit society by lowering electricity prices [14]. It's a cheap, flexible storage support for renewables. Similarly, by lowering the total cost of ownership of e-vehicles through the possibility of reward, V2G could enforce the uptake of EVs, creating additional environmental benefits.

V2G infrastructures are indeed still currently expensive. It has yet to be determined whether the benefits of V2G are sufficient to justify the costs or when it will become economically viable. The costs come not only from the charger, but also from its efficiency and the additional wear and consumption of the batteries state of health (SoH).

V2G's operation depends on several enabling technologies and infrastructures. These include vehicles, chargers, controls and communication protocols, as well as market structures and the overall policy framework.

A summary of the technical and infrastructure stack used to deliver V2G services is described [15]:

- The Energy Market: are the parties who will require altered demand or generation profiles to meet the energy needs (e.g. manage peak demand). They provide signals indicating timing and level of service wanted.
- The control layer: optimises the multiple needs of the energy market and customer preference to create EV charge requests
- The cloud: is the bridge between the orchestration engine and the customer interface and their charger/car.
- The charger and vehicle (WB and EV)
- The customer's will to provide consent to requests by the aggregator

The charging infrastructure (3rd point) is the component under investigation in this paper. It supplies electric energy for the recharging of electric vehicles. So far, the vast majority of the charging stations installed and available on the market allow exclusively unidirectional flow.

There are four EV charging modes. The first three refer to AC (alternate current) charging, while the fourth sets the conditions for fast DC (direct current) charging. In this work, a DC charging station is tested that is V2G-capable. Unlike the AC charging station, a DC charging station contains an AC/ DC converter embedded in it.

1.5 V2G services

V2G requires a smart charging system to transfer electricity from the grid to the batteries of EV and vice versa. With regard to the grid, the services provided are popularly referred to as V2G ancillary services, bidirectional or uni-directional.

The uni-V2G use has some advantages over the bi-V2G, such as less battery degradation, lower cost and initial investment, relatively simpler control, minimal social barriers and the absence of deep study on bi-V2G's performances. The other side of the coin is the multitude of additional grid services that will become available with the introduction of bidirectional V2G [15].

As a matter of fact services such as peak shaving, reactive power control or renewable energy storage support will have a much smaller impact if only the management of charging times and the power of the different EVs is considered.

The principal schemes for bidirectional enabled systems are proposed below.

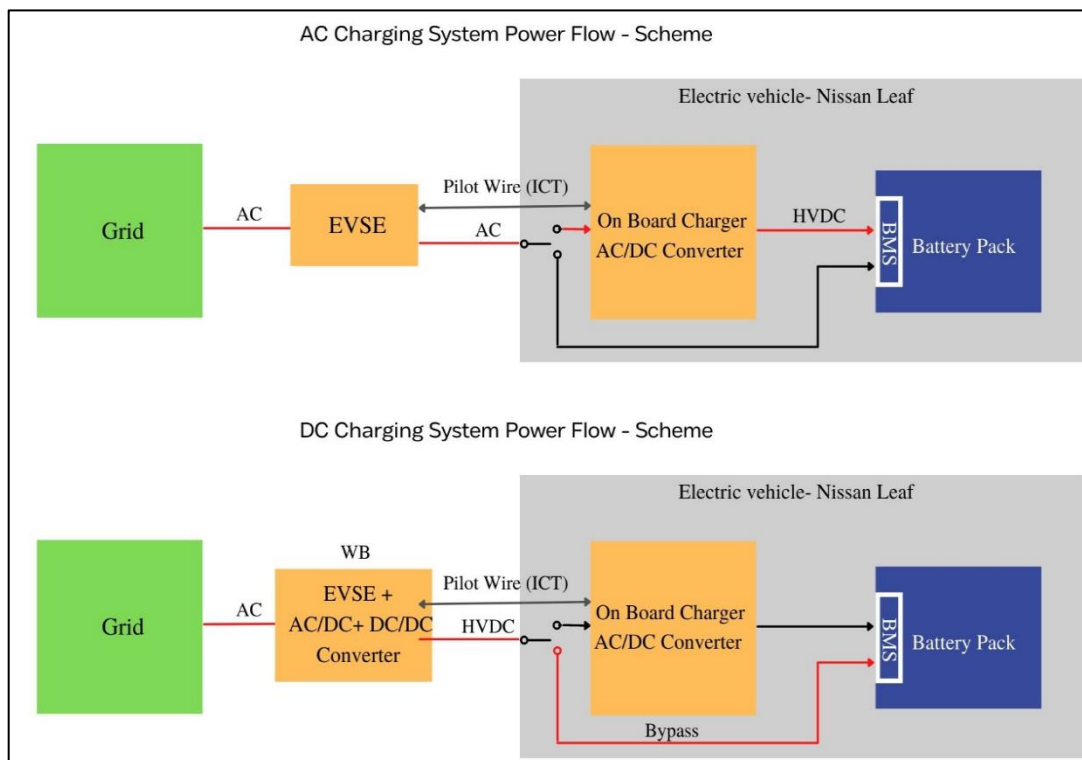


Figure 1-4 bidirectional power flow architectures

The *Figure 1-4* shows the two main types of charging architectures that allow bidirectional charging flow. The power flow is highlighted using the red line.

The first consists only of a EVSE that can supply AC power to the vehicle. In this particular case, there is no wallbox (WB), since there is no active conversion of power inside the device. Rather, it is used the internal converter of the EV itself, which is then connected to the DC terminals of the rechargeable battery.

The second type of infrastructure, on the other hand, represents the field of study of our interest and consists of a charger capable of converting the three-phase or single-phase signal of the grid into a direct current signal. This infrastructure is more powerful and the WBs that use it usually have a two-stages architecture. A first stage consists of an AC/DC rectifier/inverter and a second DC/DC converter stage that adjusts the voltage to that of the battery.

The power can flow both towards the EV and the grid.

Bi-V2G is expected to have a higher potential commercial value than V2B or V2H for most applications, because the distribution system operator may be willing to purchase energy from customers during times of peak demand and use the battery capacity of the EVs to provide ancillary services [15]. The other two application cases are mainly used only to provide an energy balance to the hub to which they are connected, for self-consumption.

The system architecture associated with bidirectional V2Gs can be classified into centralized and decentralized architectures. In a centralized architecture, the role that plays

as the central control for the management of the charging and discharging events is called aggregator [14].

An aggregator must be able to participate in the electricity market through different ancillary services of the grid by organizing and optimizing the EVs charging and managing the load profile. A simplified architecture of the V2G system highlighting the role of an aggregator is shown in *Figure 1-5*.

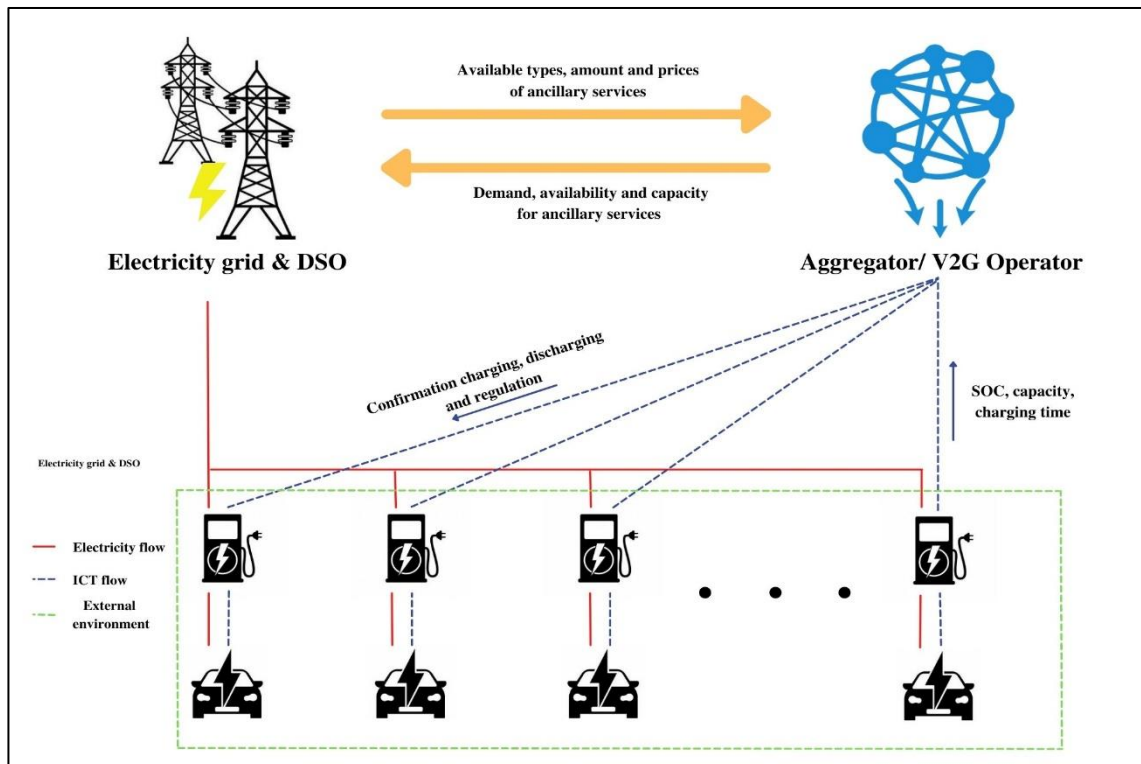


Figure 1-5 V2G ancillary services aggregator management

A closer look reveals that the aggregator acts as an interface between EV fleets and the electricity grid. It connects to each vehicle in the EV fleet that has a service contract with it. Data such as SoC and departure times from the vehicle management system are used as a reference for the charging schedules or participation in grid services [15].

Then, the aggregator enters another contract, this time with the grid operator, and agrees with this entity to determine the type of service and the regulation capacity to be provided to the grid or the power needed by the aggregator to charge the EVs.

Regarding the development of these systems in the context of reference, which is the Italian one, with the resolution 300/2017, ARERA [16] gave the green light to the process of enlarging the number of regulatory service providers, launching a series of pilot projects with Terna.

In this context, the “Unità Virtuali Abilitate Miste” (UVAM) currently represent the reference form of aggregation in Italy [17].

V2G, managed through UVAM, could be an interesting opportunity for EVs owners, to the extent that it could enable a stream of revenues for the benefit of the owner potentially able to make the investment in an electric car more attractive.

Together with the other projects underway at Edison, the study of the performance of a prototype of a bidirectional column has been included in the context of the possibility of developing such aggregation services in an office-like parking lot with V2G-enabled columns.

This application scheme is based on the availability of vehicles parked in the company's lots for extended periods of time during the morning and afternoon hours. In this way, the bidirectional nature of the installed WBs can enable different services [14].

The *Figure 1-6* shows a summary of the different types of V2G, the services offered and the related optimisation objectives and constraints.

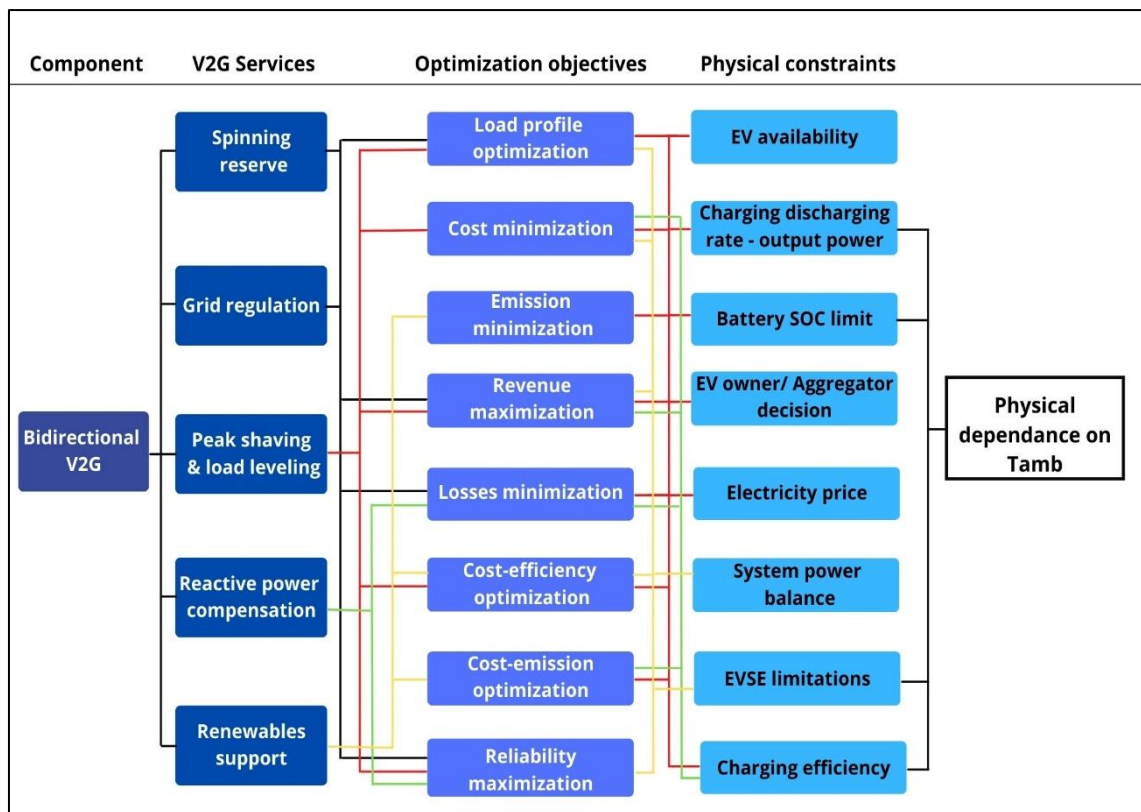


Figure 1-6 ancillary services summary, focus on Temperature effects on optimisation constraints

As projects are developed outdoor, it can be seen the evident dependence that many of the limitations acting on the services themselves deriving from the climate in which they are inserted. As in the previous figure is clear that, in this kind of aggregated projects, the WBs and the vehicles are exposed to external temperature conditions through their operation.

In fact, when the temperature is particularly cold in the winter months or when the WBs are exposed to the sun during the summer, different effect on the EVSE could be experienced.

The observable effects are divided into effects acting on the storage system and therefore on the battery of the vehicle itself or limitations affecting the performances of the WBs. Our study is part of this framework, which tries to answer these questions by distinguishing the effects on the recharging system from the well-known ones acting on the batteries.

2 Temperature effect on EVs

This chapter addresses the consequences of extreme thermal conditions (beyond standard operating conditions) on the components used to charge electric vehicles addressing in more depth the workframe of this thesis. Before presenting the tests carried out at the Officine Edison labs in collaboration between the Politecnico di Torino and Edison, we review what has been learned in this field so far.

Given the great variability of the European climate, which brings summer heatwaves in the Mediterranean area contrasted by severe winter conditions in the north of the continent, it is important to establish the performance of a product across the entire spectrum of temperatures that can affect it.

Since we did not have a large enough climate chamber available, we decided to study the effects of certain thermal conditions on wallbox (the converter) leaving the vehicle (Nissan Leaf) battery outside the controlled volume.

Therefore, the thermal effects of the batteries are not considered and the temperatures will not affect its performances.

The final paragraph introduces the selected tests in light of the information available in the literature.

2.1 Effect of Temperature on batteries

The effects of temperature on the physical parameters of batteries for automotive purposes are well known, many studies have found important findings in this field and as they are summarised in this chapter.

It is important to have an idea of what these phenomena might be, even if the battery is not thermally conditioned in our case. The reason for this is to have a clearer explanation of the phenomena that occurred and compare them with what has been studied in the literature.

Indeed, when comparing the results obtained with those already published, it is always necessary to compare the different experimental conditions. If the results found are in contrast with what can be found in the literature, it is necessary to keep an eye on the differences in order to understand whether the divergent data collected are due to a specific behavior of the device under test (DUT) or to the unequal experimental set-up. To do this, it is necessary to be aware of the effects that temperature can have on non-involved components.

Starting from 1991, with the first commercialization of rechargeable lithium-ion batteries, this specific type of battery has taken on more and more footing to become hegemonic in the electricity storage market. Given its high energy density, which allows the dimensions to be kept limited, and its high safety compared to competitors, it is now the standard for every application in the electronics field.

In EV applications, the temperature of the Li-Ion battery affects the availability of energy, the discharge performance (during starting and acceleration) and the charge acceptance during energy recovery through regenerative braking [18-19]. The temperature also affects the battery life and the frequency of its replacement. Therefore, batteries should be operated in a temperature range that is optimal for performance and lifetime [20].

When looking at these effects, we have to divide between:

1. Influence on battery power
2. Influence on available energy (capacity)
3. Influence on lifetime (SoH)

The effects on the life span of the component are not of interest, as our aim concerns the characterization of the performances, therefore phenomena such as thermal runaway are not analysed.

Batteries work best at room temperature, and any variation between hot and cold will alter performance and/or life. Operating a battery at higher temperatures temporarily improves performance by lowering internal resistance and speeding up chemical metabolism, but such a condition shortens life if it persists for a prolonged period.

Speaking of performances, the phenomena inherent in the battery itself are explained by the Arrhenius's law which describes the electrochemical processes within the system. The Arrhenius equation defines the relationship between temperature and the rate at which the reaction proceeds inside the battery [20]. It shows that the speed increases exponentially as temperature rises above standard conditions:

$$k = A \cdot e^{-\frac{E_a}{RT}}$$

Having:

- k = chemical reaction rate
- A = const.
- E_a = Activation energy
- R = Gas constant
- T = Temperature [K]

Different temperatures affect the internal chemical reaction rates, and internal resistance and efficiency of all types of batteries. Charge times will then vary as temperatures change. The effects will now be divided into those relating to high temperatures and those relating to low temperatures

- **Effect of heat**

As the temperature of the battery increases the chemical reactions inside the battery also quicken. At higher temperatures one of the effects on lithium-ion batteries' is greater performance and increased storage capacity of the battery.

A study by Scientific Reports [21] found that raising the temperature from 77 degrees Fahrenheit to 113 degrees Fahrenheit resulted in a 20% increase in maximum storage capacity.

We report the results, we see how the short-term performances are benefited by the temperature increase.

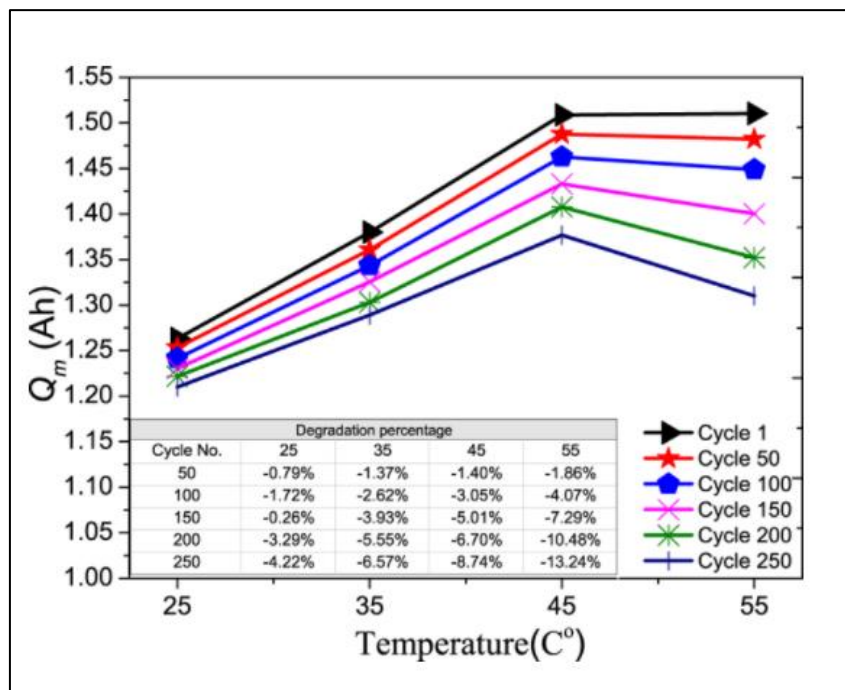


Figure 2-1 temperature effect over battery's storage capacity

At the same time, however, high temperatures damage the electrolyte of the battery, leading to a rapid degradation of performance and storage capacity even after a few charge-discharge cycles.

- **Effect of cold**

The performance of LiBs will degrade at temperatures below 0 °C. Prolonged exposure to cold temperatures also has a big impact on battery performance and safety.

At first, the low temperatures will affect the property of electrolytes. With the decrease of temperature, the viscosity of the electrolytes will increase, reducing the ionic conductivity. The internal resistance will subsequently rise due to the increase in the resistance of the directional migration of chemical ions.

The increase of charge-transfer impedance [11] in LIBs is also an important factor that contributes to the performance degradation at low temperatures. This means that it requires more effort by the battery to charge, in turn lowering the capacity.

Another consequence of this effect is the reduction of the current drawn when a low-temperature battery is connected to its rapid charger at DC or to the internal converter of the vehicle itself.

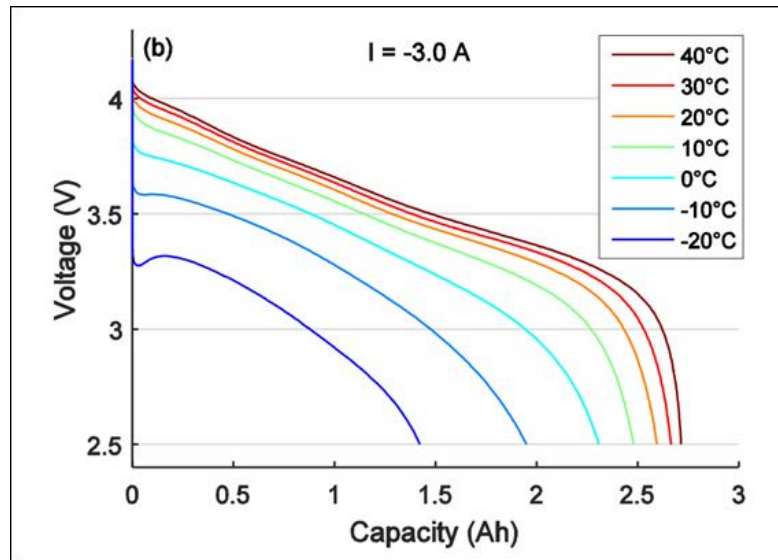


Figure 2-2 battery characteristic curves according to temperature

When the converter applies the voltage to the battery terminals, since the internal resistance is greater, the current that is able to flow inside the electrolyte will consequently be lower

Finally, a detail on the discharge and charge behaviour of the battery that can affect the recorded performances is given by the fact that the charge-transfer resistance is higher for charging than for discharging. Thus, charging a battery is in general thus more difficult than discharging it.

2.2 Thesis objective and test selection

The literature on EV infrastructure planning and policy in the light of the temperature effects on EV fast charging are limited. Past studies typically assumed the EV charging process with a constant rate of charge the effects of temperature on EV charging were neither accounted for nor discussed.

The growth of an electric charging infrastructure in different countries brings several challenges related to its installation. One of these challenges is related to weather conditions, which are extremely heterogeneous due to the different latitudes where fast-

charging stations are located and whose influence on charging performance is often neglected or unknown. It is quite clear that temperatures are a factor of great impact on the potential development of EVs and all related services as in *Chapter 1.5*.

When electric vehicles (EVs) are exposed to extreme temperatures, their performance and charging are limited. For the foreseen adoption of EVs, it is not only important to study the technology behind it, but also the environment it will be inserted into.

Temperatures of $-30\text{ }^{\circ}\text{C}$ to $+40\text{ }^{\circ}\text{C}$ are frequently observed in Europe [33] and the effects on batteries are well known. However, this condition is not as well-known and is being studied as regards their effect on the chargers connected to such EES. Furthermore, there is no accurate study on the subject in the literature that can give indications to the manufacturers regarding the management of temperatures by the device.

The impact on the grid due to the performance of bidirectional chargers operating in G2V or V2G, under extreme conditions requires analysis. These systems are very expensive compared to conventional unidirectional fast chargers and they are often designed to be included in the horizon of supply of the grid with the ancillary services. However, certain services make sense only if the resulting economic return justifies both the higher initial investment in these systems and the user's willingness to provide such services

The only studies that report actual research on the effects of temperatures on the potential of the fast chargers concern unidirectional systems [22]. These studies, moreover, focus in particular on the effects on the entire charging system, examining both the WB and the vehicle battery's EES.

The temperature dependence of charging and power consumption, particularly the effects of low temperatures, has been shown to affect electric vehicle charging performance in several ways [22]. The authors in reference [18, 19, 22] note that charging capacity decreases at negative temperatures as the internal resistance of the battery increases, causing the maximum voltage to be reached earlier.

The efficiency and availability of operation of these systems is a fundamental parameter. Since these factors can be influenced by the external conditions to which they are subjected, it is useful to have an appropriate study on these effects. Furthermore, there are few, if any, studies on the effects of outdoor temperatures on their performance for these bidirectional systems.

Charging station deployment often needs to consider the rate of EV charging because a longer duration of charge means a need for more charging stations for a given demand.

These results may therefore lead to a reassessment of the geographical distribution of charging infrastructure, so that, for example, the need to deploy a greater number of WBs in the geographical areas where temperatures are more critical may be considered

Also, the availability of full capacity can be at stake in critical temperature regimes. As a matter of fact, to maintain the integrity of the components inside, power electronics when operated at extremely high temperatures are often limited in their performances.

Finally, the study concludes that the main limitation for the number of chargers in a multi-charging station is the harmonic limits and not only the power capacity of the upstream current transformers.

As the number of EVs charging at the same time increases, the total flowing current also increases. These particular appliances often produce distortions in the currents withdrawn and injected creating many issues in the distribution system. With many of these devices simultaneously connected, the harmonic limits can be easily exceeded [23]. This clearly leads to the impossibility of having many devices connected at the same time, a great limitation looking to the future.

Thus, if we combine the loss of power with the impossibility of connecting several vehicles simultaneously in the same section of the distribution network, we obtain the panorama of interest for the proposed study. These simultaneous effects could therefore severely limit the areas of application and the applicability of V2G technology.

Following this literature review, the following tests were selected of particular interest: conversion efficiency, availability of charge and discharge nominal power, standby power consumption, harmonic distortion and THD.

3 Standard selection and description

This chapter is entirely devoted to the description of the standards and the reasons that led to their selection.

The objective, as described at the end of the previous chapter, is to evaluate how and to what extent the thermal conditions to which the bidirectional charger under study is exposed affect its performance in the context of using this technology for the V2G potential.

The tests indicated above can be divided into two macro categories, one represented by the performance tests, the other aims at verifying the compliance of the WB in the grid interconnection.

The test plan for the performance evaluation is designed to test and evaluate the vehicle's capability to provide power to the grid, and to evaluate the vehicle's ability to connect and disconnect from the utility. The reference testing procedures over which the study is based are presented by the National Renewable Energy Lab which has provided a complete list of tests that must be performed to evaluate the performance of a charging station. Since there is not yet a standard that addresses V2G requirements, NREL has collected many performance tests from various standards and adapted them for V2G operation. This test plan does not include all the tests required to meet interconnection requirements, but in exchange some additional performance tests are included in the test plan to verify the V2G-capable vehicle's continuous output power, efficiency and losses.

The interconnection tests, on the other hand, being defined by specific pass-fail criteria, are instead taken from IEC EN 62909 [46] which specifies general aspects of bi-directional grid-connected power converters (GCPC). The International Electrotechnical Commission (IEC) is a worldwide organization for standardization comprising all national electrotechnical committees (IEC National Committees).

these tests and procedures are all to be referred to the environmental test framework which instead are managed by another IEC standard: the BS EN 60068 [25] standards.

The first section deals with the environmental tests as a whole, referenced to the BS EN 60068 [24] standards. Then, the procedures performed and the connection standards are presented and listed for greater clarity on how the results were achieved.

3.1 Environmental testing

Environmental testing, also called environmental conditioning, can be defined as practices in which specimens are subjected to natural or artificial environmental conditions

mimicking storage, installation, use, and transportation conditions. Then their performance can be monitored, and reliable conclusions can be made [24].

There is vast scale of environmental tests. First, there are climatic tests that are done for studying how products and parts can handle different climatic and weather conditions. Usually, in these tests, temperature and humidity are the main parameters that are monitored. These conditions can be still so that temperature and eventually humidity remain at the same level for the whole duration of testing. The other possibility is that there are different temperature and humidity cycles where these quantities vary at a desired range. In addition to temperature and humidity, other environmental conditions can be studied: for example how sea water corrodes materials, how air pressure affects cargo in planes, or how the radiation of sun affects materials.

Since the device is a prototype that is not easily replaceable, during this study it was avoided the exposure to a different hygrometric content or corrosive environment inside the chamber. The effect of still temperature on the performances was the only parameter explored.

The bidirectional charger under scope has been placed inside the chamber. The measuring equipment was maintained outside due to its temperature limitations. The power cables have been passed through specific cable entries on the side of the chamber's control volume. These passages were then insulated with cotton wool in order to prevent dispersion towards the outside of the chamber as much as possible.

It should be noted, however, that the performances given in the chapter relative to the experimental layout refer to ideal test conditions. Since the cable entries are a disturbing element in the thermal conditioning system, these ideal conditions cannot be considered to have been met despite the insulations applied. This leads to a reduction in the stability range given by the thermal chamber, which must be taken into account in test phase.

Several standards have been analyzed for the climatic tests in this thesis, below are the reference standards with a brief description of the control parameters. The climatic tests performed are classified into dry hot and dry cold test as there is no humidity control performed. There are many different standards that are used to test environmental stress to different kind of products and there are also many regulations that can help to decide the best methods for every kind of different testing situations.

The standard including all environmental tests is called IEC EN 60068 [24], and this standard is separated into three parts. The part one describes the basic knowledge of environmental testing and requirements. The second part includes all tests for different applications and how to execute them. The third part includes supporting documentation and guidance, in other words all the background information.

These standards also differ for the presence inside the thermostatic chamber of a forced convection fan that heats up the specimen inside the controlled environment. In this case the fan behind the heater element was covered with cardboard as it cannot be controlled in the air outlet speed. This topic will be discussed in more detail during the pretest phases.

3.1.1 Environmental testing - Test A: Dry Cold & Test B: Dry heat

The standards and the testing conditions are similar for both the Test A and Test B described by the IEC EN 60068-2 [25], for this reason these tests are described in the same chapter.

This standard deals with environmental tests applicable both to heat-dissipating and non-heat-dissipating specimens. The object of the dry heat (and dry cold) test is limited to the determination of the ability of components, equipment or other articles to be used, transported or stored at high (low) temperature.

These particular tests are subdivided as follows [25]:

1. Dry heat test for non-heat-dissipating specimens
 - with gradual change of temperature.
2. Dry heat tests for heat-dissipating specimens
 - with gradual change of temperature
 - with gradual change of temperature, specimen powered throughout thermal conditioning

A specimen is considered heat-dissipating only if the hottest point on its surface, measured in free air conditions (i.e. low air velocity circulation), is more than 5 K above the ambient temperature of the surrounding atmosphere after temperature stability has been reached. This condition is always verified in our system even at the lowest power exerted.

This last one test is our proper scope of interest throughout the thesis work in this performance evaluation process. This procedure is specifically for heat dissipating specimens which are subjected to a critical temperature level for a time long enough for the specimen to achieve temperature stability and which are required to be powered throughout the test period.

3.2 Performance tests (NREL procedure and standards)

Vehicle-to-grid (V2G) prototype vehicles are being developed and tested at the National Renewable Energy Laboratory (NREL) [26]. Utilizing bi-directional power electronics can allow a vehicle to not only charge its batteries from the electric utility grid during charge but also can provide power back to the grid during discharge. This leads to the need to characterize the device in both types of use, which may differ not only in the results but also in the trends shown.

The objective of this document mentioned above is to provide an interim test plan for evaluating V2G applications. The test plan is designed to test and evaluate the vehicle's capability to provide power to the grid.

The main tests to be conducted concerning a V2G system that are of any interests to us are:

- Performance test:

1. continuous input power of the system

2. conversion efficiency
3. standby power consumption

- Network connection test:

1. power factor
2. harmonic content of the currents

These tests have been extrapolated from standards such as IEC EN 62933-2 [46], IEEE 1547.1 and UL 1741; or from studies conducted on V2G systems.

The capability of continuous power output or consumption, means being able to provide the system with continuous power flow to and from the vehicle when subjected to abnormal conditions.

This may be the case if the ambient temperature set exceeds or approaches the limits specified by the manufacturer, or if the voltage levels of the supply become abnormally high or low.

One main part of the discussion will aim at verifying the WB's ability to continuously supply power at the maximum set point when the voltage values are close to the limits (derating conditions). It will also be examined whether continuous operation is possible at thermal conditions beyond the admissible limits, i.e. whether there are methods to control the delivered power or the internal temperature to avoid immediate shutdown.

3.2.1 Conversion efficiency test

The purpose of the test procedure is to measure the energy efficiency of battery chargers coupled with their batteries, which together are referred to as battery charger systems. This term covers all rechargeable batteries or devices incorporating a rechargeable battery and the chargers used with them.

This evaluation is intended to establish the conversion efficiency of the inverter between the vehicle battery and the AC output as a function of output power level. The bidirectional nature of the DUT must be represented in this test as the performance of the converters can vary a lot depending on whether the power flow is exiting or entering the vehicle storage system.

It's to be evaluated how efficiency changes when four parameters change according to the following experimental procedure in both working modes [26]:

- Power exchanged
- Battery state of charge (SoC)
- Mains voltage (AC)

-Ambient temperature

From NREL, the procedure to be followed in order to perform this test establishes:

1. Maintain the ambient air temperature of the test chamber/room within $\pm 3^{\circ}\text{C}$ of the nominal operating temperature specified in the wallbox information datasheet. Write down the ambient operating temperature
2. Maintain the vehicle in an environment before testing to ensure that the DUT is relatively warm at the beginning of the test. This will bring the DUT to a stable operating temperature in a reasonably short period of time.
3. Connect the DUT according to the instructions and specifications provided by the manufacturer.
4. Set the simulated utility to provide the nominal AC voltage.
5. Set (or verify) all DUT parameters to the nominal operating settings.
6. Verify the battery SOC.
7. Set the V2G DUT to provide as close as possible to 100% of its rated output power.
8. Record all applicable settings
9. Measure and record the following values at 30 second intervals for at least 3 minutes (continuous sampling at higher data rates is preferred):
 - Input voltage (DC and AC)
 - Input current (DC and AC)
 - Input power (average DC + AC RMS)
 - Output voltage (AC)
 - Output current (AC)
 - Ambient temperature ($^{\circ}\text{C}$)
 - Inverter temperature at heat sink.
10. Repeat step 9 for the remaining power levels or similar manufacturer's adjustable power levels.
11. Repeat steps 2-10 for test conditions by changing AC voltage.
12. Repeat steps 1-11 for maximum and minimum allowable ambient temperatures as specified in the DUT datasheet.

This is a performance test, so there are no specific pass/fail criteria. For each power level at each test condition, calculate and report: average DC input power, average AC output power and the efficiency computed as the ratio of the previous two depending on which one is the input and which one the output power flow.

3.3 Power quality tests

This section contains various tests to determine the safe V2G interconnection to the utility grid. These tests are required by CEI/IEC 61000-3-2 [47], CEI/IEC 62909-1:2017 [46], CEI/IEC 61727-2004[44].

The massive increase in electric vehicles (EVs) expected in the near future poses a challenge for infrastructure design and dimensioning. In a changing sector, the integration of EVs into electricity grids can bring severe challenges for electricity grid operators, especially in terms of power quality. It is important to assess the potential impact of EV integration on the grid in order to ensure standardized grid operation.

These are pass/fail tests and their purpose is to verify the compliance of the wallbox to be connected to the grid. A time series of three-phase instantaneous current measurements should be collected for each operation condition, which are at the rated input active power and the rated output active power of the EES system in the two modalities. The requirements related to the measurement are according to IEC EN 61000-4-7[45].

3.3.1 Power factor

A poor power factor refers to an excess of reactive power in the system. This reactive power cannot be used to do real work and is therefore wasteful and costly. A high value of this parameter allows the system to reduce energy costs and avoid equipment overheating, unwanted shutdowns and failures.

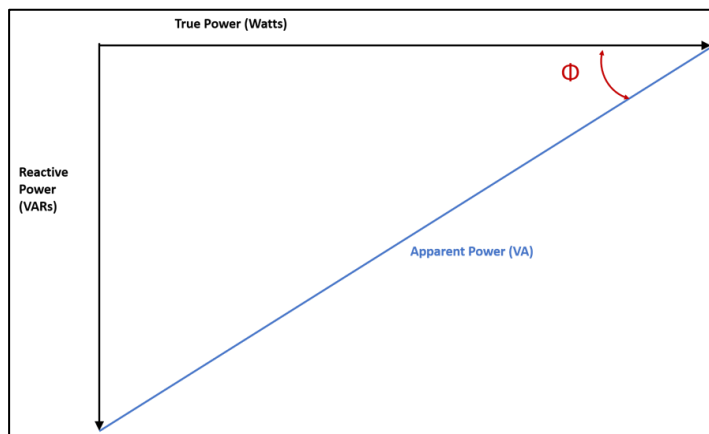


Figure 3-1 power factor visualization

The standard defines the "power factor" as the ratio between the active power (in kW) and the apparent power (in kVA).

The apparent power in turn is the square root of the sum of the active and reactive power squared. Considering the tension V and the current I for each phase we have that the expression of the power factor is calculated with the following formula:

$$PF = \frac{P}{S} = \frac{VI \cos \varphi}{VI}$$

Where:

P = Real Power [kW]

Q = Reactive power [kVAR]

S = Apparent power [kVA] = $\sqrt{P^2 + Q^2}$

In accordance with Distribution Code 4-1-10, the V2G system shall not inject reactive power into the utility network, while the drain of reactive power shall be limited to a power factor of 0.9. This limit applies unless otherwise agreed upon with the utility. The standard specifies that the storage system seen as a load from the grid must have a delayed power factor of more than 0.9 if the output power is more than 50% of the converter's rated power, in this case 5 kW.

3.3.2 Current harmonics

The main cause of the harmonics generation are the “non-linear” loads. Before talking about harmonics, we need to define what is a “linear” load and what a “non-linear” load.

On one hand a linear load draws instantaneously proportional current to the applied voltage, i.e., its impedance is maintained constant along the whole alternating period [27]. For public electricity supply of 50 Hz sinusoidal voltage, this will mean a pure sinusoidal current also.

Linear loads can be classified as resistive (electrical heaters, incandescence light bulbs), capacitive (capacitors usually found as part of systems or equipments), inductive (transformers, motors), or combinations of some of them.

On the other hand, a non-linear load changes its impedance with the instantaneously applied voltage leading to a non-sinusoidal current consumption [28]. In other words, there is no constant relationship between the current and the voltage of this load in the alternating period. The simplest circuit that represents a non-linear load is a diode rectifier.

Harmonic distortion is a deviation of the current or voltage waveform from a perfect sinusoidal shape. In the case of nonlinear loads, such as EV charge controllers, current distortion is very common due to the need of power electronics switches to convert power from an AC to a DC. It is expected that more and more electric vehicles (EVs) and plug-in hybrid electric vehicles (PHEVs) will be used soon. The potential impact of these vehicles on the power quality of the electricity grid is poorly understood. Harmonic distortion of chargers with currents of 20 A per phase or less is regulated by law in the EU.

Harmonics are sinusoidal voltages or currents having frequencies that are integer multiples of the supply frequency (50 Hz). Low voltage and current harmonics depend on the characteristics of the distribution system, the type of service and the connected equipment. This analysis will be focused on this last point of interest. To ensure that the equipment connected to the utility system is not affected, the charging station output should have low current distortion. Since the voltage waveform is accurately given by the PA, only the current harmonic component is measured.

The Harmonics Test aims to measure the individual current harmonics and the total-harmonic current distortion (THD) of the charging station under normal operating conditions. Harmonic Distortion is described as the interference in an AC power signal

created by frequency multiples of the sine wave. Total Harmonic Distortion is used to measure the effective value of harmonic distortion.

$$THD_I = \frac{\sqrt{I_2^2 + I_3^2 + I_4^2 \dots + I_n^2}}{I_1}$$

I_n = is the value of the nth current harmonic order

I_1 = is the value of the fundamental frequency's harmonic

This theoretical background needs to be applied in the various experimental cases found in this thesis work. These mathematical methods of evaluating the interference on the wallbox supply current signal must be compared with the limits required by the standards.

They are different if the device is seen by the grid as a load (G2V) or as a real voltage generator (V2G). In this last case, the standard aligns with the one relating to photovoltaic systems, since from the grid point of view the V2G system is a storage system in DC (battery of EV) coupled with a two-step inverter: the first consisting in a DC/DC converter to adjust the unstable voltage level given by the SoC, the second one being an inverter or DC/AC converter. This simplification makes the EVSE similar to a photovoltaic system with storage able to discharge the energy towards the low voltage network.

3.3.2.1 Harmonic limits in load configuration (G2V) – CEI/IEC 62933-2-1:2018.

A time series of three-phase instantaneous current measurements should be collected for each operation condition at the rated input active power. The requirements related to the measurement are according to IEC 61000-4-7. The individual harmonic current components for frequencies up to 40 times (2000 Hz) the fundamental grid frequency and the total harmonic current distortion should be calculated in each operation condition of the EES system and should be reported.

Class	Measurement	Conditions	Maximum allowable error
A	Voltage	$U_m \geq 1 \% U_N$ $U_m < 1 \% U_N$	5 % U_m 0,05 % U_N
	Current	$I_m \geq 3 \% I_N$ $I_m < 3 \% I_N$	5 % I_m 0,15 % I_N
B	Voltage	$U_m \geq 3 \% U_N$ $U_m < 3 \% U_N$	5 % U_m 0,15 % U_N
	Current	$I_m \geq 10 \% I_N$ $I_m < 10 \% I_N$	5 % I_m 0,5 % I_N
U_m, I_m are the measured values (see definitions) U_N, I_N are the nominal input ranges of the instrument U_N, I_N are the nominal input ranges of the instrument			

Figure 3-2 harmonic's measurment allowable errors

Two classes of accuracy are suggested for instrumentation measuring voltage and current harmonics. The maximum allowable errors in *Table 3-1* refer to single-frequency and constant signals, in the operating frequency range, applied to the instrument under rated operating conditions to be indicated by the manufacturer.

The harmonics limits are specified by the standard about the Electromagnetic compatibility (EMC) - BS EN 61000-3-12:2011.

Minimum R_{sce}	Admissible individual harmonic current $I_h/I_{ref}\%$				Admissible harmonic parameters %	
	I_5	I_7	I_{11}	I_{13}	THC/I_{ref}	$PWHC/I_{ref}$
33	10,7	7,2	3,1	2	13	22
66	14	9	5	3	16	25
120	19	12	7	4	22	28
250	31	20	12	7	37	38
≥ 350	40	25	15	10	48	46
The relative values of even harmonics up to order 12 shall not exceed $16/h$ %. Even harmonics above order 12 are taken into account in <i>THC</i> and <i>PWHC</i> in the same way as odd order harmonics. Linear interpolation between successive R_{sce} values is permitted.						
a I_{ref} = reference current; I_h = harmonic current component.						

Table 3-1 individual harmonics limits G2V

In this specific standard named above in the part from 3 to 12 limits for harmonic currents produced by equipment connected to public low-voltage systems with input current $> 16A$ and $\leq 75A$ per phase.

These harmonics limits need to be confronted with the measured ones to comply with the standard the measured harmonics should be lower in all their components and in all the phases.

3.3.2.2 Harmonic limits in generator configuration (V2G) – CEI/IEC 61727:2004

As far as operation as a real voltage source is concerned, the reference document mentioned in the standard on the energy storage system is referred to the “Technical Requirements for Connecting PV Systems to low voltage Distribution Networks”. This standard can be adapted to a battery pack connected to a WB in V2G, since in both cases, with regard to the distribution network to which the system is connected, it is a direct current energy generation system connected to an inverter that feeds a three-phase alternating current into the electrical distribution network.

The purpose of this test is to measure the individual current harmonics and the total rated current distortion of the V2G system under normal operating conditions.

Total harmonic current distortion shall be less than 5 % at rated generator output in accordance with IEC 61727:2004 [44]. Each individual harmonic shall be limited to the percentages listed in *Figure 3-3*.

Odd harmonics	Distortion limit
3 rd through 9 th	Less than 4,0 %
11 th through 15 th	Less than 2,0 %
17 th through 21 st	Less than 1,5 %
23 rd through 33 rd	Less than 0,6 %

Even harmonics	Distortion limit
2 rd through 8 th	Less than 1,0 %
10 th through 32 nd	Less than 0,5 %

Figure 3-3 individual harmonics limits V2G

The even harmonics in these ranges must be less than 2.5% of the lowest listed odd harmonic limits.

This is a pass/fail test and the V2G system is considered compliant if the individual current harmonics and the total distortion of the rated current do not exceed the limits specified in the reference standard. For a multi-phase V2G system, each of the phases must comply with the specified limits.

4 Experimental layout

This chapter focuses in describing in detail the functioning and the operating conditions of each of the piece of equipment provided by the Politecnico of Torino and Edison S.p.A. inside the laboratory of the Officine Edison in Turin. The measurement layout and the supply chain were part of the university's laboratory section, while the prototype of the wallbox coupled with the storage system and the thermostatic chamber was granted by Edison itself.

Inside the laboratory, in an area shared between the structures of Edison S.p.a. and those of the Politecnico of Torino, belonging to the "EC-L: Energy Center Lab", a structure has been set up to house a prototype, not yet on the market, of a well-known manufacturer of chargers for BEVs. This is a prototype for the European market that aims to exploit the potential of bidirectional charging. In particular, it should be able to connect the EVs to the low-voltage three-phase grid to feed power into the grid when needed to balance the distribution system in an operation mode called vehicle to grid (V2G).

In this study horizon, the university has built a structure that can combine accurate measurements of electrical parameters with a system for powering the equipment that is repeatable and precise. The latter remains a fundamental aspect of the scientific research process. Indeed, it should be underlined that a consistently different supply would lead to consistently different and even contradictory results. Even though the measurements (by definition) cannot be the same if they are taken at two different points in time, it is expected that the trends and behaviors do. For example, power quality aspects such as the point-by-point assessment of harmonics often play a role in very small differences, and often a product is confirmed as compliant or non-compliant with distribution market rules (e.g. the limits of the harmonic contribution that develops in the flows) based on very small differences.

Furthermore, everything must be able to manage the bidirectionality of the device, the fundamental feature of the product.

To enable repeatability, the WB is powered by a linear power amplifier (PA). This amplifier is very precise and has low latency. Via its integrated software, it is possible to control both the frequency and the RMS of the voltage waveforms to be reproduced with high accuracy. It then feeds itself through the network in the laboratory and generates, on the one hand, the connection voltages of the WB and, on the other hand, the images of the currents generated by its internal generator. This second aspect will be discussed in more detail in the section on measuring devices.

The voltages thus generated then feed the WB passing through the protective box. The DC side of the system begins downstream the WB after the rectification of the three-phase signal into a single DC output.

On the DC side, the current measurements are made via conventional probes, the AC side relies on the signals coming from the amplifier; while for all voltages we rely on deriving the measurements via junction boxes.

The currents, once measured, are sent to the HBM through BNC cables, while the voltages signals are acquired using banana plug-plug cables. The central console, then processes all these quantities involved.

In order to have a brief description also of the vehicle side of the experiment the type of charging implemented by this system is mode 4, defined by the IEC EN 61851-24: 2014 standard, i.e. the DC connection between the vehicle and the column through a type C connection with a CHAdeMO charging station, shown in *Figure 4-1*, whose reference standard is IEC EN 62196-3: 2014. On the right side, on the contrary, there is the corresponding Nissan Leaf's input socket.



Figure 4-1 CHAdeMO plug and Nissan's socket

The first further development work on the experimental set-up consisted of positioning the WB correctly within the thermostatic chamber for thermal conditioning. The placement should be such that the WB should be easily manipulated from the outside to change the position of the temperature measurement on the heat sink in real time.

On the other hand, it had to allow the power and network cables to be safely routed out of the chamber, and it had to be able to present a derivation method suitable for the normal use of the unit.

In the next image (*Figure 4-2*) the complete experimental layout used during the case study's experiences is depicted drawing the attention to the power and signal connections characterizing the setup. The chapter will, then, focus over the description of every component presented in the general layout explaining how they work interacting with each other in order to make the experiment easily replicable in the future.

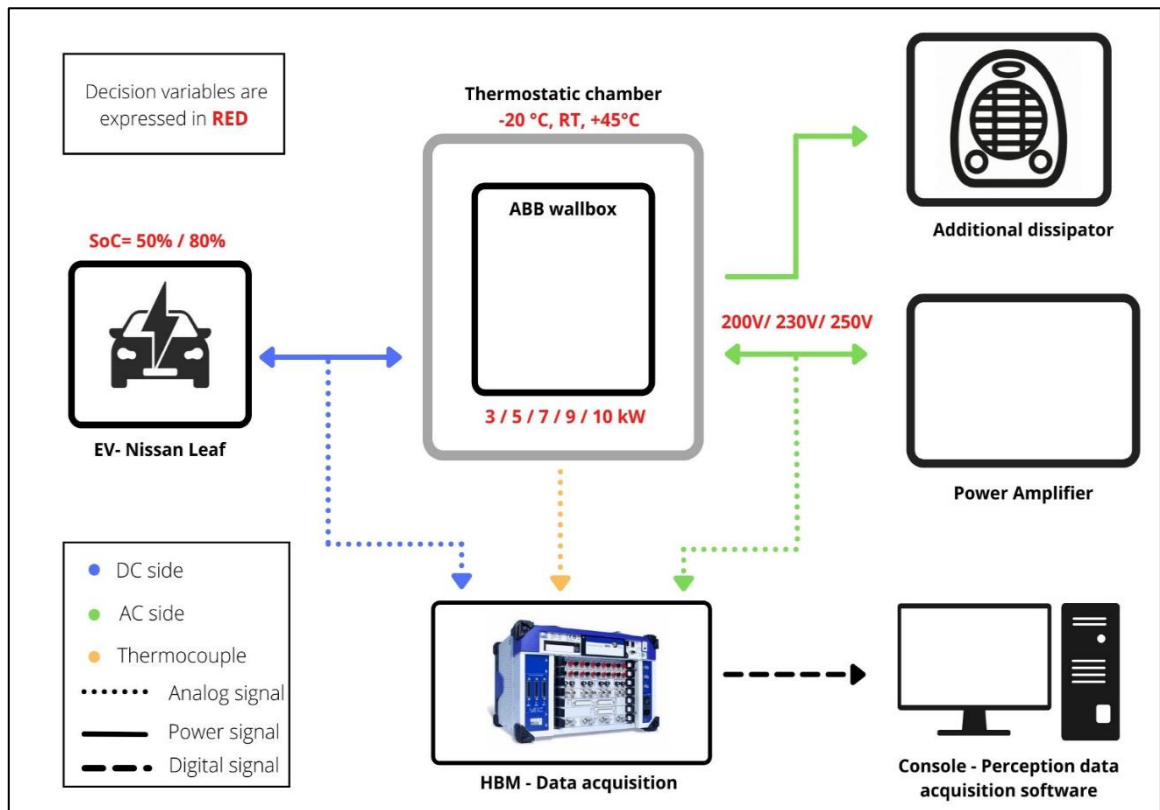


Figure 4-2 Experimental layout summary

Another interesting aspect of the layout concerns the presence of a second load connected in parallel to the power amplifier. This setup is due because during vehicle-to-grid behavior, the energy discharged from the battery is dissipated directly on the PA. The power amplifier then needs to be able to continuously dissipate the entire 10 kW of power supplied by the vehicle.

This feature cannot be granted by the PA alone especially when the WB is operating at the lower limit of the connection voltage generating high current. However, the possibility to have continuous dissipation is fundamental. The WB must reach a thermal equilibrium condition inside the chamber before the starting of the acquisition. Since several minutes are needed, the layout should be built to continuously dissipate the power discharged.

To solve this technical issue, an additional dissipator, consisting of a resistance heater with a nominal power of 9 kW, is connected in parallel with the amplifier. In this way, the currents are divided between the two consumers and there is no overloading of the PA.

4.1 Physical components

In this section we will introduce the components used in the layout described above, their functional logic and the basic properties that describe their operation and scope.

A more detailed section will be devoted to the instruments for measuring and controlling the system temperature, a special area to which I have devoted my thesis analysis.

4.1.1 Safety devices: Protection box and Emergency Power-Off button

To ensure a safe supply to the charging station, an electrical protection box was designed and installed in the EC-Lab before the tests began. The WB is then not directly connected to the grid of AC, but via the protective box, in which the appropriate protective devices are installed. Since the operation requires the connection to the PA, like in the interconnection grid tests or the performance tests with non-nominal voltages, a power cable is derived from the protection box to connect this external power source to the wallbox. This means that supplying the WB, also the protection box is fed in both the operational conditions.

The installation of these protection devices was carried out as part of the previous thesis on this WB prototype, so the process will not be discussed in detail.

The only significant difference from the previous installation concerns the positioning of the DUT, moved from a support grid to the thermostatic chamber. The following *Figure 4-3* show the safety and emergency devices listed here.

In summary the main components of the security system are made up of:

- Residual current device (RCD): 230/400V, $I_n = 40A$, AC: 30mA, DC: 6mA;
- Magneto-thermal breaker: 230/400V, $I_n = 32A$;
- Emergency power off (EPO) button.

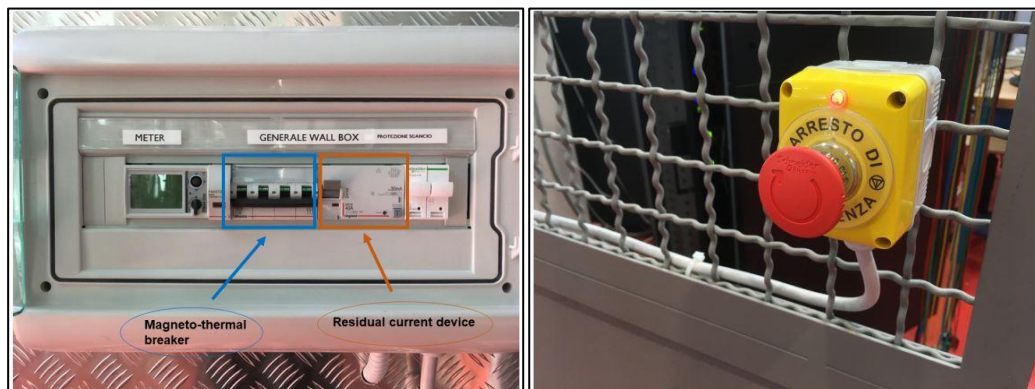


Figure 4-3 protection box (left) emergency button (right)

4.1.2 Power source: the Power Amplifier Spherea Puissance Plus PA-3x7000-AC-DC-400V-54A-4G

The power amplifier used in this thesis has been manufactured by Spherea Puissance Plus. It is a four quadrants 21 kVA (7 kVA per phase) amplifier that can be operated in AC [29].



Figure 4-4 Power Amplifier (left) and display (right)

Four coupling modes are available:

- LVAC - Low Voltage Alternate Current
- HVAC - High Voltage Alternate Current
- LVDC - Low Voltage Direct Current
- HVDC - High Voltage Direct Current

Each mode has 4 operative ranges. The ones for LVAC are

- 135 V - 54 A
- 200 V - 36 A
- 270 V - 28 A
- 400 V - 18 A

Since we need 250V at most, the third range is the one that has been selected.

However, only the first mode is of interest for this analysis. The regulation chosen is the voltage type. A touch-screen display in the front panel is used for the local control.

Using this control display, the desired operating mode is chosen. To protect the other devices connected to the amplifier in case of a wrong amplifier operation, a maximum amplitude current equal to 20A is set as the maximum value for a limit duration of 0.2 seconds.

The amplifier is also the main actor of the dissipation of the power received by the WB in V2G. The dissipation capacities of the PA are connected to the internal resistance which can be manually increased via the display. Since this mode created instability during its use, it was decided, as already mentioned, to add a second load connected in parallel to the amplifier to share the dissipated currents.

Another screen returns the measured currents and voltages in real time. On the right side of the *Figure 4-4 (right)*, LEDs show the possible faulty behavior as in figure.

4.1.3 The thermostatic chamber

Nowadays, it is crucial to develop products in such a way that they can withstand all the environmental stresses that can occur in the “real world”. Appropriate equipment is needed to obtain this information.

It is always possible to test these conditions “on field”, directly where the action takes place therefore where the products are normally used, but instead an environmental test chamber is usually a better alternative. With test chambers it is possible to control different climatic conditions such as temperature and humidity; keeping these parameters under control is then possible to give an accurate estimation of the actual behavior of the component in critical conditions. Some chambers are even able to accelerate the effects of climate conditions. In this way, the lifetime, or the effect of the environment over the performances of different products can be estimated relatively accurate. In this thesis we will focus on the latter opportunity of investigation.

As mentioned before this work is carried out in collaboration with the laboratory “Officine Edison”, the EC-Lab, which has provided the thermostatic chamber used across these observations. The chamber’s manufacturer is Angelantoni.



Figure 4-5 Discovery chamber by Angelantoni

The chambers used for environmental testing can be distinguished into two groups

1. Thermostatic chamber: only control of the temperature inside its volume, the humidity cannot be actively operated with this instrument
2. Climatic chamber: there is both the possibility to act on the humidity and on the temperature

The chamber provided in the EC-Lab is a thermostatic one; even if the instrument would be enabled to operate also on the humidity, the condensation tank is not connected to it.

Another distinction parameter concerns the operating range, we will discuss this in the next section dedicated to the detailed description of the functions and features of the chamber.

4.1.3.1 Functioning of Discovery by Angelantoni

The environmental testing chamber used across this thesis was provided by Angelantoni, named Discovery. The measurements of the chamber were 919 mm wide, 1765 mm high and 1786 mm deep. There were two racks where products to be tested are put. The internal compartment which is the useful volume for the tests execution measured 601mm x 694mm x 801mm. The chamber’s general specifications of usage can be found in *Table 4-1*.

SPECIFICATION	UNIT OF MEASURE	VALUE
Useful volume	liters	337
Temperature range	°C	-40 / +180
Temperature precision	± K	0,1 ÷ 0,3
Maximum internal thermal load	W	1300 (+25°C)
Refrigerant gas		R404
Maximum weight that can be loaded on each shelf	kg	50
Speed of temperature variation: Heating	°C/min	4.5
Speed of temperature variation: Cooling	°C/min	3

Table 4-1 thermostatic chamber specifications

It is also possible to do different kind of test programs with the chamber, to do cyclic tests where the chamber changes temperature or keeps these values in a desired level for a certain period. Also, the changing rates of temperature and RH can be modified to satisfy the needs of tests by giving specified time for steps in program.

The chamber's frontal door is kept closed by an electromagnetic handle functioning only when connected to the mains.

The machine can be operated locally via the touchscreen panel on the front, with this method it is possible to run previously saved programs or simple setpoints for static temperature control, furthermore it is also possible to indicate the execution speed by specifying a rate per minute of temperature change; if this is not indicated, the chamber will execute the setpoint at maximum speed as in *Table 4-1*.

Cooling and heating are the two functions needed to control temperature. It's also important that the test chamber can distribute the desired temperature evenly on every spot inside of the chamber. The design chosen by Angelantoni to heat the chamber is an electric fan heater that consists of a fan and resistive coil. The coil package is heated to a high temperature, and air is conducted through it using the fan, so through the ventilation system, air is conducted to the chamber itself.

Cooling system works on the same principle as refrigerators. There are four components to the closed system: an expansion valve, an evaporator, a compressor, and a condenser.

A block diagram of this cycle can be seen in *Figure 4-7*.

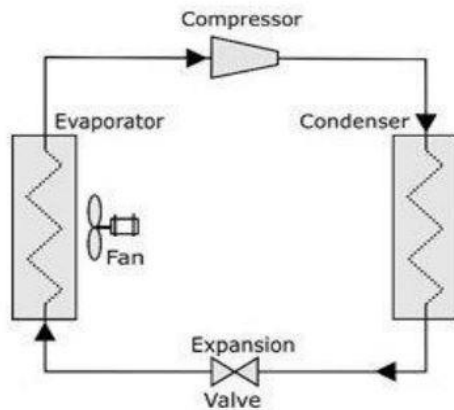


Figure 4-6 refrigerant liquid's cycle

First the cold and low-pressure liquid refrigerant is conducted to the evaporator through the expansion valve. It changes into gas in the evaporator and cools the air there. Then, the fan blows the cold air to the chamber.

Next, the low-temperature low-pressure refrigerant continues its way to the compressor where it changes to a high-temperature and high-pressure gas. Then the refrigerant continues to the condenser where it relinquishes its heat and it turns back to liquid.

Now the liquid goes back to the expansion valve and the cycle can start again from the beginning.

The Angelantoni's chamber is then equipped with an internal thermostat below the compartment which is part of the control system which implements a feedback function for regulating the temperature in the chamber itself. To this are added 4 PT100 resistors as in *Figure 4-8* are connected in Wheatstone bridge which will be used during the tests to check that the entire volume of the chamber has a similar temperature since an heat dissipating specimen will be tested.



Figure 4-7 Chamber's PT100s for temperature control

These PT100 have been numerated from 1 to 4 to keep better track of the temperature's fluctuations inside the chamber itself.

The control of the operations can be performed with three different ways:

- Local control using touchscreen on the chamber frontal side
- Remote control through API: MyKratos 2.0
- Remote control through APP: MyKratos 4

In this thesis only the functioning using API has been explored and exploited.

4.1.3.2 Winkratos 4.0 usage

The software functions are subdivided into “areas” logically associated to specific operations:

1. **Manual mode:** allows operator to set the point to be reached, the slope with which to operate. The test is activated by the operator and continues until it is stopped by it.
2. **Programme mode:** used to handle the test made with the internal editor, the profile created is run till a maximum of 100 times.

Different users can operate simultaneously the chamber with a hierarchical order made up of 5 levels which allow different access to the machine functions. From the level 1 which has the lowest grade of priority able only to monitor the system status, till the level 4 user which can modify all the different system’s settings. Another level called Admin is present whose sole function is to manage other users.

The connection between the PC and the chamber was established using the internal Wi-Fi connection present inside the chamber.

Since, according to the environmental testing the slope of the thermal conditioning has a maximum value, some profiles for heating up the specimen and successive cool down are drawn. One kind of cycling test has been done to assess the derating strategy at high temperatures and the possibility to restore the full power output once the ambient returns in the standard range.

For each test a recording session can be started or interrupted at any time and the data acquired can be exported in ASCII format. The recording data from the thermostatic chamber have been used in during the preliminary tests to verify the functioning of the chamber itself. For the temperature’s measurement on the WB during the proper performance assessment a type K thermocouple has been calibrated. The reason can be found in the fact that using the recording means of the chamber a fixed sample rate of one acquisition every 5 seconds.

Since a greater accuracy is needed to assess the specimen’s temperature an external transducer connected to the DAQ was chosen. In this way the temperature could be monitored more frequently especially during the derating behavior shown by the WB during the extreme operation at 45°C.

4.1.4 The wallbox: il DUT

Vehicle to grid (V2G) technology allows electric vehicle (EV) batteries to store energy and discharge it back to the electricity network when it's most needed like in peak load periods. This two-way exchange of energy provides your business with several economic, environmental and operational benefits and it is possible using a bidirectional converter like the DUT. The provider has launched a new commercial charging service using vehicle-to-grid (V2G) technology in partnership with Nissan.

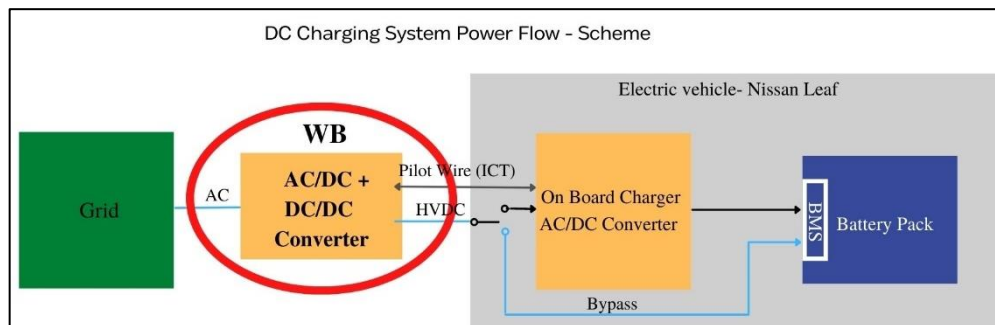


Figure 4-8 DUT architecture layout

The *Figure 4-8* shows the architecture of the V2G charging station to illustrate the role of WB in it. It is a device that is part of the power electronics landscape and is nothing more than a converter. Because of this, many WB reference standards are directly derived from those relating to photovoltaic systems. From the point of view of the grid, as a matter of fact, there is not a big difference between the two systems when they are connected to it.

As specified in the *Figure 4-8*, this converter is composed of an AC/DC and a DC/DC step. Keeping it short, a description is provided with the main characteristics to provide an overall description of the components according to some reference papers [34] [35] [36].

- AC/DC-converter:

These converters are the basic components that allow the grid to interface with the battery: unidirectional single-stage chargers are based on this type of converter. Numerous studies have highlighted three common AC /DC topologies: half-bridge layout, full-bridge layout, bridgeless layout.

Each configuration can be selected according to some characteristic parameters: number of switches, load on the switches (voltage and current), size of passive components (capacitors and inductors), low harmonic content and highest achievable power. Among the advantages of these configurations:

- Lower current per switch (considering the same power each switch operates at half the current of the previous case) leading to lower switching losses with respect to the half bridge
- Higher efficiency for higher output power
- DC output voltage with a lower harmonic content (notch filter is still necessary)
- Simplest control and lower number of components with respect to other configurations

- DC/DC converter:

Looking at the second stage of a dual stage charger, classic dc/dc converters such as buck, boost and buck/boost topologies are commonly adopted.

The V2G WB technology allows for the two-way energy flow; both recharging an EV's battery when electricity is at its cheapest, and discharging excess energy to sell back into the grid.

Starting from the datasheet provided by the manufacturer, some technical specifications can be mentioned and discussed for a complete understanding of how the device works

The WB maximum power in G2V and V2G (respectively 11 kW and 10 kW) is available only when the WB is connected to the internet network through an ethernet connection cable. The communication's protocols in both online and offline operation will be explored during the pretest phase. During our tests the 11kW charging was not available.

The WB works in Mode 4 of charge through a CHAdeMO connector (currently the only one suited for bidirectional functions).

The device is equipped with its own energy management and power control system logic that adapts the charging/discharging power to the settings selected through API using LabView control panel or APP when the DUT is online, while if the WB is not connected to the internet a charge of 7 kW automatically starts regardless the battery SoC level. The transaction's logic will be then defined in a dedicated section during the pretest phase.

The user can choose, when the WB is connected to the internet, whether and how the bidirectional operations happen thanks to some parameters: the amount of energy available for V2G operation (% of SoC), the EV charging schedule, the minimum charging/discharging power (3kW), the set point selected by user and the minimum SoC value below which no discharge of the vehicle is allowed which is 35% (MBP, Minimum Battery Percentage).

The WB is available only with a CHAdeMO connector. The device declares the following functions:

- Adapting the charging power to the set points selected by the user through API
- API visualization of the battery SoC (sampled every 10 seconds)
 - setting via API of the SoC schedule (selecting a time interval to reach a minimum level of SoC requested) and immediate charge setting
- the visualization of the AC real-time power flow (sampled every 10 seconds) through API
- APP control of multiple EVs charging

In the following tables there are summarized all the most important features of the wallbox.

Two tables can be derived for this peculiar device used across this study. The first one (*Table 4-2*) is relative to the installation parameters required by the device itself for the correct operation. In those prescribed ranges the provider ensures the continuous operation

of the WB, during the environmental tests the prescribed limits were tested and eventually validated.

From datasheet the device's working ambient temperature range between -25°C to +50°C. An unspecified derating starting from 40°C is then mentioned in the datasheet, no particular description of the behavior below -25°C is eventually described.

	PARAMETER	SPECIFICATIONS
Size and weight	Size	370mm*610mm*135mm
	Weight	25 kg without gun cable
Ambient conditions	Operation temperature	Operation temperature -25 °C to +50 °C
	Relative humidity	< 95%, non-condensing
	Altitude	Maximum 2000 m above the sea level
	Cooling	Force air cooling
Noise	Noise level	Maximum 70 dB(A)
EC charge cable	Lenght	3500 mm

Table 4-2 WB's general installation specifics

Given the nature of the tests carried out, parameters of great relevance are the dimensions of the device that have determined the possibility of using the same in the thermostatic chamber for the execution of the environmental tests and the specifications on thermic operational limits.

Charging Mode	Mode 4 (DC)
Connection standard	CHAdeMO
Frequency	45-65 Hz
AC input	340-440 V _{rms} (p-p)
Stated peak efficiency	96%
Max AC current	20 A (charging at 11 kW)
DC output	(G2V) 150-500V (V2G) 150-450V 36.7A (11kW) 33.3 (10kW)
Efficiency (declared)	95.9%

Table 4-3 WB's working specifics

The second table (*Table 4-3*) describes the operating specifics of the device from the input voltages and power level to the proper output connection.

Features like the available AC voltage levels and maximum currents are used as input variables in the operation of the Power Amplifier as mentioned in the previous paragraph. The stated efficiency needs then to be validated.

Differently from the AC voltage connection level which depends from the mains conditions and the power output requested, the DC connection depends directly from the battery operational conditions, therefore from SoC.

The vehicle used for the test is a 2019 Nissan Leaf e+ equipped with a 62 kWh lithium-ion battery. The EV can be charged via both DC and AC as it has CHAdeMO and Mennekes (Type 2) inputs respectively. Only the CHAdeMO connection is of interest for this wallbox operation. The vehicle has been charged and discharged multiple times over many different tests and thesis works so the EES's performances should not be considered in these works.

4.1.5 Electrical quantities measurement: general layout

The DUT in charging operation functions as a AC /DC converter or rectifier. For G2V use it takes AC current from the mains (or from the PA), converts it to DC, acts as rectifier and supplies power to the EV battery.

For V2G operation, the battery supplies DC power, which is converted to AC power by the WB. To have this kind of power flow the WB behaves as an inverter, like the inverter that converts the DC current and voltage from a PV panel to an alternated signal.

This twofold functioning highlights how it is of fundamental importance to acquire the electrical parameters both on the AC side and on the DC side in order to have an accurate description of the performances.

The device in its two operative configurations needs to comply with some regulations; to be sure that those standard are fulfilled in the test phase it's fundamental to correctly acquire the voltage and current signals in both AC and DC sides in the two operating conditions. These signals can be collected through tools and probes, such as the probes used for the direct current described, or via BNC connectors that take the signal directly from other components, i.e. the alternating currents acquired directly from the amplifier.

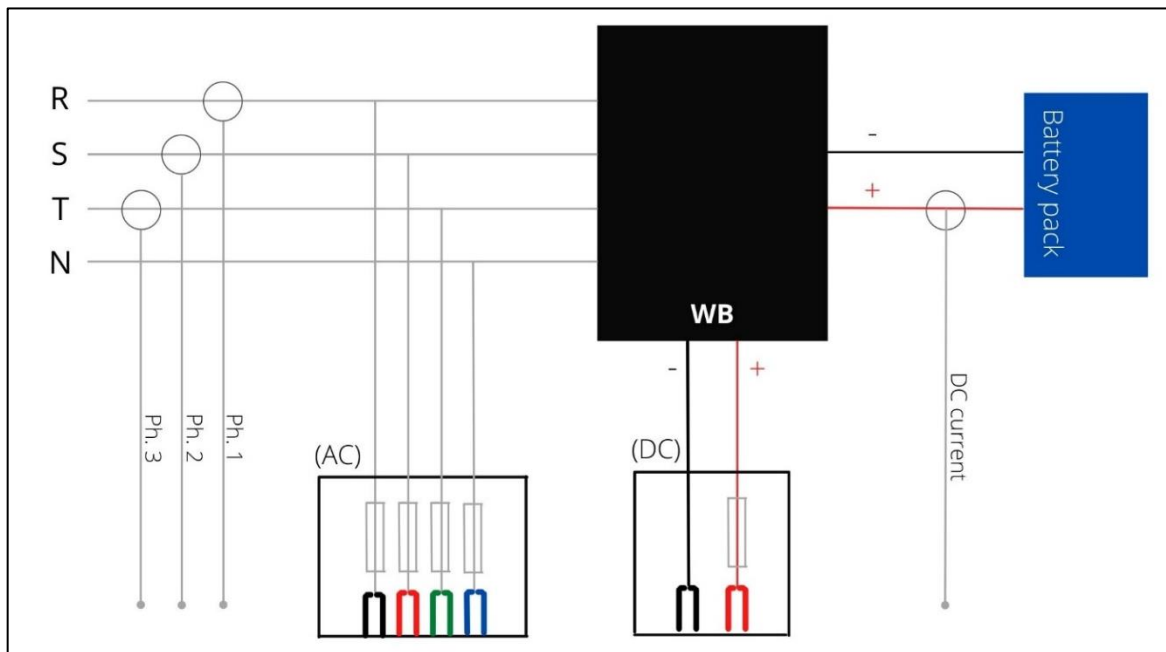


Figure 4-9 electrical quantities measurements general layout

Currents are transmitted through BNC coaxial cables, while the voltage signals using a banana connector.

The two black boxes in *Figure 4-9* (AC and DC) above are the junction boxes for voltage measurements, while the grey circles on the line depict the ongoing current acquisitions.

4.1.5.1 Voltages measurement

To have the voltage signals two different junction boxes have been used. The junction boxes are portrayed in the *Figure 4-10* below, it can be seen the junction cables entering the boxes and the banana cables exiting going towards the HBM plugs. Two signals are needed for DC, 4 signals for AC (3 phases and the neutral).



Figure 4-10 Junction boxes for voltage signals

For the DC voltage measurements, the WB cover has been removed and both the DC power supply polarities (positive and negative) have been derived into one of the two junction boxes. This voltage is therefore also representative of the battery's voltage across the terminals. There is only one 500 V, 2 A fuse in the DC junction box since two fuses would have been superfluous, as the DC current value on the positive and negative cable is the same. Through a banana plug-plug cable, the signals are finally transmitted from the box to the DAQ.

To obtain the AC voltages, a similar procedure was carried out. This time, four 1.5 mm² wires (three phases and the neutral) were diverted downstream from RCD to terminate in the AC junction box. In the box, each wire passes through four 400 V 4 A fuses before providing their voltages at the bushings.

4.1.5.2 Currents measurements

To assess the performance of the converter the voltage and the direct current flowing in and out of the EES must be acquired with precision and accuracy to comply with the IEC standards of evaluation. In the following section it is described where these values are collected before presenting the measurement instruments with their features.

In this case since the acquisitions are performed with different ways: we split the discussion to provide an accurate description of both the measurement procedures.

- **DC side**

The power supply from the wallbox, exits the thermostatic chamber to feed the EES inside the Nissan Leaf. The power terminal follows compliance with the CHAdeMO standard. CHAdeMO is the original DC plug developed by five Japanese automakers that have been trying to promote this plug as a global standard since 2010. The CHAdeMO cable contains two power supply wires (one positive and one negative) and DC power can flow in them.

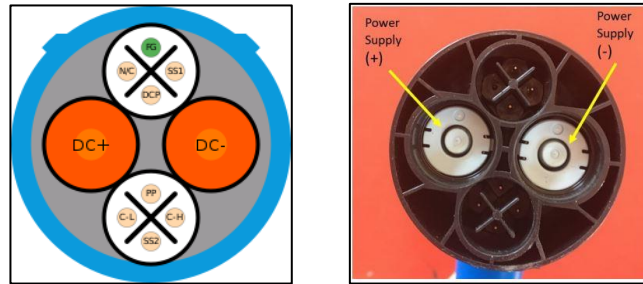


Figure 4-11: CHAdeMO supply conductors with polarities

Inside the supply cable are these two conductors in *Figure 4-11*. Since current clamps measure the current flowing through a conductor and convert it into a voltage signal that can be displayed and registered on an oscilloscope, it makes no sense to clamp the current clamp to the cable DC in which there are two conductors with opposite flow directions: the value read by the device would be zero because the effect of the two conductors balances out, one being the positive and the other the negative. Only clamping the probe on one of these two supply wires can be helpful, providing the real DC current value.

Fortunately, the CHAdeMO socket under the bonnet divides the driver to reach the connections of the Nissan Leaf's EES, which is located inside front car trunk. In this way, the positive conductor is separated from the negative and it is possible to measure the actual value of the DC current with the terminal probe.

The signal is then led to the DAQ via a rather long BNC cable. The BNC cable is shielded so that it does not introduce any sources of interference into the signal recorded by the unit. In *Figure 4-11* it is reported the current clamp used for the recording connected to the positive conductor.



Figure 4-12 Hioki 3274 DC current clamp

- **AC Side**

The current measurements on the AC side of the WB are not carried out directly upstream of the DUT. In the previous thesis work the protection box supply power cable has been stripped. In this way the three phase wires are exposed and the probes could be placed, each probes was then connected via BNC to the DAQ.

In this case, instead, the currents were registered directly from the output of the PA. This measuring difference introduces a different error contribution in the recorded quantities that will be translated in a different error propagated in the conversion efficiency. An esteem of the error propagation and the different errors of the measures will be carried out accordingly.

Since the real time simulator is not connected for these tests, as it is not strictly necessary, the AC variables are taken directly from the output signal of the amplifier. The input terminals of the amplifier are connected to the internal generator output cables of the amplifier. The output signal in turn is connected to the oscilloscope to proceed with the acquisition. The accuracy of this measurement is specified in the data sheet of the PA. This topic will be introduced and discussed during the error propagation analysis



Figure 4-13 AC current images signals

4.1.6 Double load configuration: additional dissipator

During the discharge phases (V2G), a problem with power dissipation was found at a maximum power of 10kW.

In previous studies, for the continuous at this power setpoint on the PA's dissipator, a second additional 8-ohm resistor was used according to the specifications of the amplifier itself, in addition to the standard resistor already inserted. This allowed the power to be delivered for a longer period without overheating the heat sink inside the PA.

After stability problems were encountered in this mode, it was decided to use a different configuration: a junction box to connect the amplifier in parallel and an external triphase heat sink capable of handling up to 9 kW. The operating diagram is shown in the following *Figure 4-14*.

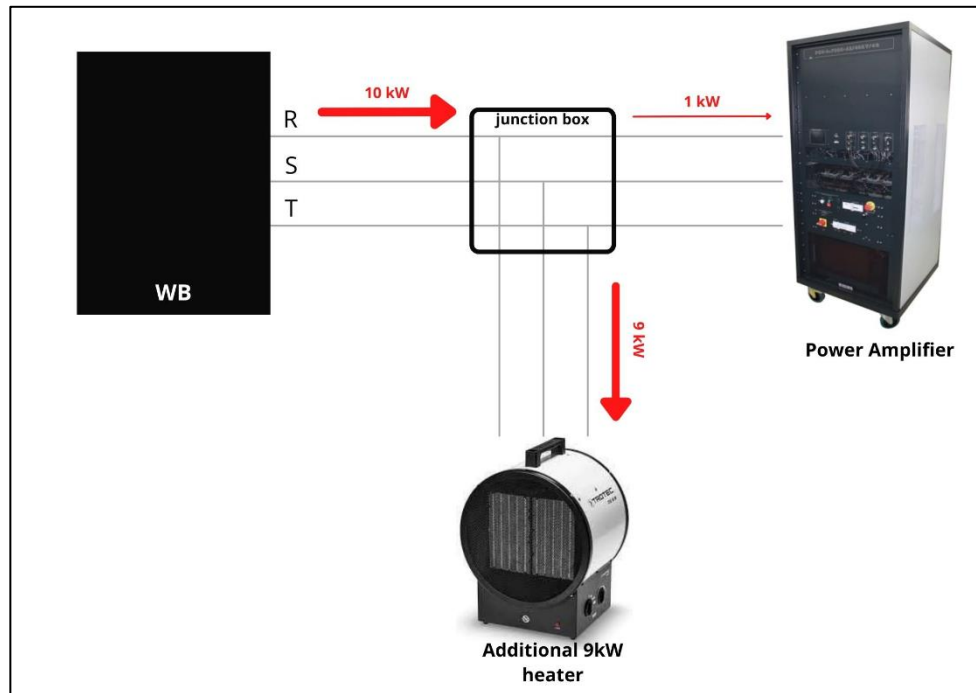


Figure 4-14 Parallelo load configuration

The *Figure 4-14* shows the operating diagram on the AC side, when the battery was discharged and a power of 10 kW was fed to the amplifier. Using a diagram of the power flow, it can be seen the direction of the power flow. Since the dissipator feeds the internal resistor with two phases and the circulating fan with the third one, it was always kept at full output so as not to create dangerous imbalances between the phases of the amplifier. It was therefore constantly drawing 9 kW when in use.

It should be emphasized that, on one hand, this technique was not necessary when V2G tests were carried out at high voltages. This is because at high voltages the absorbed currents were obviously lower and therefore the heat developed by the Joule effect decreased. As a matter of fact, the losses associated with the Joule effect, which are directly related to the ΔT exerted on the resistor, depend on the ohmic value of the resistor and the square of the current flowing in it. Since this value must be equal to the total power applied to the amplifier (10 kW, as mentioned above), the temperature developed will be much lower when the current is reduced (e.g. when the supply voltages are higher).

On the other hand it should be borne in mind that this method, in which the currents are divided in parallel with the external heater and only measured as they flow through the amplifier, irreparably affects the measurements and results in currents being recorded on the AC page that are much lower than those actually exerted by the WB. The procedure is therefore due to divide part of the current into the additional dissipator for the time necessary to condition the WB in the chamber.

When the thermal equilibrium was reached, the total value of the currents flowing through the amplifier can be recorded by switching off the dissipator, because the short duration of these recording would not create any overheating issue during the recording.

4.1.7 Data Acquisition System: HBM- GEN7tA

Data acquisition (DAQ) is the process of measuring an electrical or physical phenomenon such as voltage, current, temperature. The DAQ is the last link in the operating chain of the measuring device, in which analogue signals are processed and converted into digital and then into discrete measurements.



Figure 4-15 HBM - GEN7tA

The GEN7tA is a transient recorder and data acquisition system. In the project it is used for visualization, monitoring, recording and post-processing of electrical quantities. Through an RJ45 connection it is possible to visualize all measured quantities remotely on a computer on which the proprietary software Perception is installed.

Perception software requires a HASP (hardware against software privacy) key that is an hardware-based protection. Perception is used both for visualization during the test execution and for the data and variables storing. Indeed the formula used will be discussed in the next chapter but it is important to highlight that the content of those created variables cannot be stored without the use of the logfile function. This function allows the DAQ.

The 1 Gbit Ethernet interface is capable of transferring the recorded data to the PC at 100 MByte/s allows electrical signals to be logged at high-resolution, and at up to 2 MS/s.

4.2 Temperature measuring devices

A reliable temperature measurement, which can be recorded as a voltage signal, is essential for the study of environmental testing. Several devices are used to track temperature changes:

- one thermocouple
- 4 PT100 RTDs.

The thermocouple was used for measurements on the surface of the heat sink, while the PT100s served as a control instrument. Since the fan was covered so as not to affect the convection mechanisms studied by the manufacturer WB, the PT100s were essential to ensure the homogeneity of the temperatures inside the chamber, so that the control volume was conditioned in the same way at each of its points, without major differences between them (no more than 5K). This procedure was chosen because it was not possible a priori to know the position of the internal temperature control device in the unit itself.

Let's briefly describe the physical operating principles of these 2 transducers, as this is an essential part of the choice for temperature measurement and thus of the following work. Transducers take energy of some type (i.e. mechanical or thermal) and convert it to another type, typically electrical.

4.2.1 Thermocouple Type K

A simple description of a thermocouple is two wires made of dissimilar metals connected at one end that transfer thermal energy as a voltage measured across the two 'cold junction' ends. Thermocouples are flexible, inexpensive, and provide fairly accurate temperature measurements. The phenomenon describing the thermocouples behavior is known as Seebeck effect.

The Seebeck effect refers to the development of an electromotive force between two points of an electrically conductive material when there is a temperature difference between these two points. A simple thermocouple system, is comprised of two wires and a device to acquire the voltage signal. The wires are sheathed internally with sheathing of different colors. This prevents any contact along the wire and allows identification of the positive/negative leads of the wire. *Figure 4-16* below shows the type K thermocouple used in this thesis experiences, with a welded tip.

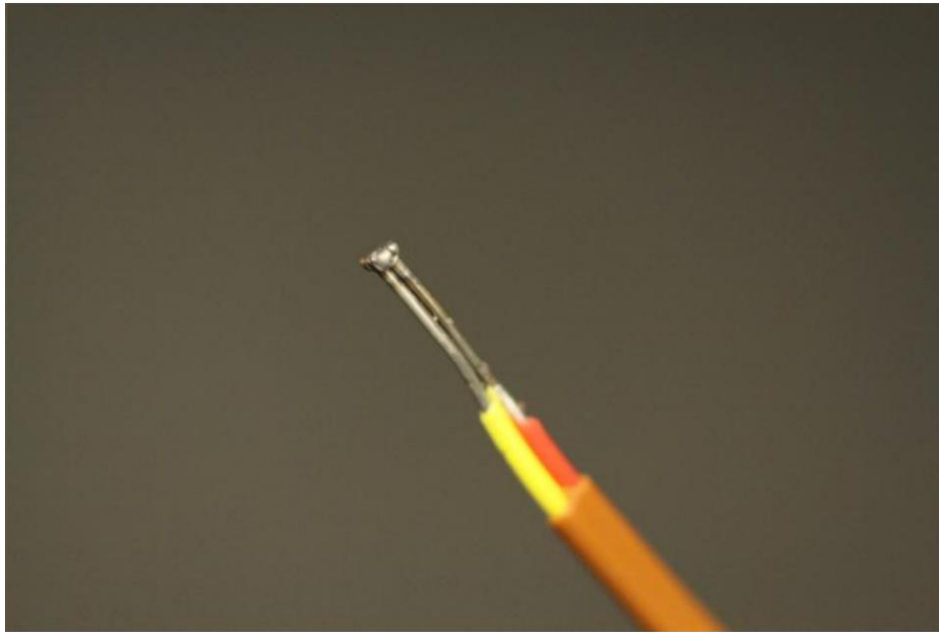


Figure 4-16 Thermocouple type K used for testing

Thermocouple ‘type’ refers to the materials that comprise each wire in the thermocouple. A type K thermocouple is comprised of Chromel (a nickel chromium alloy, yellow sheathing) and Alumel (nickel aluminum alloy, red sheathing). The type K thermocouples have a possible range between -250°C and 1330°C . The yellow lead is positive, and the red lead is negative. The other two ends of the thermocouple are connected to a data acquisition system (DAQ) or a voltmeter to measure the temperature.

4.2.2 RTDs

The resistance thermometer (RTDs) generally consists of a filamentary metal element wrapped around or placed on an insulating support (frame), with the sensitive element surrounded by a protective sheath.

The operating principle of resistance thermometers or metal resistance thermometers is based on the change in electrical resistance of the metal contained in the sensor as the temperature to which the sensor is exposed changes. For metals, there is a linear relationship between the resistance and the temperature. The metals most used in the manufacture of these sensors are platinum (the chemical name is Pt) and nickel (the chemical name is Ni). As a matter of fact, these two metals have excellent properties that favor their use in the field of thermal measurements: they have a high resistance and are very stable.

Metal resistance thermometers are identified by the abbreviation of the metal they contain: if platinum is used, the designation is Pt, if nickel is used, the designation is Ni. The abbreviation is usually followed by the value of the nominal resistance at the reference temperature (0°C).

The pt100 is only used for environmental control inside the test chamber. As it is equipped with external cable entries for the various power and network cables, it is not perfectly isolated from the external environment. This means that the internal temperature is not perfectly homogeneous and can therefore affect the results obtained if it is not carefully monitored.

5 Test Preparation

This chapter deals with all the preliminary procedures for carrying out the tests. Indeed, the acquisition activities were preceded by some technical and logistical assessments that were carried out in order to have a clear picture of the standard procedures that would then be followed when carrying out each registration.

A first section is dedicated to the thermal parameters, from the calibration of the measuring instruments to the definition of a standard for the thermal conditioning of the component. This latter parameter is particularly important for the study of the performances in different thermal regimes because, starting from the assumption that a change in component temperature can also lead to a change in performance, it is necessary to ensure that the DUT and its internal components are in thermal equilibrium at the desired temperature before the beginning of each test

A second section is instead dedicated to the integration of WB into the measurement chain, with the definition of the decision variables within the DUT and the remote control through a API of the device. As a matter of fact, when the WB is operated locally is limited to certain operating conditions, whereas when the DUT is connected to the Internet, the availability of V2G and of different operable power setpoints opens up.

Thirdly, the formulae for processing the measurements collected are defined. The procedure for initiating the test is defined so that it is clear, open to discussion and repeatable in the future.

Finally, a section is devoted to the analysis of the error introduced in the measured parameters and the transmission of the same in the final results, which are presented in the next chapter.

5.1 Thermocouple calibration's procedure -80BK-A

Thermocouples are calibrated initially by their manufacturers. Changing the measuring device (from multimeter to oscilloscope) without having the characteristic equation of the generated signal available from the manufacturer, a recalibration is necessary. In this specific case the thermocouple choice fell on the instrument integrated in the Fluke multimeter.

Calibration is a type of characterization whose aim is to define the metrological properties of a measuring instrument. This is done by comparing measurements with a reference device defined as a sample [30]. Calibration is also used to determine the trans characteristic of the instrument.

Indeed, many measuring instruments are transducers; they convert the quantity read into a signal (typically electrical in nature) that can be more easily read and processed by suitable indicators. Knowing the relationship between the quantity read and the signal produced allows the relative indicator to be set correctly and thus the measured quantity to be read accurately.

The logic used for the calibration process is called calibration by comparison. In this method, the calibration is made so that the same quantity is measured as is measured by the sample instrument. The accuracy of the calibration results from the comparison of the two measurement results.

To calibrate a thermocouple, various types of measuring equipment, standards, and procedure based on Department of Mechanical and Aerospace Engineering Buffalo [30]. First, a control temperature must be established that is stable and provides a constant temperature; it must be uniform and cover a large enough area that the thermocouple can adequately be inserted into a thermal bath as in *Figure 5-1*.



Figure 5-1 thermocouple calibration

A second type k thermocouple produced by the same manufacturer as the first one and identical in all respects to the one to be calibrated is used as sample instrument. The two instruments therefore possess the same accuracy and precision.

This second thermocouple, however, is coupled to his Fluke 87V-MAX Multimeter which then reports the correct temperature recorded.

The thermocouple to be calibrated is inserted together with the sample one in the same volume of heated water like in figure.

The volume was taken large enough to easily accommodate the thermocouples and to be insensitive to external conditions.

Following this scheme, the measurements were produced at regular time intervals by inserting the thermocouples into the volume and recording the value signaled by the multimeter and the voltage signal acquired by the HBM. To proceed smoothly without having to deal with infinitesimal numbers (since the voltages involved are in the order of mV) a display gain of 30000 °C/V was adopted so that the measurements produced were better visualized.

Once a good data set of observations was obtained, they were recorded to study their linearity. Indeed, a strong linearity is expected in the relationship between the recorded temperature and the measured voltage, so that future values can then be placed on the appropriate linear regression line.

Linear regression attempts to model the relationship between two variables by fitting a linear equation to the observed data. One variable is considered the explanatory variable and the other the dependent variable.

Before attempting to fit a linear model to observed data, a modeler should first determine whether there is a relationship between the variables of interest, but since we are working

with a known to be transducer, we are certain that the relationship between the recorded data and the displayed one is real.

In statistics, linear regression is a linear approach to modelling the relationship between a scalar response and one or more explanatory variables (dependent and independent variables). In linear regression, relationships are modelled using linear predictor functions whose unknown model parameters are estimated from the data. Such models are therefore linear models.

This property can be checked with the coefficient of determination R-squared [31]. The coefficient of determination R^2 is a statistical value that allows you to understand if a linear regression model can be used to make predictions. R^2 value can vary between 0 and 1.

- $R^2 = 0$ indicates a model whose predictive variables do not explain the variability of y around its mean at all. In practise, if you were to use only the mean of y instead of the independent variables inserted into the model, you would get the same explanatory value. This situation occurs when the y estimated by the model is exactly the same as the mean of y . In this case, the corresponding correlation index is also equal to 0.
- $R^2 = 1$ indicates a model whose independent variables are able to fully explain the variability of y around its mean. That is, if you know the values of the independent variables, you can predict exactly what the value of y will be. This situation only occurs when all points in the scatter plot lie exactly on the regression line. After all, if the R-squared is equal to 1, the correlation index r is also equal to 1 or -1. So in this case there is no prediction error when you use x to predict y . In other words, the observed values of y exactly match the values of y estimated by the model.

The larger the R-squared value, the more the model usually has high predictive power: the larger the R-squared value, the better the ability of the explanatory variable to predict the values of the dependent variable.

The R-squared index assesses how much the individual observations deviate from the regression line. If you build two regression models for the same data set, the model with the largest R-squared is generally the one that has the smallest deviations between the observed and expected values of y .

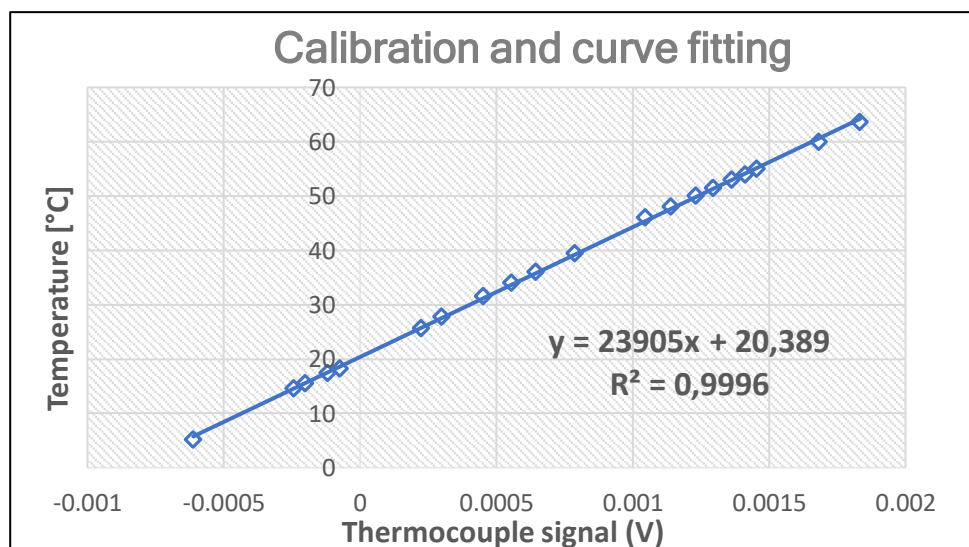


Figure 5-2 calibration curve fitting

In the *Figure 5-2* it is clear how much linearity is observed by the transducer. The value of R-squared, which approximates our data set with the following equation, is very high, indicating an excellent approximation in terms of future observations. It will be therefore possible use the equation shown in the graph to obtain the gains and technical offsets of the instrument, with a very high probability that the value measured by this prediction will be reliable.

Since the calibration procedure is in any case affected by variations in external conditions and by the inaccuracy of the measuring instruments, it is repeated three more times.

Finally, an additional test is carried out for temperatures below zero with the thermal chamber and a solution of water and sugar to avoid solidification.

In this second plot (*Figure 5-3*), the characteristic curves that have emerged are reproduced. Near the zero crossing of the instrument, the inaccuracy of the instrument increases, leading to a greater variability of the recorded data set; while for measurements far from zero there is a convergence of the recorded data.

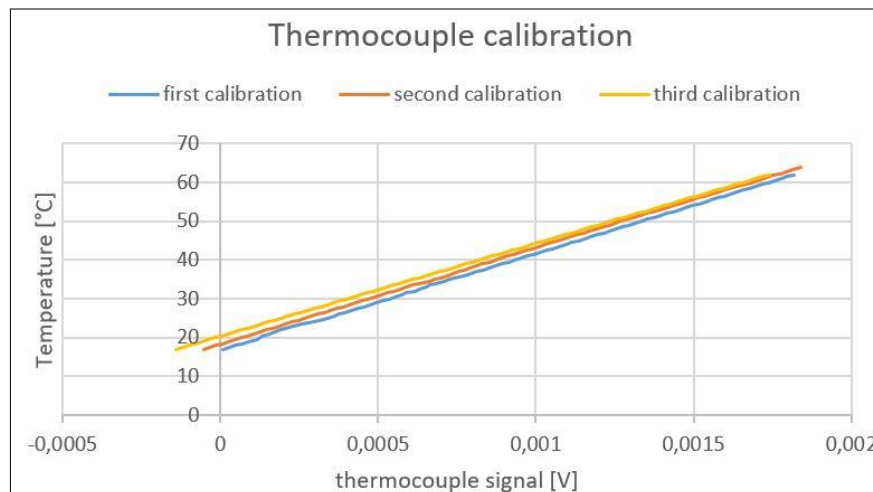


Figure 5-3 thermocouple's calibration curves

An average of these curves, which may be representative of all the measurements made is then derived. The equation resulting from the fitting is then used as the basis for the measurements during the experiments.

After the characteristic equation of the thermocouple was determined, the acquisition point was chosen. The point that exerted the highest temperature when the WB was in operation was therefore selected

With the help of some graduate students with experience in the field of power converters, it was possible to identify by an external inspection the areas where the suspected power exchange could take place. Two zones were identified, one in the lower part where the DC/DC converter is likely located and one in the upper zone where is probably to find the AC/DC stage. Several tests were performed in G2V at a standard power of 7 kW and the thermocouple was used after calibration to investigate the two previously identified zones. Thus, with this procedure, it was possible to identify the location where the thermocouples

should be placed. The instrument was then positioned and fixed at the point where the acquisitions described were to be made.

5.2 Thermal conditioning procedure

The expression "environmental conditioning" or "environmental testing" covers the natural and artificial environments to which components or equipment may be exposed so that an assessment can be made of their performance under conditions of use to which they may be exposed in practice.

Temperature chambers used for "environmental conditioning" or "environmental testing" are not described in any publication, although the method of maintaining and measuring temperature has great influence on test results. Thermal conditioning is the controlled application of heating and cooling to achieve a change in the properties of the item being observed.

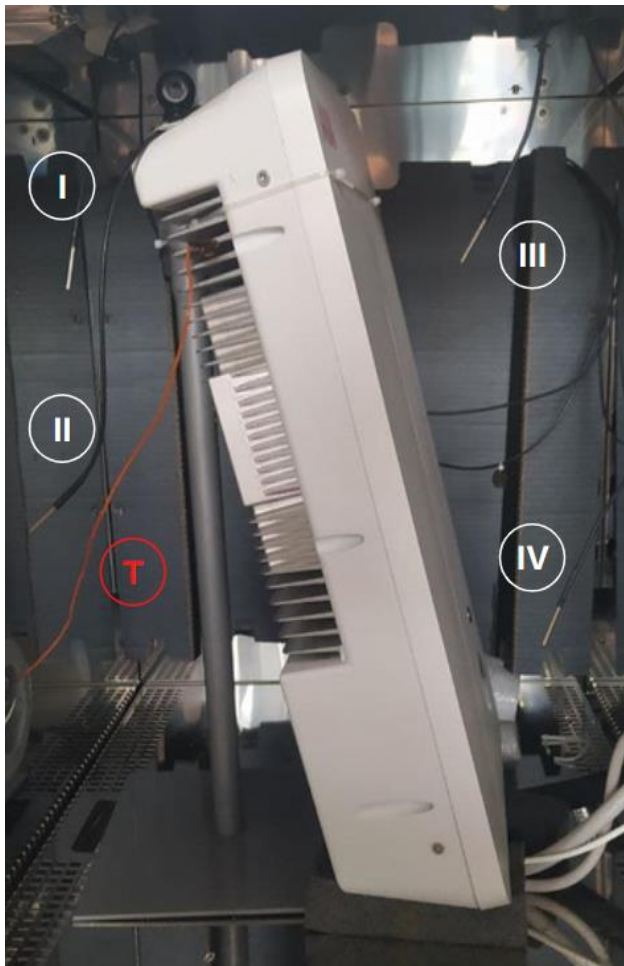


Figure 5-4 temperature control
white: control RTDs red: thermocouple

According to the standard IEC EN 60068: 2007 and following the specific procedures Bd and Be, depending on whether or not we want to power the device during conditioning, can proceed with the positioning of the device in the test chamber. Here we try to describe how the measures were positioned in order to obtain a reliable representation of the thermal evolution to which WB is subjected.

The WB has been positioned vertically so as not to modify the power dissipation mechanism as it is intended

by design. The forced convection cooling strategy can be strongly influenced by the orientation of the device itself.

For the same reasoning it is needed a low air velocity state: the conditioning airflow within the working space has to be low enough so that the temperature at any point on the test specimen is not reduced by more than 2 K by the influence of the circulation of the air (if possible, not more than 0,5 m/s). This testing parameter is controlled by acquiring the signals of the 4 RTDs of the thermostatic chamber. The placement of the sensors is presented in *Figure 5-4*. To fix the sensors to a preferred height, cable insulating tape was used. The RTDs were numbered from 1 to 4 to keep track of their different signals.

At the same time this airflow should not be enough strong to modify the airflow over the heatsink exerted by the DUT's cooling fans. The reason lies in the fact that having a strong

airflow from the chamber over the WB could influence the device temperature's build up. A protective screen was then used between the chamber's heater and the device.

It is fundamental, for the testing procedure, that the device reaches thermal stability before the start of the acquisitions. The factor influencing the so-called conditioning times is the thermal capacity of the WB. A serie of 5 tests is completed in order to establish the acclimatization times of the WB inside the thermostatic chamber.

This process was used in the preliminary phase to define a schedule of the laboratory experiences that could be held. Without an accurate definition of the pre-acquisition conditioning times, it would not be possible to estimate the development times of the different experiments.

The thermal conditioning estimation was carried out as follows.

Starting from the consideration that the greatest temperature difference to which the machine will be subjected, considering the choice of thermal regimes (-20°C, RT, +40°C), would be 30°C; for assessing the conditioning time the initial temperature was taken equal to 0°C with the final temperature of + 30°C.

Before starting the experience, it was necessary to ensure that the WB was in perfect equilibrium at 0°C, in this regard a constant regime was maintained at this temperature for about 2 hours.

At any time, thermal equilibrium is considered reached when a temperature increases or decreases of less than 2°C in a time span of 5 minutes is recorded by the thermocouple. In the next figure a single recording is shown as an example of the thermal conditioning evaluation procedure.

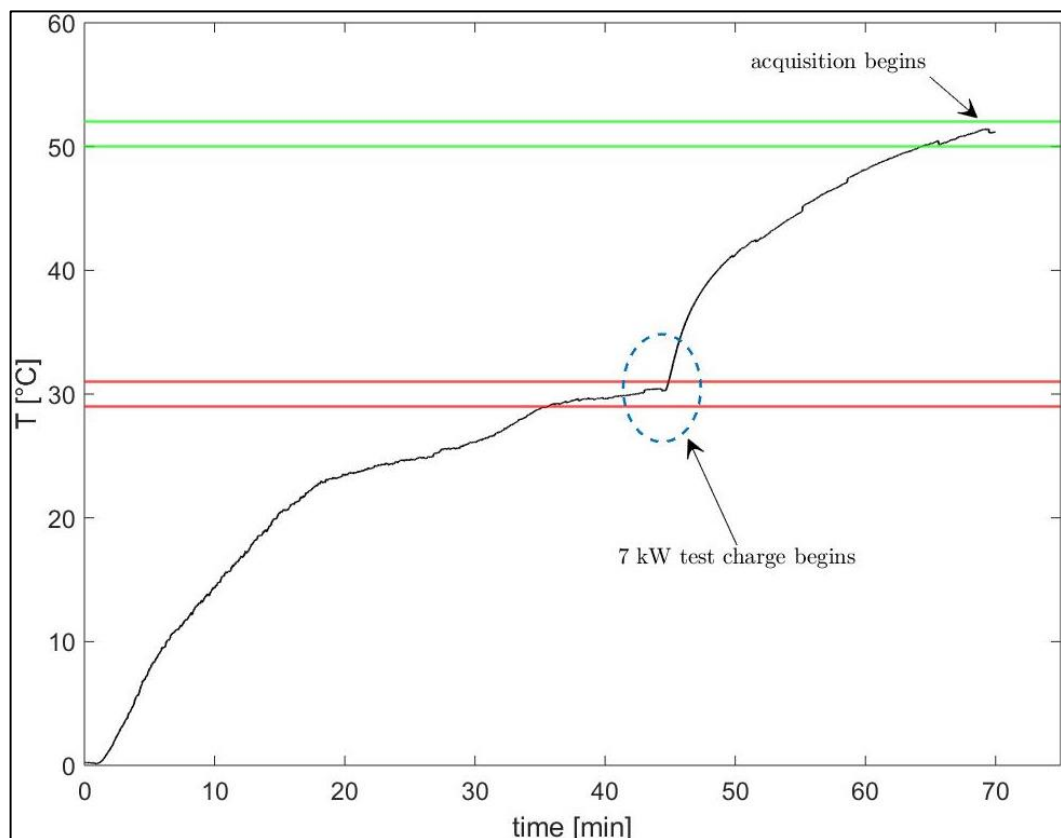


Figure 5-5 thermal conditioning time

The dataset in establishing the conditioning time was made up of 5 different recordings starting from five different initial temperatures always experiencing a temperature difference equal to 30°C.

As it is highlighted in *Figure 5-5*, 40 minutes is the time for the conditioning of the unpowered WB to increase the temperature value of 30°C. To reach a thermal stability with the working WB, a total of 70 minutes (40 + 30) were necessary. This second conditioning time it is strongly dependent from the working power setpoint of the WB during conditioning, In the 5 recordings always a different power was used to complete this second conditioning. All the similar observed times are reported in *Table 5-1*

Power setpoint	Total conditioning time
3 kW	55 min
5 kW	60 min
7 kW	70 min
9 kW	75 min
10 kW	80 min

Table 5-1 thermal conditioning time at different power setpoints

Once this important parameter has been established a standard procedure is defined for carrying out the measurements at the various critical temperatures established.

The specimen initially into the chamber, is at the temperature of the laboratory. Usually the temperature registered inside the Officine Edison laboratory were around 20°C with a minimum of 18°C. The specimen shall then be switched on and electrically loaded checking whether it is capable of functioning properly. This step is of main importance, because before working on the thermal conditioning of the device, the functioning of the communication protocol must be verified. As a matter of fact, it was not uncommon to have experiences that were nullified by malfunctioning of the WB's API control. The communication protocol is explored in the following paragraph. After this additional check the WB is shut off and the conditioning can begin.

The temperature is then adjusted to the temperature appropriate to the degree of severity (-20°C, RT, 40°C).

After temperature stability of the test specimen has been reached in accordance with what has been shown and described in the previous image, the WB is supplied with power till the second plateau is reached. Then the relevant quantities are recorded.

5.3 Communication procedure through API

This section aims to define the components, their connections and the sequence to be followed in order to enable the WB to perform different and successive power setpoints exploiting the online operation.

As a matter of fact there are two distinct modalities of operation enabled by the DUT. The first one serves the purpose of an accelerated monodirectional DC charge with a conductive charging process able to deliver a rated power of 7kW to the ESS of the vehicle.

According to the definition from the Italian plan for the electric infrastructures, the charging system under test falls into the category of accelerated type. This definition comprises the EV supply equipment (EVSE) able to supply the battery pack with a power between 7kW and 22kW.

In offline mode only charging is allowed, the device in this case behaves as a V1G fast charger enabled for one-way power exchange. This operating mode is the simplest one to adopt, it is much more user friendly than the online modality and allows for the push-and-charge use.

On the other hand, the online mode aims at a different mode of use. As a matter of fact, it enables not only to operate at higher power setpoints for the charging mode, but it gives access to the potentiality of V2G mode. The nominal power of the charging column is 11 kW, while the nominal discharge power measured is 10 kW. Both values are referred to the AC side, which means that in V2G mode seen from the DC side the wallbox absorbs more than 10 kW due to the WB conversion efficiency.

Using the API control software implemented in a set of LabView control panels, it is possible to send charging and discharging requests to the column via an Internet connection. The commands can be managed either through an API platform or through the app, which can only be used to send vehicle charging commands. The APP was never used across this study, so it is no further analysed.

The DUT has three different status: OFF, STANDBY, ON

The status of the WB is shown by a led stripe on the frontal side of the device which states the actual condition of the WB. In the following *Table 5-2* is presented the taxonomy of the visual signal given by this led light.

Led color	Status
RED	OFF
BLU	STAND BY
GREEN	ON

Table 5-2 visual LED signal's taxonomy

Unfortunately, there is no visual signaling that the device has been successfully connected online, the only way to verify the correct online operation is to look at the power delivered in real time by the WB. The frontal led will turn green when the WB is in ON state independently if it is connected or not to the internet network. This aspect could become a matter of discussion in design phase in order to provide an easier experience.

As it has been already mentioned the online communication between user and WB is made possible through two different ways: API and APP requests. The API requests are sent through a LabView project. In order to begin the transaction, it requires parameters such as

the User ID, EV ID, the EVSE ID; this allows the user to obtain the access authorization token and secondly to execute the commands.

The LabView control panel grants the user to set the operating power of the wallbox and the scheduled time interval to which the setpoint is referred. For the V2G operation the power setpoints are considered as positive, while in G2V mode the power flow is considered with negative values. Furthermore, the AC power is expressed in Watts.

Several authentication issues have been encountered when using the DUT via the API, due to the product's lack of flexibility when encountering power-on procedures that differ from the standard protocol. For this reason, a procedure was selected to clarify the procedures to be followed.

The main problems encountered were mainly related to the inability to establish communication between the cloud and WB if the product was turned on while the CHAdeMO connector was already plugged into the vehicle, or after a shutdown not preceded by the disconnection of the plug from the vehicle itself.

In both cases the DUT was not able to operate in V2G mode like it was disconnected from internet. This behavior was encountered every time a switching on or a turning off the device was not anticipated by the disconnection of the CHAdeMO plug.

A second communication issue occurred when the WB was connected to the Ethernet cable after it was already in STAND BY. In this case the DUT could not detect the connection with the ethernet cable, and it was not possible to establish a communication with it. This caused that the wallbox was visible through the control panel and its status was correctly updated by it, but it was not possible to communicate power setpoints.

Despite these problems, it is important to keep in mind that laboratory use is not the same as the use intended for the final consumer or the V2G service provider. As a matter of fact, the cases where the Internet connection is interrupted or the device suddenly shuts down without the vehicle being unplugged are rare, if not eliminated, under normal operating conditions. These eventualities can happen, but often they are errors or malfunctions.

In any case, to avoid problems or malfunctions in future studies, a standard procedure is established that takes into account the possible workflows. Starting from the standard situation with the WB being shut off and disconnected from internet:

- Connect the Ethernet Cable to the WB
- Turn on the switch in the electrical cabinet
- The wallbox's frontal led turns red
- Wait for the WB to establish internet connection and to be ready to charge (blue led): this could take several minutes
- Log in to the Server via Client ID to get the access token, the token is unique for each transaction. The setpoint Labview panel will automatically perform this operation as follows

- Open the SETPOINT panel in LabVIEW to set a new transaction's schedule. Every setpoint

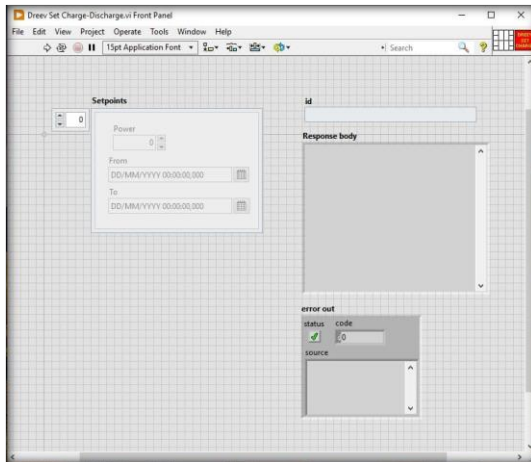


Figure 5-6 LabVIEW setpoint panel

- Set the schedule of desired setpoints in Watts through API. Many successive setpoints can be arranged in an array using this panel in *Figure 5-6*. Any given setpoint is characterized by the power value (positive in discharging, negative in charging) and by a chosen date and time according to the Central European Time. The array will identify the first given setpoint with the 0 index, the second one with the 1 index and so on.
- Wait for confirmation from the software: if the 400 error is displayed, the chosen scheduled overlaps with an other active schedule.
 - Once the code is run, if the current transaction will be characterized by an id and the chosen time and date
 - Push the front button to start the transaction with the cloud:
 1. The led turns green
 2. The wallbox starts following the scheduled setpoints
 3. If there is no setpoint scheduled the wallbox won't start any charging process, the led will turn green anyway, since the communication with the cloud is established
 - Press the button to end the ongoing transaction (the led will turn again blu)
 - Unplug the vehicle
 - Turn off the switch in the electrical cabinet

As said before it is fundamental to unplug the vehicle before switching it off keeping it unplugged before the beginning of the next experience. If the wallbox is shut down and repowered while the CHAdEMO socket is still plugged into the vehicle, the wallbox could incur into behaving like it is not online, thus providing only the 7 kW G2V operation.

The LabView panel communication commands are described in the following section. Different operations and controls are possible using this software. Three different panels have been developed to allow the control over the operation of the WB during the experiments. Also, future setpoints and the current status are communicated in this way.

Controlling the last SoC and power flow is always possible through the STATUS panel which refreshes its data every 10 seconds. It will also report the setpoints communicated in the last 24hrs (in this case the time will be reported in UTC not in CET). If the transaction

has not already begun the STATUS reported will be referred to the last one. In this panel it is also possible to check if the Vehicle connected is the correct one checking the related id:

All the communications sent to the WB go through the cloud, the same logic applies as in the case of control via app (even though not in the scope of this document). Therefore, is mainly important the frequency with which the wallbox interrogates the cloud, this greatly influences the behavior of the device as soon as it is turned on.

Two different situations have occurred:

- The wallbox, after its standby operation, when is operated starts with a 7kW charge for less than a minute and after that brief transient the output power goes to zero waiting the scheduled setpoint or directly follows the scheduled setpoint, if the selected time has already passed.
- The wallbox avoids the first transient since, during the standby period -blue light, the device has already interrogated the servers.

Unfortunately, this warmup time cannot be uniquely defined without consulting the communication setup, according to some evidence collected during some experiments these are the results.

The standby start time is considered when the wallbox led turns from red to blue, the standby end time instead is the moment when the button is pressed. The incorrect behavior defines when the device starts with the standard 7kW G2V operation

Standby start time	Standby end time	Standby total time	Incorrect behavior
09:10:00	09:25:00	00:15:00	YES
10:05:00	10:11:00	00:06:00	YES
13:41:00	13:50:00	00:09:00	NO
16:23:00	16:28:00	00:05:00	NO
16:50:00	17:03:00	00:13:00	YES

Table 5-3 communication time tabel

The *Table 5-4* highlights that the device interrogates the cloud quite often, this behavior can be considered harmless since in our lab the device is subjected to frequent shut down and start up, while in a domestic/industrial operating condition this won't happen frequently, but only due to faults.

At the end we can add a little reminder that using the "Setpoint" panel we can communicate a whole schedule of multiple successive setpoints and for this very reason they need to be communicated together with a time stamp associated. Conflict between communicated time intervals will invalidate such setpoints. since the cloud is synchronized to the English time zone, the timestamp in the status window is displayed according to the UTC time zone.

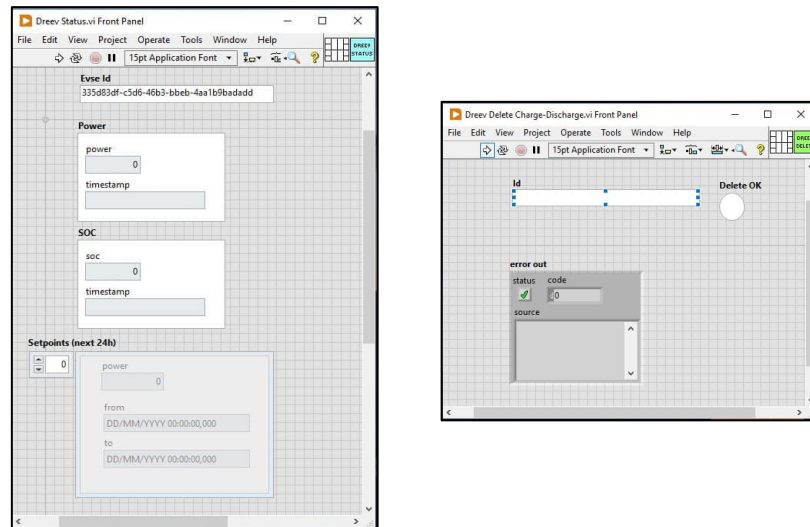


Figure 5-7 LabVIEW STATUS panel (left) DELETE (right)

To delete a current or a future setpoint, simply use the LabView project DELETE. The executed command coupled with the ID of the desired setpoint will delete that command from the WB schedule. If the setpoint ID is not specified, the current setpoint or the one closest to execution will be deleted.

5.4 Operative limits of the DUT: choice of the decision variables

Starting from the data provided by the manufacturer, it is possible to establish the limits of operability within which to proceed to test the DUT.

The operating limits from the WB point of view can be assigned to 2 main categories made up of 4 elements: on one hand there are the external variables like the minimum and maximum SoC and the minimum and maximum supply voltage; on the other hand, there are the internal variables like the minimum and maximum output power and the working temperature range. The latter characteristic named is the most important one for the scope of this thesis work.

In terms of the SoC, the first limit is ascribed at the V2G mode: if during a discharge the percentage reaches the 35%, the discharging process is automatically stopped. If a further discharge is requested via API at this point, the wall box does not respond to the command. This limitation did not have any impact on the tests performed, as the effect of the percentage of battery charge on charge and discharge performance has been addressed in previous work and the results would be redundant. However, in order to have a comparison with the results previously obtained, two SoCs were considered.

- SoC=50%
- SoC=80%

The second external variable introduced is linked with the supply conditions of the WB. The voltages are fed directly from the PA for its precision in reproducing waveforms and it

is known that the voltage level is a parameter that could influence the behavior of the DUT. To have a complete control over this parameter, it is crucial to operate using a controllable voltage source such as the linear power amplifier. Relying on the voltage fed by the distribution network could introduce an unacceptable degree of randomness to the results.

According to the datasheet the operating limits would be a phase-to-neutral minimum voltage of 198V and a maximum one of 254V. For safety reasons, these values have been shifted toward the nominal value. In summary, the values for the voltage between phase and neutral applied across PA are 200 V, 230 V, and 250 V, respectively.

The power limitations are taken straightforward from the datasheet: the WB presents a minimum power threshold of 3 kW both in charge and discharge. Every power setpoint lower than 3 kW (absolute value) is automatically raised up to such value. The setpoints are then organized as follows: with step of 2kW between one and the other, 5 setpoints have been derived for both charge and discharge: 3kW, 5kW, 7kW, 9kW and 10kW. These values refer to the AC side in both operating configurations. Originally, the maximum set point that could be served by WB was 11 kW; it was lowered to 10 kW, as with V2G, because undefined problems made it impossible to operate at maximum charging power during testing.

This technical limitation did not particularly affect the results, since the thermal effect associated with the single additional kilowatt of power supply (AC in G2V) would not have had a significant impact in order to change the conclusions drawn.

As mentioned above, the aspect of greatest interest in performing the intended tests is the working temperature. The information provided by the supplier is general in its nature, as the data sheet indicates that the instrument operates at an ambient temperature between -25°C and +50°C. The provider then mentions an unspecified power derating from 40°C without describing the behaviour at -25°C in more detail. The WB is therefore expected to behave according to standards within the specified range, with particular attention to behaviour at temperatures above 40°C. In *Table 5-4* are listed then the variability range of the thermal level during tests.

T_{min}	-20°C
T_{nom}	RT (20°C)
T_{max}	+40°C
T_{derating}	>45°C

Table 5-4 WB temperature specifications from datasheet

These considered variables fall within the horizon provided by the possibility of bidirectional power flow between EV and distribution grid. Therefore, this pool of different conditions is doubled due to the possibility of operating both in V2G and G2V.

Within these selected temperature range, the other influencing parameters will be made to vary in succession. The total of the performance tests will consist of 180 observations, 90 for each operating mode (V2G and G2V) from which the results obtained for the two SoCs considered, the 5 power setpoints at the 3 different supply voltages, branch out. This wide field of observation can help the analysis to be complete and comprehensive of the performance's trends to be able to create maps in which visualize the relationship between the parameters of interest.

An additional note can be added at the SoC level.

There are two different SoCs that are communicated during the test that can be examined. Although this is not a fundamental variable, it is fair to consider it. The first SoC available is the actual SoC, which is the physical percentage of the state of charge of the battery itself. For security reasons, this percentage is not the one transmitted through the electric vehicle's diagnostic system and through the wallbox's cloud. This second SoC value is defined as the "state of charge indicator" and is transmitted to the WB's API every 10 seconds.

Since this second SoC value is the one communicated to the end user, the tests are based on this value. The "display" value is calibrated in such way that it communicates a slightly lower value when the state of charge is low and a slightly higher value when the maximum capacity of the battery is approaching. The reason for this decision is that we do not want to tempt the end user to over-discharge the battery or, on the contrary, to charge it beyond a certain threshold (95%), because such extreme use risks damaging the component itself. This logistic decision is an intelligent way to limit the depth of discharge of the EES system in order to extend its useful life without reducing the capacity to 80% of the nominal value.

The chosen variables are summed up in the *Table 5-5*:

VARIABLE	UNITS	VALUES
<i>Temperature</i>	°C	-20, RT (20), 40
<i>AC Voltage</i>	V	200, 230, 250
<i>Power</i>	kW	3, 5, 7, 9, 10
<i>Working mode</i>	-	G2V, V2G
<i>SoC</i>	% Full capacity	50, 80

Table 5-5 list of decision variables

5.5 Data acquisition and processing

The DAQ (by HBM) was used to measure, monitor, record, and analyze the electrical quantities. In this section, the software viewpoint is explained.

The user interacts with the DAQ through the proprietary software Perception installed in the central console for remote control of the quantities registered. The software allows the

measured waveforms and electrical signals to be visualized in real time. The signals from the thermocouple or current probes are all analog voltage signals that are transmitted to the acquisition board via suitably insulated BNC cables. These signals are then transmitted in digital form to the software, which can analyze them by implementing real-time formulas or processing the entire signal over a defined period.

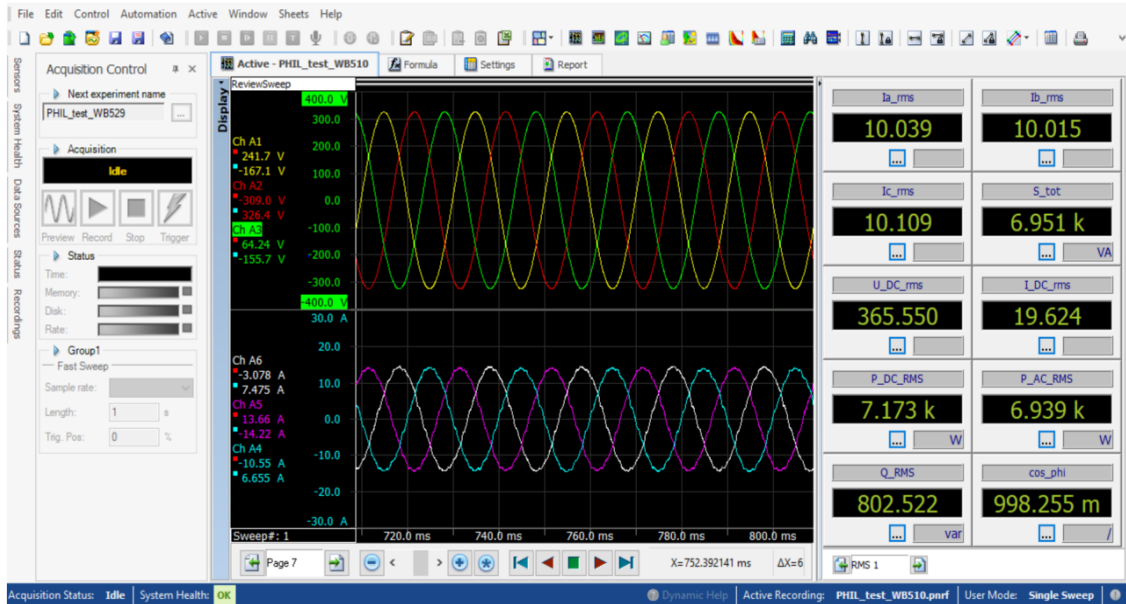


Figure 5-8 Perception software panel

The DAQ is characterized by two recorders (A and B) with 6 input channels each. By counting all the currents, the voltages and the signal of the thermocouple, the occupied channels are 9 which are divided between the two different recorders.

Different acquisition setups were created as different types of experiences were conducted simultaneously on the Officine Edison laboratory. Each setup was characterized by different measurement devices that were characterized by different acquisition parameters (offset and engineering unit multipliers). These different setups were organized into workbenches. Each acquisition session was named after the experiment performed.

Since the real-time formulas were not used for analytical processing of the results, they are not discussed. Across this study the formulas, called Single Sweeps, were used to calculate the quantities recorded within a given time interval.

The signals not characterized by a periodic function (e.g. the continuous signals of direct current and direct voltage) after their acquisition are processed by an integral for the calculation of the average value, and their value oscillates during the acquisition period, due to the noise of the signal, around their average value. In order to use them in the calculation of the power in a given time interval, the following formula is then used.

$$X = \frac{1}{t_{end} - t_0} \cdot \int_{t_0}^{t_{end}} X(t) \cdot dt$$

If the measurement is instead characterized by a waveform with a specific period and a specific amplitude, the calculation of the average value is useless. If the offset is not erroneous, this method would even result in zero measurements. Therefore, to calculate the rms value of these signals, you must use the rms value (RMS), which is defined as the square root of the mean square.

$$X = \sqrt{\frac{1}{t_{end} - t_0} \cdot \int_{t_0}^{t_{end}} x(t)^2 \cdot dt}$$

For common waveforms such as the pure sine wave, the relationships between the amplitudes (peak-to-peak, peak) and RMS are fixed and known, as they are for any continuous periodic wave. However, this is not true for any waveform that may be neither periodic nor continuous.

The RMS is calculated for all the waveforms acquired.

The calculation of the real power on the AC side passes through an analytical analysis which is slightly different from the other quantities as it depends on its instantaneous value. As a matter of fact, the instantaneous value is first calculated as the sum of the products of the instantaneous values of voltage and current in the three phases.

The electrical quantities in uppercase represent the RMS values, those in lowercase the instantaneous ones

$$p_{AC}(t) = i_R(t) \cdot v_{RN}(t) + i_S(t) \cdot v_{SN}(t) + i_T(t) \cdot v_{TN}(t)$$

This value is then filtered. Finally, the RMS value is applied in order to obtain a value not linked to the time instant.

$$P_{AC,RMS} = I_R \cdot V_{RT} + I_T \cdot V_{TN} + I_S \cdot V_{SN}$$

After this processing we can derive the final parameters of interest for our analysis. The results coming from this analytic elaboration, automatically performed inside Perception, are then saved in logfiles since most of the times we are just interested in the results, not in the waveform shapes.

The structure of the logfiles isn't of any interest so it will be overlooked. The final reference formulas used were:

Apparent Power	S [VA]	$v_{RN} \cdot I_R + v_{SN} \cdot I_S + v_{TN} \cdot I_T$
DC Power	P_{DC} [W]	$U_{DC} \cdot I_{DC}$
Reactive Power	Q [Var]	$\sqrt{S^2 - P_{AC}^2}$
Power factor	$\cos\Phi$	P_{AC}/S
G2V efficiency	η_{G2V}	P_{AC}/P_{DC}
V2G efficiency	η_{V2G}	P_{DC}/P_{AC}
G2V dissipated power	$P_{diss,G2V}$	$P_{AC} \cdot (1 - \eta_{G2V})$
V2G dissipated power	$P_{diss,V2G}$	$P_{DC} \cdot (1 - \eta_{V2G})$

Table 5-6 Single Sweep relevant formulas

Where:

- V_{RN}, I_R = voltage and current phase R;
- V_{SN}, I_S = voltage and current phase S;
- V_{TN}, I_T = voltage and current phase T;
- U_{DC}, I_{DC} = DC side voltage and current.

This argument applies to the analysis of conversion efficiency, but obviously not to the analysis of the harmonic content of the generated currents. In this case, the fundamental parameters will not be the construction of the analysis formulas, but the acquisition frequency and time and the analysis will be subsequently performed not using Perception, but in an external computer environment such as MATLAB. This topic will be discussed in detail later in this chapter in the context of the experimental results obtained.

5.6 Test execution procedure

This procedure represents the temporal succession of the activities aimed at recording and acquiring the parameters of interest.

According to the standards introduced previously, the performance tests must be continued for a minimum duration of 3 consecutive minutes, having to acquire sinusoidal quantities (both in V2G and in G2V) the acquisition frequency must therefore be at least sufficient to represent these sinusoids at the frequency network (50Hz). In order to have data that can also be used for the analysis of harmonic distortion, it will be kept during each test at 200

kSample / sec, when it won't be necessary this kind of accuracy the data will then be downloaded at a lower temporal resolution.

The general initial procedure to conduct the test is described below in steps.

The first step is to turn on the DAQ and prepare the measurement display station:

- connect the USB key with the Perception license
- connect the ethernet cable for digital data communication,
- turn on the software
- select a workbench

Then start connecting the measuring instruments and preparing them for acquisition

- Clamp the DC current probe (on one battery cable underneath the bonnet)
- Set the offset (it is important to carry out this task before connecting the EV since it has been observed a small current flowing inside the conductors even with no setpoints)
- Connect the BNC corresponding to the 3 current images of the PA to the HBM or alternatively clamp the 3 AC current probes

Once the measurement setup is connected and it is possible to verify the proper functioning of them on the oscilloscope; the experiment can begin. The connection and verification procedures will be described.

- Check open state of the switches (protection box)
- Connect the plug of the protection box supply power cable with one socket of the junction box
- Connect the PA to one second socket of the junction box and the additional dissipator to the third. It is not important the order, the power flow will flow according to the voltage difference exerted at the connections

Once the measurement setup is connected and it is possible to verify the proper functioning of them on the oscilloscope; the experiment can begin.

- Control that the EV is unplugged and the WB is connected to interne (for the communication issues introduced before)
- Switch on the power amplifier
- Set the PA using the frontal display.
- Select the coupling mode LVAC (low voltage alternate current) since the PA could also control a DC voltage. It has to control the voltage level, behave as a voltage generator: the current varies according to the power setpoint.
- From the touchscreen display window "Configuration" impose a maximum current of 20A, there are many safety devices that prevent damage to components, but it is also important that the amplifier stops supplying in the event of an overcurrent. After selecting the options, it is needed to press validate button to initialise the parameter
- In case of G2V operations, turn off the additional dissipator before starting the experiment (at maximum power output): the additional current to be fed to the heater will shut down the amplifier since it will feel an overcurrent at its terminals.
- From "Program " window impose the voltage range of interest (270V), the 50 Hz frequency and the sinewave form (it will produce a perfect sinewave). Selecting, then, the voltage level of reference (200V, 230V, 250V) and by checking the output box it can be validated. Now the PA is in operation

- Close the protection box switches. Now the WB will start feeling the voltage and it will be switched on
- Wait until the WB led turns blue
- Plug the CHAdeMO connector into the EV
- Push the WB button
- Verify that the WB led turns green
- Verify that the 7kW won't start (often it will begin for few seconds before stops). If a continuous charge is present the WB is not connected to internet, it must be disconnected from the power source and powered again.
- Verify that the WB feels the DC voltage at the battery's terminal, if the voltage visualized is null, the WB is not connected to the EV even if it is online. It must be disconnected, switched off pressing the button, and switched on after it completes the standby procedure. After it will be correctly connected.
- Verify that all the waveforms (AC and DC voltages and currents) are correctly visualized on Perception
- Set a Temperature level of interest using the chamber display if it is just needed a stable temperature or the editor in case it requires a cycle profile
- Wait the thermal conditioning time
- Send the power setpoint request through the LabView project or the other function (Immediate Charge, SoC schedule) through the app.
- Check if the request has been received correctly.
- As the power flow starts wait for the second conditioning , when the temperature is stable start the recording.

The electric car that was used in the laboratory tests is a Nissan LEAF, whose battery has a capacity of 60.0 kWh.

5.7 Error analysis

This brief section is devoted to the introduction of a short analysis performed to identify the degree of error in the measurement of recorded conversion efficiency. As a matter of fact, different measuring devices were used in the tests, depending on their availability. This is especially true for the measurement of the AC side currents.

During the test campaigns, as mentioned above, we used the measurements recorded through the BNCs, from which the images of the currents reported by the generator PA were derived.

However, these images do not correspond 100% to the actual recorded current signal. Indeed, as indicated in the amplifier data sheet, these current signals have a well-defined percentage error.

During the experiments, further comparative tests were performed with current probes, which are certainly more suitable and accurate in measuring the sinusoidal values of the currents, but certainly more inconvenient when it has to be analyzed large observations amount. As a matter of fact, two types of probes were available in the laboratory, both supplied by the Politecnico.

One was two other two available Hioki probes similar to those used for DC, and the other was two clamp probes: the PICO TA 189 that we show in the figure. These two more accurate measurement method can then be used to correct the acquisitions of the PA images confronting the results.



Figure 5-9 PICO TA 189 clamp on probe

This table shows the relative uncertainties as described in the data sheet. These are percentage values of the nominal measurement recorded. Since the errors have no sign, they are not variances, either positive or negative.

	% Error
Amplifier	1.5%
PICO	1%
Hioki	1%

Table 5-7 errors

The errors can be divided into two macro categories:

- Systematic errors
- Random errors

On the one hand, the former usually have the greatest influence on the quality of the measurement and may be due to errors in instrument calibration or human error in the measurement process. On the other hand, the random errors are fluctuations around the mean value of the measurement, which usually have less influence on the quality of the measurement, but cannot be predicted.

It goes without saying that the first one can be at least partially corrected, while for the latter only an improvement of the instrument itself can have an effect.

It is also necessary to point out how errors, starting from raw measurements, propagate when subjected to mathematical processing. For example, in the studied case of conversion efficiency V2G and G2V, the current measurements from AC are subject to the error of the meter, while the voltage measurements taken directly are subject only to the error of the DAQ (negligible, about 0.02% of the acquisition range).

The currents and voltages are then multiplied together and summed to be reported along with the current and voltage on the DC page, which themselves have been recorded with some relative uncertainty. This equation explicates all this discourse.

$$\eta_{G2V} = \frac{P_{out}}{P_{in}} = \frac{P_{DC}}{P_{AC}} = \frac{U_{DC} \cdot I_{DC} \cdot (1 \pm ERR\%_{hioki})}{\sum_1^3 U_i \cdot I_i \cdot (1 \pm ERR\%_i)} = \frac{U_{DC} \cdot I_{DC} \cdot (1 \pm 1\%)}{\sum_1^3 U_i \cdot I_i \cdot (1 \pm ERR\%_i)}$$

To calculate the propagation of these errors to the calculated quantity, the analysis can ultimately rely on statistical methods (e.g., Monte Carlo) or common sense rules developed as a result of these studies. On this basis, we can define the random error in the efficiency measurement in the different cases by defining an uncertainty around the mean value that is equal to:

- 2.5% uncertainty on the efficiency in case of Amplifier
- 2% using the probes

Since this error oscillates around the real value of the measurement, it must be reported in the analysis for correctness, but it does not affect the observed physical trends, since all the measurements are affected in the same way.

Now it is possible to proceed with the observation of the recorded signal to evaluate the percentage of error that can be corrected, since it is systematic, assuming it is present. To do this we go to analyse the raw signal of the amplifier and probes and try to find the differences.

6 Tests results and processing

This chapter describes each test performed, indicating which standard the test is from, analysing the objective, detailing the procedure and finally looking at the results.

The results are structured as follows: First, the analytical results are presented, shown from time to time in diagrams alongside the measurement setup and the value chosen for the decision variables. Then, the conclusions that can be drawn from the observation of the obtained data are presented. A third section in each paragraph is dedicated to the dissertation of the possible causes of the observed behaviours. Bibliographical searches and previous studies that could point to the trends analysed are accounted for.

6.1 Performance tests: conversion efficiency

The procedure for this test was already discussed starting from the NREL (National Renewable Energy Laboratory) framework.

The purpose here is to calculate the conversion efficiency of the charging station under different operating conditions. Since this is a performance test, there are no specific pass/fail criteria. In addition to characterizing the product, the objective is the statement of peak efficiencies and average values in the various thermal conditions analysed. The operating conditions differ depending on whether the vehicle is charging (G2V) or discharging (V2G) and on different parameters:

- Temperature
- AC supply voltages
- Power setpoint

The performance tests start with setting a temperature condition and reaching the thermal equilibrium, as already described in the proper chapter. The temperatures chosen in this analysis were selected in accordance with the information in the product data sheet and were three: -20 °C, RT (20 °C), and 40 °C. Then the different power setpoints are varied according to the working range. Finally, the AC side voltage value is changed and the efficiencies in all these conditions are calculated. This procedure is followed once for SoC=50% and once for SoC=80%.

The wallbox is supplied with the three voltage values given in the previous chapter, section threshold selection. For the test, the corresponding phase-neutral voltages are specified: 200 V, 230 V, 250 V.

The WB configuration has a 3kW minimum charge and discharge power. Therefore, the power setpoints covering the entire power settings are: 3-5-7-9-10 kW for both G2V and V2G.

Efficiency is calculated for each discrete variation of these three parameters. The power values exchanged by the system with the grid ($P_{AC,G2V}$ and $P_{AC,V2G}$) and the power values (in direct current) exchanged between the column and the battery of the electric vehicle ($P_{DC,V2G}$ and $P_{DC,G2V}$) have been recorded and acquired. A summary scheme (*Figure 6-1*) is proposed to better visualize the quantities involved.

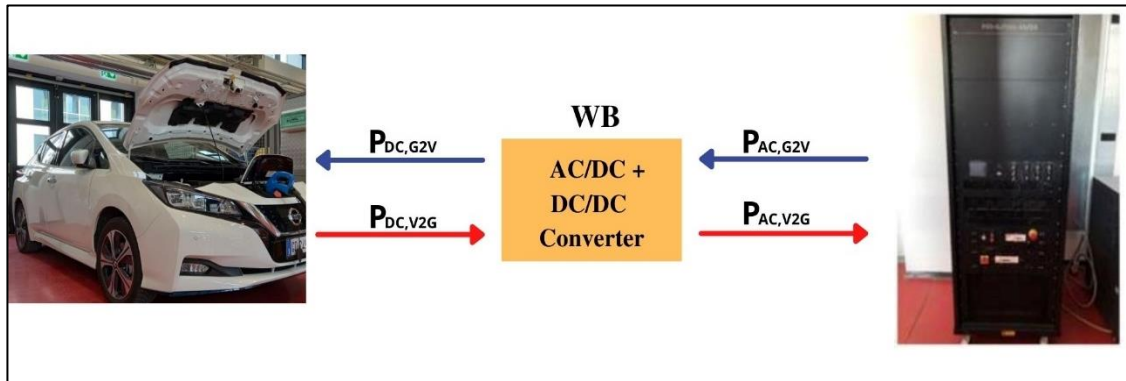


Figure 6-1 conversion efficiency power flow

The P_{AC} are calculated starting from an instantaneous value and deriving the corresponding RMS. The column efficiencies in charging (G2V) and discharging (V2G) modes were also calculated separately using the following formulas:

$$\eta_{WB,G2V} = \frac{P_{DC,G2V}}{P_{AC,G2V}}$$

$$\eta_{WB,G2V} = \frac{P_{AC,V2G}}{P_{DC,V2G}}$$

A fourth variable considered was the SoC, which is closely related to the voltage on the DC side. As mentioned above, only two DC voltage levels (355V, 385V), corresponding to 50% and 80% of SoC, were selected to allow further comparison with previous analytical work. The effect of this parameter is indeed already known: as soon as the SoC increases, the value of the voltage of the battery also increases [48]. This translates into lower current absorbed by it ; therefore, the performance of the battery decreases under stress, leading to a decrease in efficiency for G2V performances.

It is therefore clear that in our analysis the efficiency values will be lower at 80% in G2V than at 50%. With V2G, instead, this relationship is not directly evincible from physics. In this case the performances are mainly due to the constructive choices of the DC/DC converter. This is often a design decision by the manufacturer and the elements available are too scarce to characterize this type of relationship outside the experimental observations.

Since the V2G system should be intended to be used when the vehicle is charged and not in operation, i.e. at $SoC > 80\%$, one might think that the product is adapted to operate with better efficiencies at high voltages.

The individual trends are first analysed, each time highlighting a single variable of interest. Once the highlighted trends are described, the data are processed in their entirety into heat maps, which may include all the behaviours analysed above.

6.1.1 Conversion efficiency at extreme Temperature's regimes

A first result of a general nature about the effect of temperature on efficiency is shown in the *Figure 6-2*. It represents the efficiency in the two operating modes at nominal power, nominal voltage, and a reference SoC..

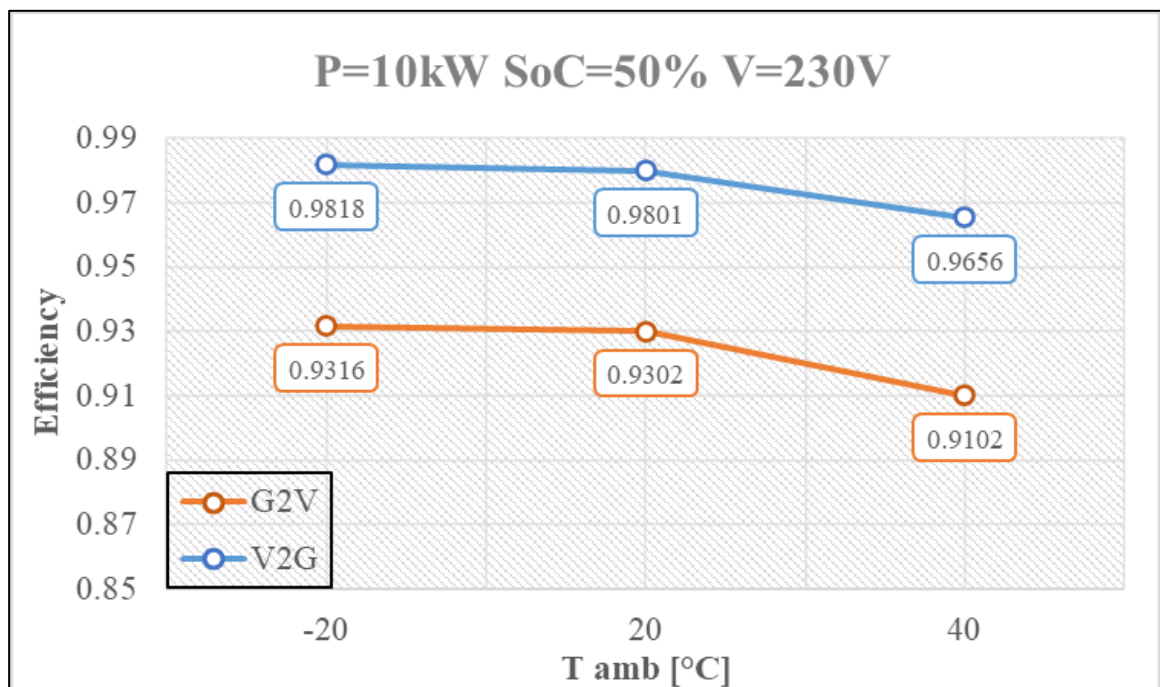


Figure 6-2 efficiency varying ambient Temperature SoC=50%

This result immediately shows a clear trend that is reflected in each of the results analyzed below. The charging behavior of the EES, i.e. G2V, has a much lower efficiency than the corresponding V2G behavior. We cannot explain this trend in detail because this is where the design variables of the device come into play, which are not known. It occurs here for the first time, but it must be considered a trend always present, that the input power in V2G is about 5 percentage points lower than the input power in G2V to produce the same output power in the two configurations.

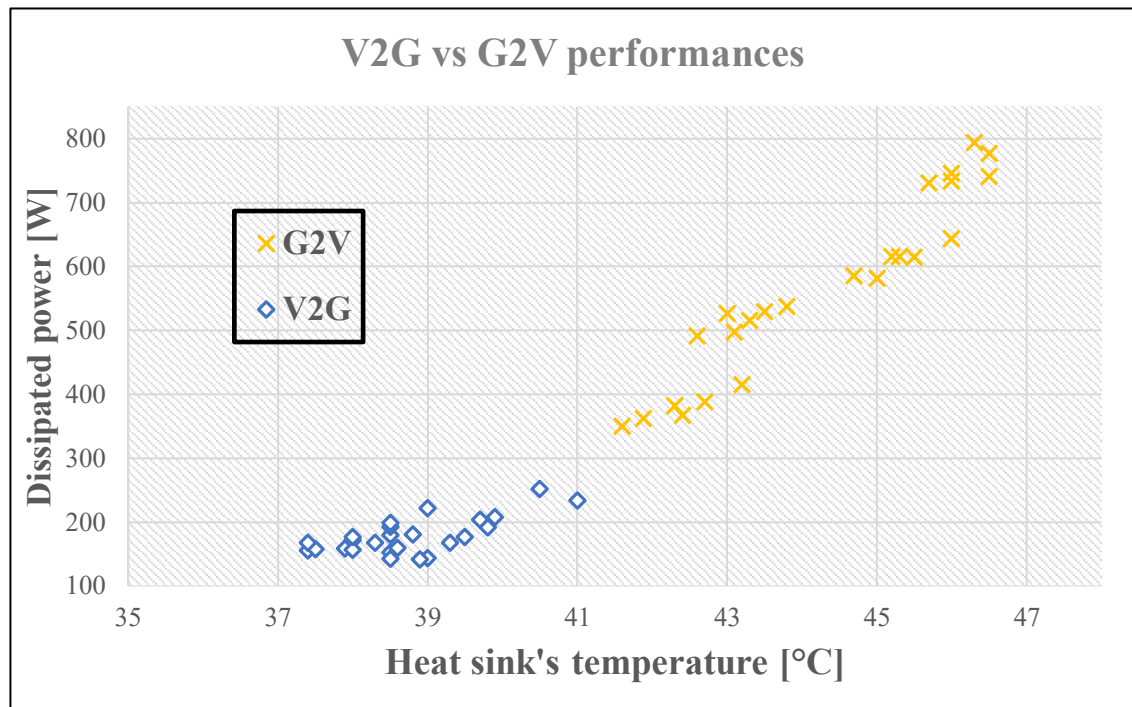


Figure 6-3 Dissipated power vs heat sink's temperature

As can be seen in *Figure 6-3* just proposed, where the dissipation characteristics of the device are related to the ambient temperature of 20°C, there is an important clearly visible difference between the V2G and G2V behavior. Even the data on the dissipated power seem to account for this difference in performances by showing high dissipated powers in G2V, greater than those V2G in any condition considered.

This observation sample relates the temperature on the heat sink and the dissipated power (which are obviously related to each other) in each operating condition recorded at a temperature of 20°C. This therefore means an observation sample of 60 different observed points that differ either by SoC, or by power setpoint or by supply voltage. The power dissipated in G2V is always greater than at V2G even when the power setpoint in G2V is the minimum, while that in V2G is the maximum.

This aspect proves to be even more of substantial importance in the next paragraph, in which it will be observed how the efficiency of the product increases (and therefore the losses decrease a lot) as the power delivered increases.

Furthermore, the result of this first analysis is quite clear with regards to the influence of temperature. A small effect is noted between -20°C and 20°C, while an increasingly consistent effect is felt up to 40°C, where a minimum in the efficiency is manifested. So, the trend is not linear; but there is a quadratic dependence with temperature above RT.

This temperature effect is what most interested the analysis carried out. It is presented here as the first result, as it constitutes the background for all the other trends related to the power set point, the voltage level leading to the creation of the heat maps.

An analysis section is dedicated to the literature review on this topic. Indeed, the bibliographic research [22, 32] seems to diverge from this observed data. Indeed, the studies carried out so far on monodirectional fast chargers have always shown a drastic drop in conversion efficiency in low temperatures regimes [32]. Indeed, it is well known that EVs are subjected to high stress at low temperatures, reducing their performances.

Cold temperatures can significantly degrade the charging speed and increase the charging time, which could make it challenging to operate EVs in northern regions. Temperature dependency of the charging process and power consumption, especially the effects of low temperatures, have been shown to affect the performance of electric cars in several ways.

The authors in reference [32] note that the charge capacity decreases at negative temperatures as the internal resistance of the battery increases, causing the maximum voltage to be reached earlier. To protect the battery, a higher voltage cannot be applied, as this would lead to a reduction in current, which would increase the charging time. The same phenomenon occurs when an electric vehicle is driven. The minimum voltage is reached earlier, the current drawn from the battery has to be reduced, weakening the acceleration capability. Furthermore, at higher temperatures ($>+40$ °C), no adverse impacts in systems with EVSE and battery are observed [32], both for charging and discharging, since the internal resistance decreases further [18][20].

This casts doubt on the data obtained, but at this point it must be emphasized once again that these reference studies were all carried out by thermally conditioning the vehicle and thus the battery as well as the converter under investigation. Therefore, the performances and trends obtained in these studies include both effects and influences. As a matter of fact, they are not characteristic just of the behavior of the converter.

For this reason, if the study excludes the battery conditioning as in this work, it will clearly get different results. It is equally clear how the conclusions drawn in these reference studies refer extensively to the effects of low temperatures on the batteries and not to the WBs of the study.

Given this bibliographic analysis and once the contributions of the non-ideality are understood, their dependence on the temperature can be studied and analyzed.

6.1.1.1 Losses dependance on Temperature

In power electronics systems the management of power loss and temperature of switching devices is indispensable for the reliability of the whole system. The aim of this chapter is to provide an analytical description of the power losses in MOSFET-based power electronics converters used in automotive applications. Power losses (P_l) in any component operating in the switch-mode can be divided in three groups [40]:

- Conduction losses (P_c)
- Switching losses (P_{sw})
- Blocking (leakage) losses (P_b) normally being neglected

Therefore: $P_{loss} = P_c + P_{sw} + P_b = P_c + P_{sw}$

- **Conduction losses**

A load switch has some inherent resistance, which causes power to be dissipated when there is a load current. The power is dissipated as heat energy from the silicon chip to the housing, the circuit board and the ambient air. The heat energy increases the temperature of the silicon chip (junction temperature) and changes the performance of the device.

Conduction losses in power MOSFETs can be calculated using an approximation using the drain-source on-resistance's value $R_{ds(on)}$ [39].

U_{DS} and i_D are the drain-source voltage and drain current, respectively. The typical $R_{ds(on)}$ can be read from the datasheet diagram supplied by the provider, where I_D is the inrush current of the MOSFET that is defined by the application. The relationship between these two parameters is the basis of the MOSFET conduction principle and can be expressed as follows [39] [40].

$$u_{DS}(i_D) = R_{DS,on}(i_D) \cdot i_D$$

Therefore the instantaneous value of the conduction losses :

$$p_c(t) = R_{DS,on}(i_D) \cdot i_D^2(t)$$

The $R_{ds(on)}$ of a power MOSFET is the most sensitive parameter with respect to temperature. Consequently, the power dissipation of the power MOSFET will also be sensitive to the temperature[38]. Looking at most of producer's datasheet the thermal behaviour of the $R_{ds(on)}$ resistance can be expressed in one equation in absolute terms which therefore depends on a reference resistance value at a given standard condition (25°C) [38].

$$R_{DS,on}(T_j) = R_{DS,on,max}(25^\circ C) \cdot \left(1 + \frac{\alpha}{100}\right)^{T_j - 25^\circ C}$$

Where T_j is the junction temperature and $R_{DS,on,max}(25^\circ C)$ is the maximum value of R_{DSon} at 25°C, which can be read from the product summary table in the data-sheet.

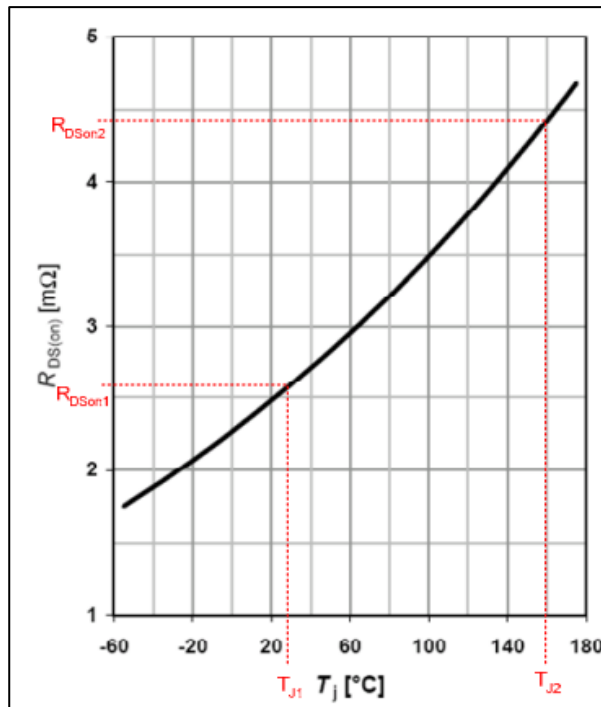


Figure 6-4 Temperature effect on conduction resistance in MOSFET

The conduction loss has a positive temperature coefficient and rise exponentially as the junction temperature increases voltage supply effect on the conversion efficiency (both G2V and V2G).

- **Switching losses**

MOSFET switching losses are a function of load current and the power supply's switching frequency.

$$P_s \propto V_{in} \cdot I_{out} \cdot f_{sw}$$

Unlike the positive temperature coefficient of a conduction loss, the switching loss has no fixed tendency to temperature and changes little in magnitude. Compared to the large fluctuations of conduction loss, it is no better than a constant.

These considerations do not only apply to MOSFETs, but can also be applied to other types of switching components such as diodes. Here we have only dealt with the influence of temperature on these parameters and have left out the physics behind the components, as it is not the focus of interest.

Thus, since the switching losses do not depend strongly on the junction temperature T_j , while the conduction losses have a quadratic dependence, we can see how the total losses in these components increase with the temperature applied to them.

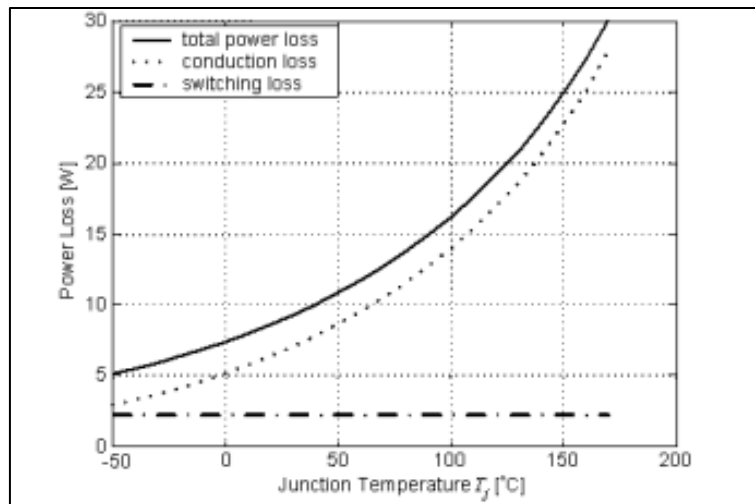


Figure 6-5 Temperature effect on MOSFET's power losses [37]

Using the example of the study on MOSFETs cited in the bibliography [37], can be seen how this diagram (*figure 6-5*) explain this dependence.

In addition, the fact that there is a strong quadratic relationship between the temperature of the components and the power losses, also explains the quadratic relationship we found in our data on the conversion efficiency.

The collected data therefore possess this trend, the efficiency tends to decrease significantly after exceeding 30°C reaching a minimum at 40°C which is defined as the maximum operating temperature of the WB. As can be seen from the following plots, this trend is present regardless of the selected power level, the mode of use (V2G or G2V) or the voltage level at which the DUT is powered.

In the following plots, the efficiency trend depending on temperature is expressed in all different conditions analyzed. The trend remains constant regardless of the conditions adopted.

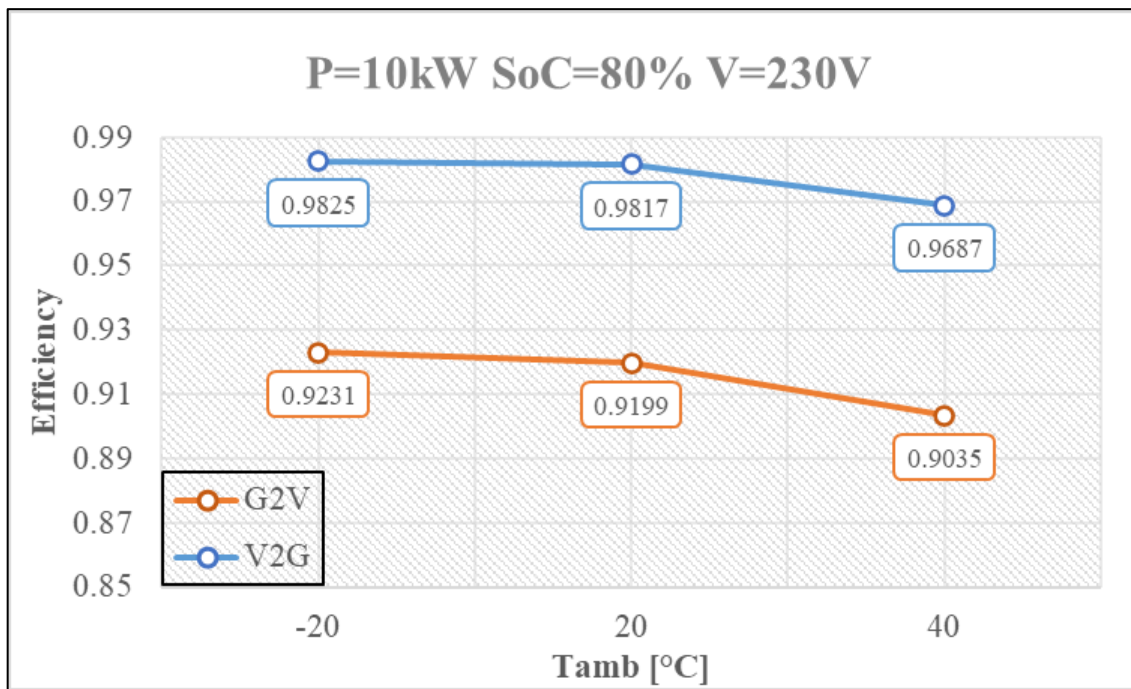


Figure 6-6 Efficiency vs ambient temperature SoC=80%

This plot (*Figure 6-6*) takes up the trend already highlighted in the first plot dedicated to the effects of temperature on conversion efficiency. However, it focuses on the effect of the other SoC setpoint analyzed.

Also in this case the trend is confirmed and the relationship between the G2V and V2G data is also similar. It remains clear that the conversion efficiency is higher when the battery is discharged rather than when it is charged.

This can be an effect given by the battery itself and its charge transfer resistance which can be higher in charge than in discharge. Or it may be an effect of the physical power conversion within the WB. On this point it is not possible to make assumptions based on one fact rather than another and therefore it remains unanswered as a question

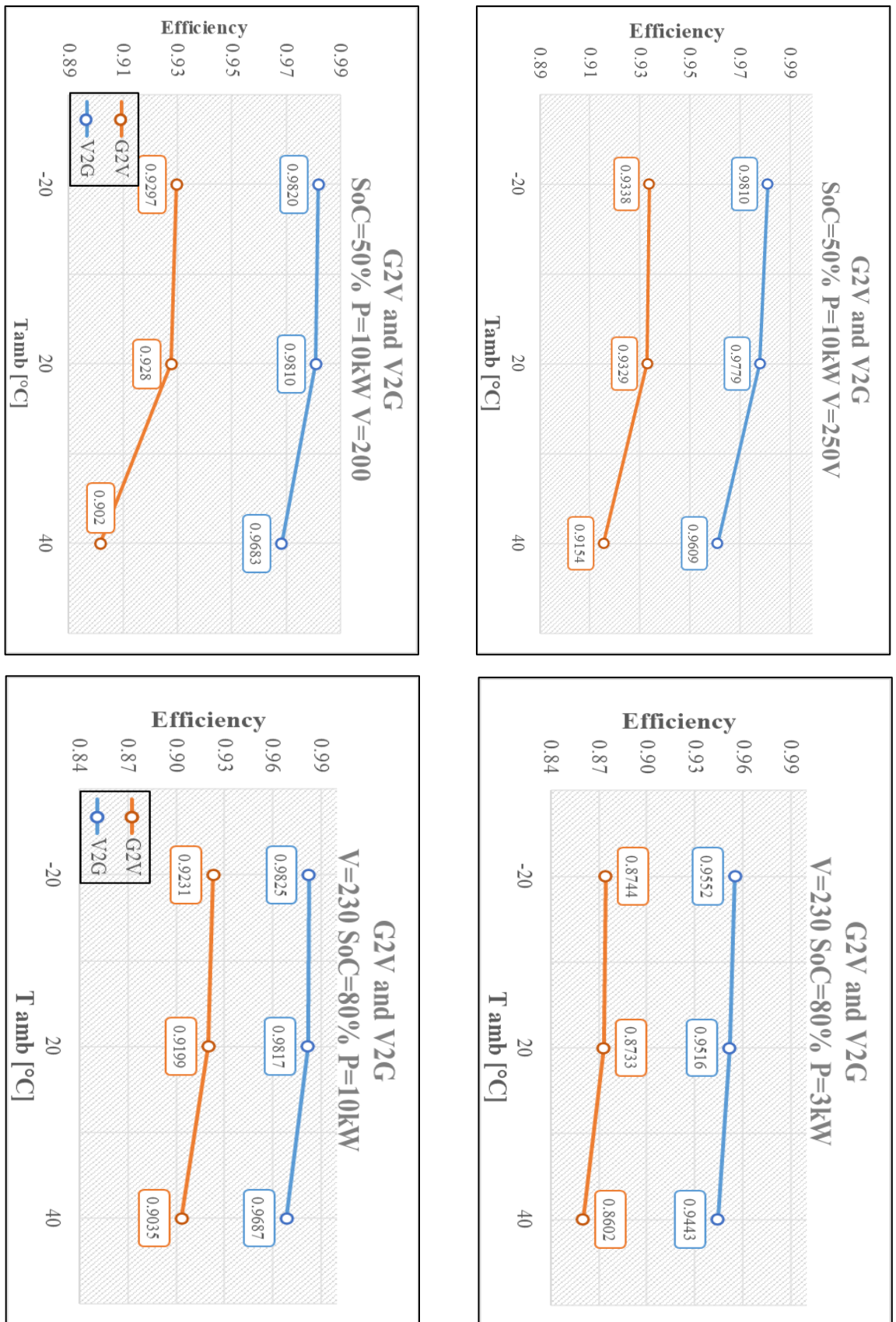


Figure 6-7 additional graphs on temperature effect over conversion efficiency

An additional parameter that can fully summarize the behavior of the WB and its dependence on temperature is represented by the average efficiency and peak efficiency.

Namely the peak efficiency as the maximum efficiency recorded at the nominal power, while the nominal average efficiency is calculated as the average of the values recorded when the wallbox is working at the nominal power.

Nominal average efficiency:

Operating mode	-20°C	20°C	40°C
G2V	0.9281	0.9208	0.9008
V2G	0.9845	0.9813	0.9657

Table 6-1 average conversion efficiencies

With a difference of 2.73% for G2V and 1.85% in V2G.

The peak efficiency:

Operating mode	-20°C	20°C	40°C
G2V	0.9342	0.9329	0.9118
V2G	0.9855	0.9827	0.9699

Table 6-2 peak conversion efficiencies

In this case the difference in G2V is 1.96% and 1.57% in V2G.

Both these results show an higher temperature effect in G2V, this is mainly due to the higher power dissipated when operating in G2V. As shown in the figure above, higher power dissipated is always present in G2V, this leads to a higher temperature of the heat sink and of the WB. This brings the temperature of the components inside the wallbox to feel a higher effect of the temperature level over the performances in the conversion efficiency.

6.1.2 Power setpoint effect on the conversion efficiency (G2V and V2G)

In this section the efficiency is compared for different power setpoints, to see the effect of this parameter on the performances.

The power setpoint is one of the most important factors for the efficiency of the WB. This is a common feature in AC/DC converters, as it was reported in the chapter relative to the experimental layout, inside the WB section [34][35][36]. Even in photovoltaics this behaviour is well known; this effect has been widely studied in unidirectional chargers, where the AC/DC step in the conversion process is the main one. Using the bidirectional WB for both V2G and G2V, an increase in efficiency is observed at each supply voltage and operating temperature as the applied power increases.

This increase in the performances related to a higher power has a plateau until the nominal power. Around the maximum power, the increase in efficiency is much less pronounced for both V2G and G2V. The plots are referred to SoC=80% as a much more significant working condition in the framework of this study of V2G potentiality.

The first two plots have G2V and V2G operation separated to highlight the impact of the power setpoint and better visualize the trend described above. This trend is then turn in all the decision-making variables.

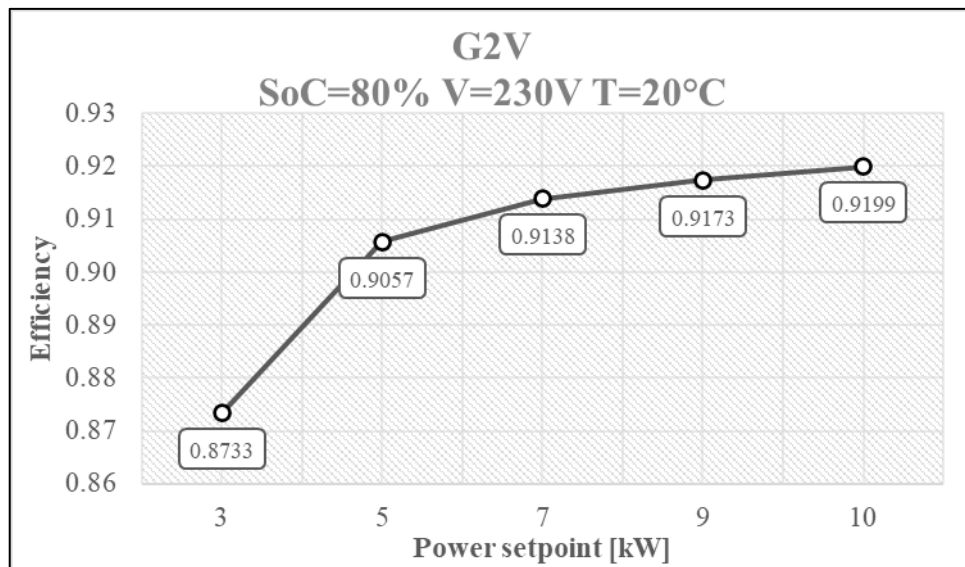


Figure 6-8 G2V power setpoint effect over conversion efficiency

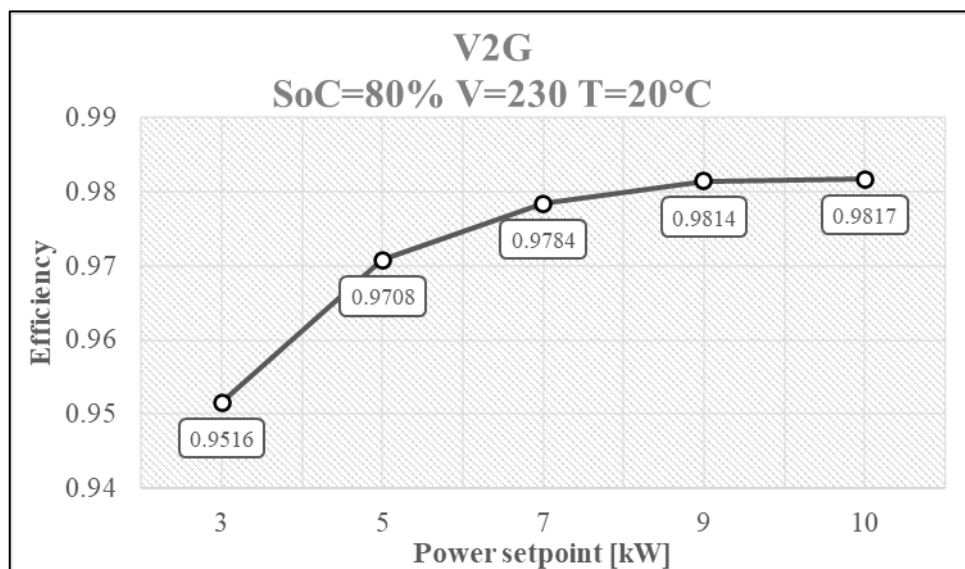


Figure 6-9 V2G power setpoint effect over conversion efficiency

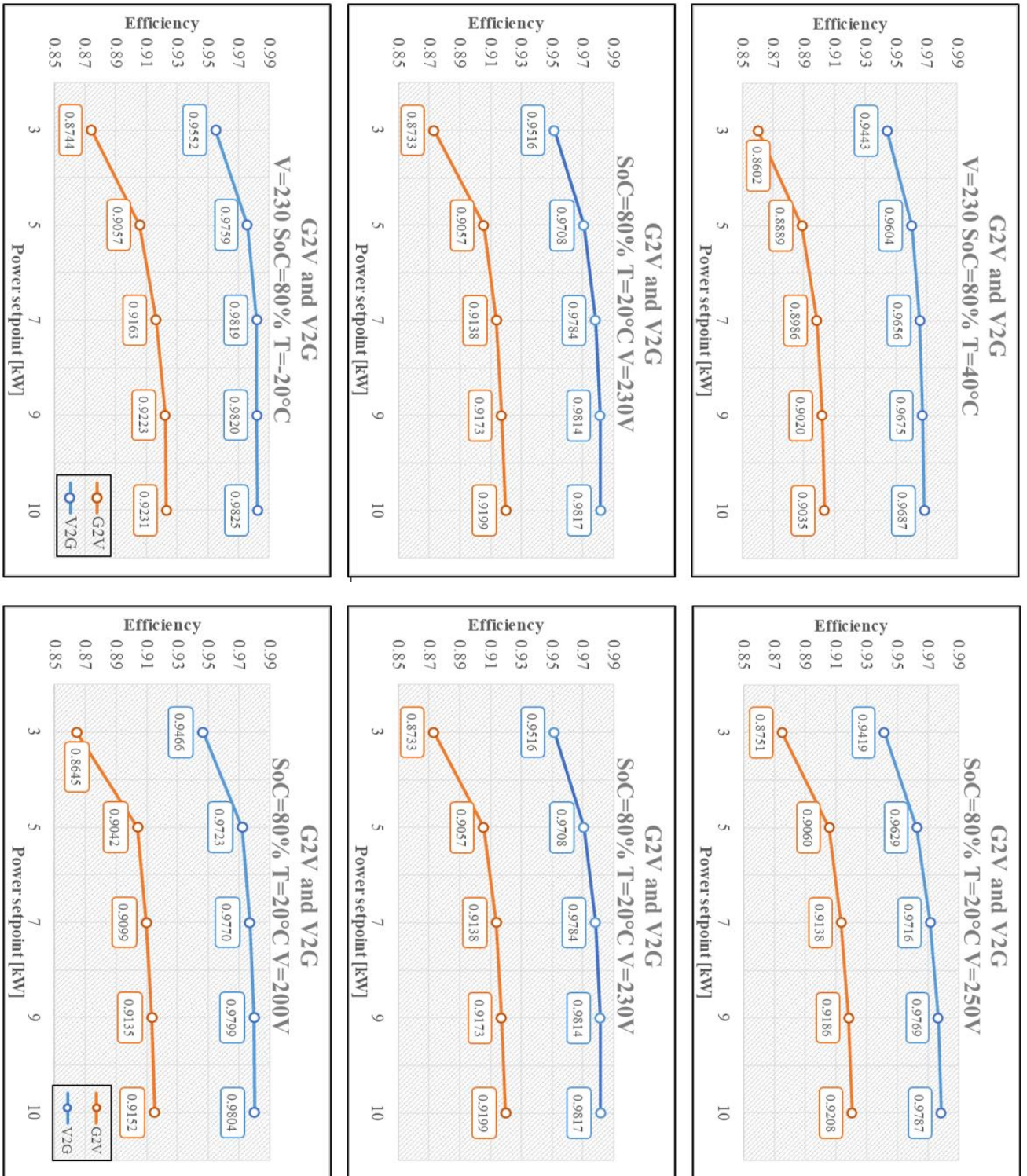


Figure 6-10 power setpoint effect over efficiency varying all decision variables

6.1.3 Voltage supply effect on the conversion efficiency (G2V and V2G)

The value of the supply voltage to which the WB is connected can have different effects on its performance. The following graphs offer an overview of the effect of this parameter on the results obtained.

This behaviour with varying voltages has been shown here at the power of 10kW. For sake of simplicity only the 80% of SoC is considered in both the operating modes. The effect of Temperature and AC side voltages is highlighted.

The trends to the other complementary values of the variables are to be considered similar, although their representation would become redundant and confusing in a single graph, therefore a graph is presented for each condition, G2V or V2G.

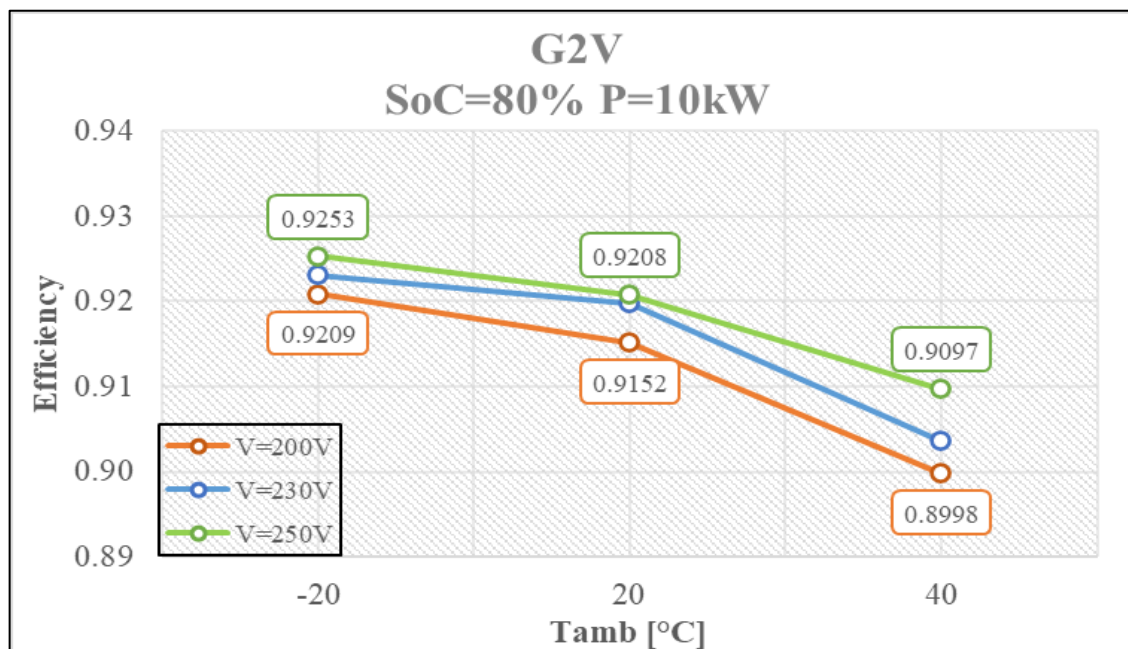


Figure 6-11 G2V AC voltage effect over conversion efficiency SoC=80%

Changing SoC does not change the present trend at 80%. It always appears that when the WB works at high voltages it has better performance, regardless of the temperature or the state of charge of the battery.

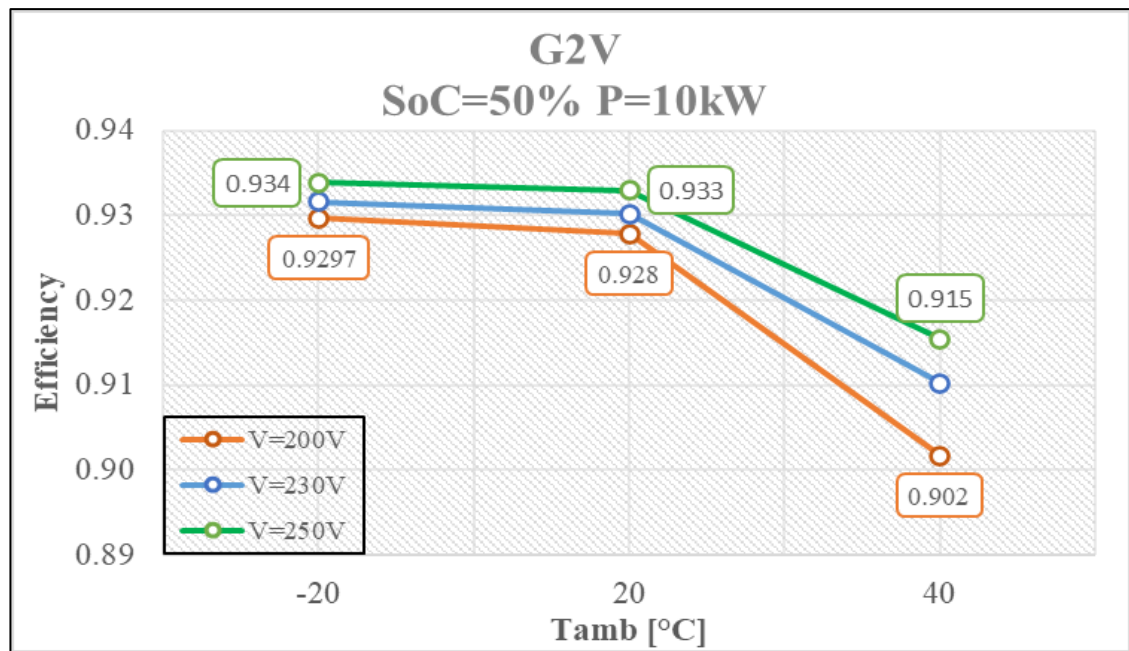


Figure 6-12 G2V AC voltages effect over conversion efficiency SoC=50%

Starting from the operation in G2V it can be seen how the efficiency increases significantly as the voltage on the AC side increases. There can be two reasons.

On one hand, the relative value of the harmonic currents generated by the device may become more significant reducing the voltages RMS, resulting in a higher distortion of the signal, which may be translated into lower efficiency. This effect is studied in the section on power quality, but it does not seem to be particularly relevant as the THDi value does not change significantly when the voltages on the AC side vary in its magnitude.

On the other hand, the voltage value can affect the current conduction within the components of WB by increasing or decreasing the Joule dispersion effect exerted on the internal resistances of the conductors themselves.

The Joule effect, also called Joule's law, is the thermal manifestation of electrical resistance. It states that the heat generated by the current flowing through a conductor is proportional to the electrical resistance, the current intensity squared and the time.

Heat inside the system under study is considered as a loss: the heat flow generated inside the wallbox is power not delivered to the battery (G2V) or to the grid (V2G). The voltage has an effect on this behavior, since: with the same power setpoint, increasing the voltage level at the WB terminals decreases the current flow, therefore with quadratic dependence the power lost as heat flow decreases. As a result, the efficiency will decrease when the flowing currents increase, therefore when voltages decrease.

The same effect acts when the WB is working in V2G, but the results obtained are quite different, in the following plots we report this effect.

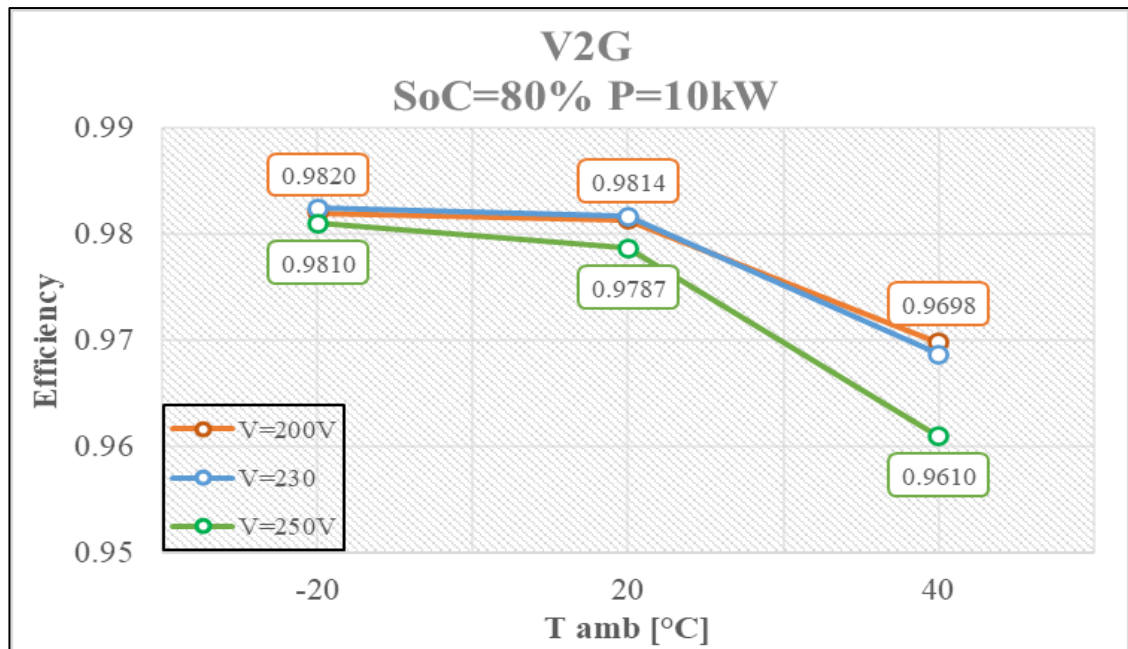


Figure 6-13 V2G Temperature effect on conversion efficiencies, voltage comparison SoC=80%

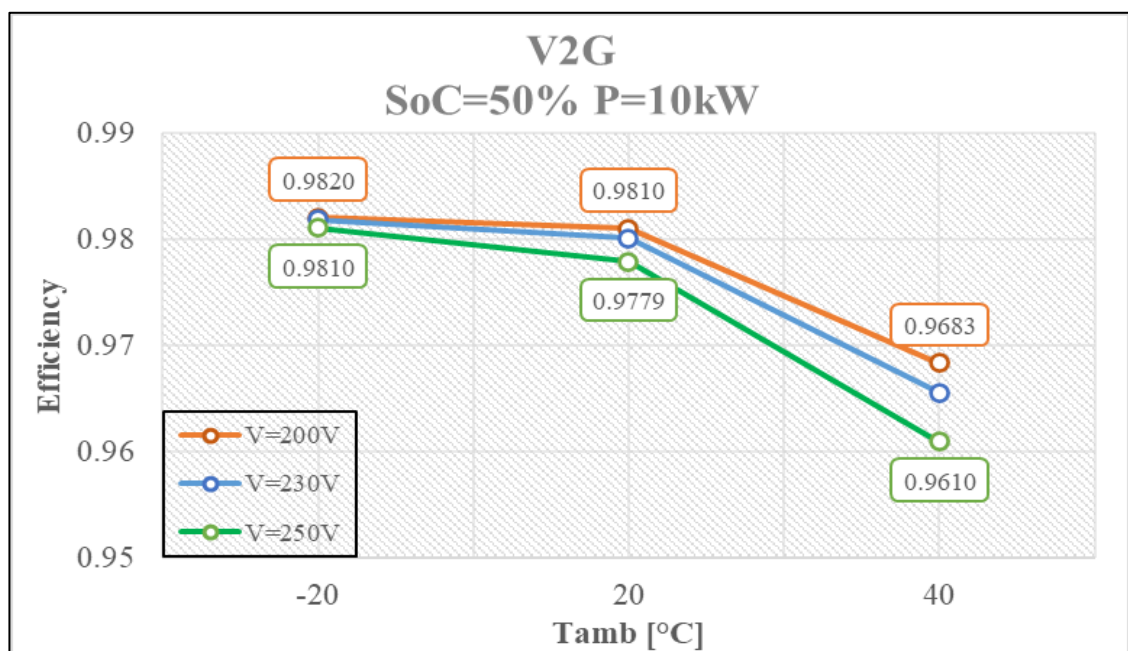


Figure 6-14 V2G temperature effect over conversion efficiency different voltages SoC=50%

In this last section dealing with the behaviour of WB as a function of the tension on the AC side, it can be accounted for this difference of trends. A possible explanation is here presented, although it immediately become clear how much this opinion is questionable. It has not been possible to carry out specific tests to verify this behaviour, so it cannot be established with certainty that the trend highlighted by the experimental campaign can be explained by this.

When the WB works in V2G, from the point of view of the network it behaves like a real voltage generator that must go to apply a prevailing voltage compared to that of the network to impose a flow of current from the WB (therefore from the battery) to the grid.

As it can be seen in *Figure 6-15*, it must happen that $U_{WB} > U_L$.

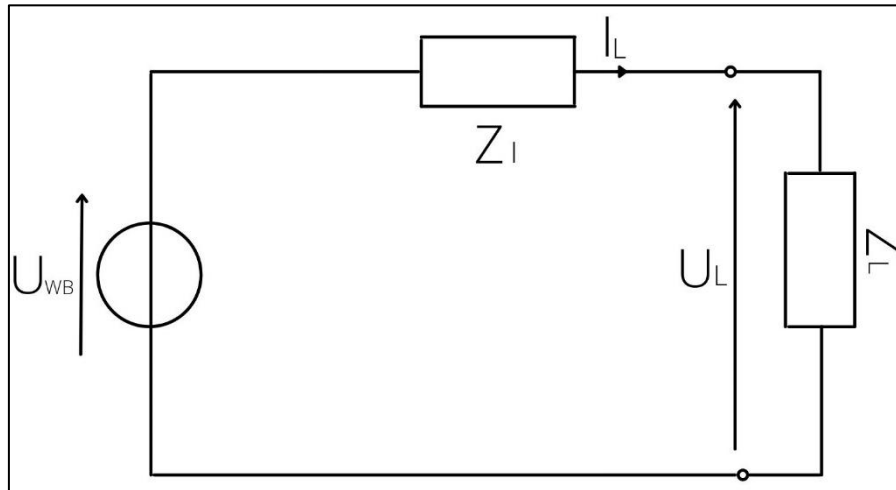


Figure 6-15 V2G real voltage generator scheme

This behavior can lead the WB to work outside its operational limits. As a matter of fact, when we go to exploit the device in V2G (having the WB a maximum p-n voltage of 255V from the datasheet) it is not possible to apply exactly 250V on the grid side for each power setpoint.

What has been noticed is that for powers above 5kW, so in order to work at 9 or 10kW, the voltage must decrease by some volts to allow the WB to work. If you try to exercise 10kW at 250V the WB goes into standby mode and cannot be operated. The voltage operative limits can then be stated as follows:

- $V < 255V$ for $P_{AC} < 5kW$
- $V < 248V$ for $5kW < P_{AC} < 7kW$
- $V < 245V$ for $P_v > 7kW$

This behavior does not pose great technical limits as the voltage difference that must be considered is minimal and not very influential. However, this may suggest that although in V2G there is also a decrease in losses due to the Joule effect when it operates at high voltages; this effect, is balanced by the fact that by operating at these voltages the WB approaches the operating limits of the connection in terms of voltages that the DUT itself must exert. Therefore, approaching the limits of its field of correct operation, it may be that efficiency and performance in general are affected.

This also seems to suggest the fact that this effect is much less marked than the effect of the voltage increase in G2V and it also appears that between 200 and 230V this difference is

almost negligible. In these two cases, as a matter of fact, the WB will work in both situations in its standard range of use, creating a less marked dependence

6.1.4 Heat maps of WallBox Performances

The sample of 180 observations is analysed according to its individual trends among the variables and how they affect the conversion efficiency as discussed in the previous paragraphs. Subsequently it was converted into a 3D MATLAB file to discuss the cross-dependence of the efficiency from temperature, power and voltage.

Each heatmap takes into consideration only one SoC, being the least important variable in the thesis study, which for the occasion is selected the one at 80% being much more significant for the V2G operation compared to 50%.

For the variability with the voltages, the three levels already described are taken (200V 230V 250V) at the nominal temperature (20°C); in the same way, the nominal voltage is considered for the variability with respect to the power.

In this way, the points of the heatmap related to conversion efficiency variability with voltage, power and temperature are 15 for each operating condition

Using a practical MATLAB tool these observational benchmarks are transformed into surfaces through a simple interpolation between the various observed points. The maps then plotted.

In the second set of heatmaps the trend described in the paragraph dedicated to the impact of the supply voltage on the conversion efficiencies is evident. This divergence between the trends found in G2V compared to those found in V2G is highlighted even more. The variation of the power in conjunction with the variation of the voltage does not appear to have a significant impact on the trends highlighted. The trends seem to be respected at each chosen power setpoint.

The first set of heatmaps instead brings with it further information than those found with the variation of the single parameter, which in turn are respected.

This cross-relation is analysed in detail after the figures.

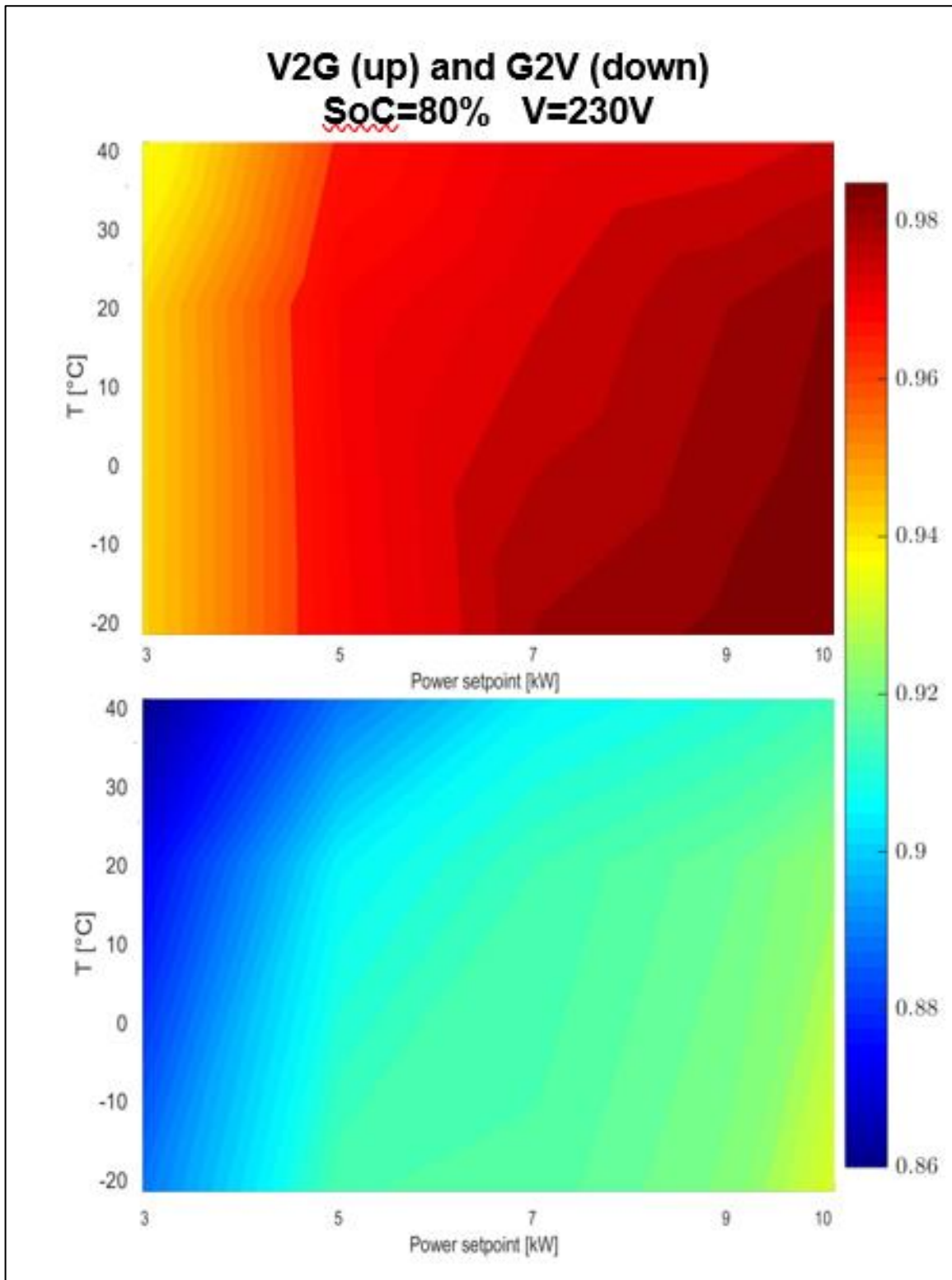


Figure 6-16 Heatmaps, WB conversion efficiency at different temperatures and setpoints

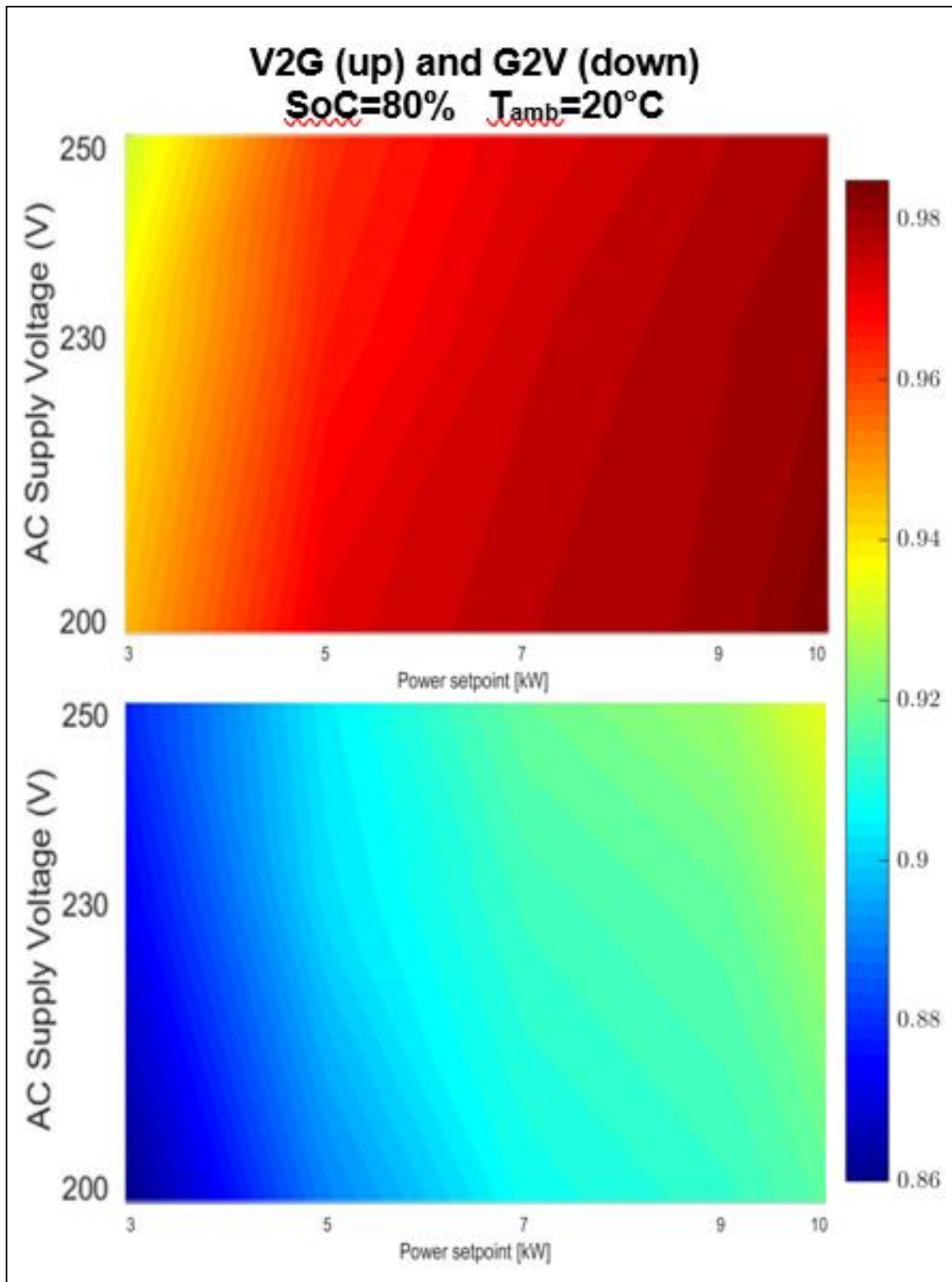


Figure 6-17 Heatmaps of efficiency varying AC voltage and power setpoint

The cross-trend concerns the interdependence between the effect of the high ambient temperature combined with that of the power setpoint.

The effect of temperature on the performance of the device is even more accentuated the higher the power setpoint at which the WB operates.

This can be seen from the diagonal trend; the efficiency of the DUT increases starting from a minimum in the upper left corner (high temperatures, low power) to a maximum in the lower right (high power, low temperatures). This diagonal trend presents de facto a greater inclination the greater the power at which it is observed.

A third note can be added regarding the difference in this cross-trend between G2V and V2G. In G2V it is in fact more prevalent and influential on the performances of the WB. The reason for this interdependence between the two variables lies in the dissipated power. In fact, taking up the results on efficiency in relation to the power setpoint, the efficiency drastically increases the greater the power processed by the WB.

However, as can be seen in the following figure, this does not lead to a stable dissipated power, on the contrary this increases up to the plateau highlighted as for the efficiencies.

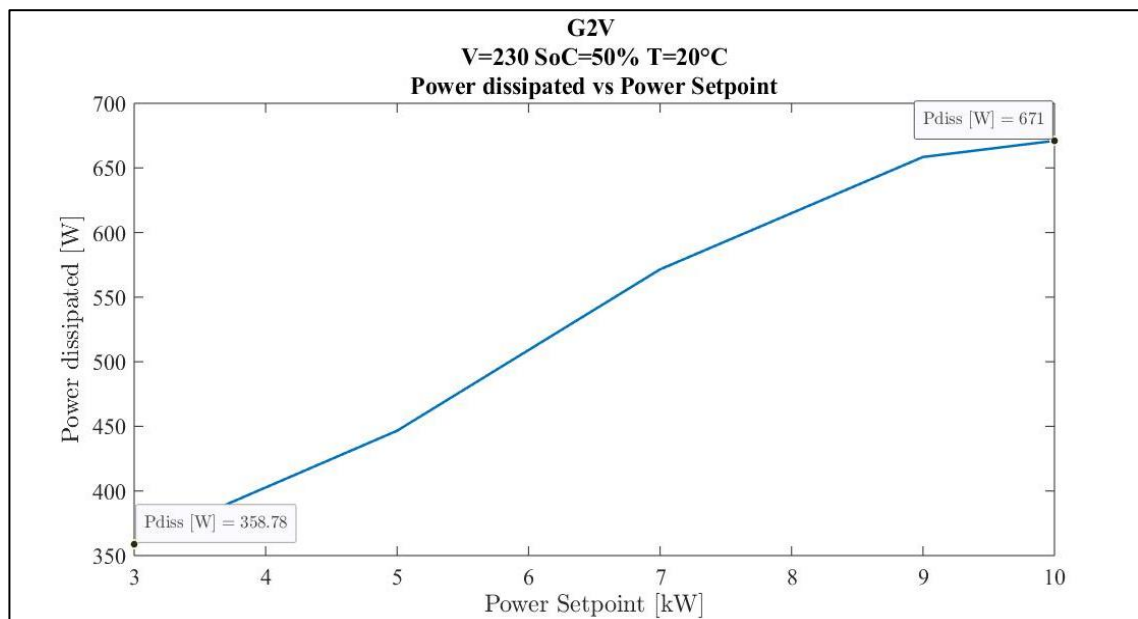


Figure 6-18 Power dissipated in G2V according to power setpoint

The increase in power dissipation leads to a direct increase in temperature, which occurs at the component itself. This relationship can be seen in the graph that relates the power dissipation and the temperature of the heat sink. As the temperature increases, the negative effect that the temperature has on the performance of the wallbox becomes even more present. The result is a trend that becomes even more effective during the transition from minimum to maximum operating power.

6.2 Derating

Derating is the operation of a device at less than its maximum capability in order to ensure safety, reduce degradation, and avoid system shutdown. This area in which the converter is allowed to operate safely is called Safe Operating Area (SOA).

Each power converter has a maximum operating temperature limit. If the temperature exceeds the upper limit, it may affect performance or cause irreversible damage. The purpose is to make the heat dissipation direction all from the case surface to the air through an appropriate thermal design.

The primary goal in the thermal design is to predict and control the converter's heat so that it does not exceed the maximum rating of temperature admissible by the WB's internal components. Heat energy is transferred from regions of high temperature to regions of low temperature via three basic mechanisms [41]:

- **radiation:** electromagnetic transfer of heat between masses at different temperatures
- **conduction:** transfer of heat through a solid medium (heatsink for example)
- **convection:** transfer of heat through the medium of fluid (typically air from ventilation).

All three of these heat transfer mechanisms are active to some degree in every application. All three of these mechanisms should be given consideration when developing thermal management.

The first two can be neglected as in our application they are relevant only to the extent that they serve to bring the heat developed by the power dissipated by the device towards the heat sink as in figure. In this last section the heat is eventually dissipated towards the surrounding environment (which in this case acts as an ideal thermostat) mainly through convection.

The heat dissipation can be expressed using this electrotechnical similarity (as in figure) where the thermal resistance is visualized as a resistor and the temperature difference as the voltage difference between two terminals. The current flowing will be represented by the heat flow passing towards the fins

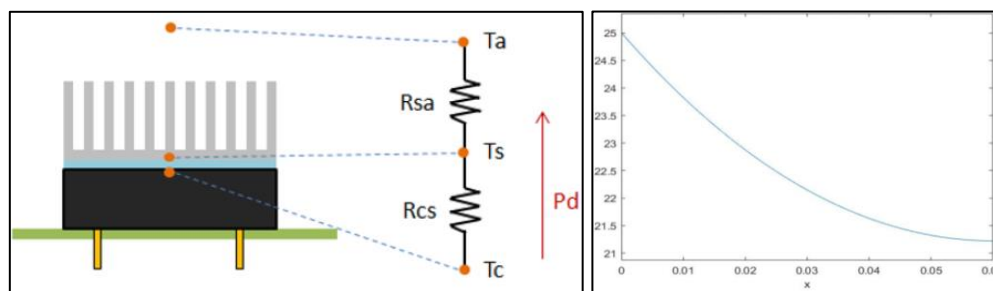


Figure 6-19 heat dissipation scheme (left) and temperature profile (right)

The temperature profile inside the heat sink fins in the 2D domain has been modeled using MATLAB and the result of the differential equation is reported above. In the graph it is possible to see the ΔT experienced by the fins inside them as their longitudinal length varies expressed in the abscissa, this result has been verified with measurements at the base and at the tip of the fins. It is therefore quite representative of how the temperature varies within them

On the market, converters are based on two convective dissipation methods with different possible fluids, in our case air [41]:

- Natural convection: where the temperature produces its own air velocity, due to the local heating of air at the heatsink surface. The air density is reduced when heated, causing it to rise, thus causing the air movement.
- Forced convection: Forced convection implies the use of fans to increase the air movement across the heatsink area. Heatsink to air thermal resistivity can be improved by as much as a factor of 10 when compared to natural convection.

The last one is the strategy chosen by the manufacturer of the DUT.

The DUT relies on a series of fans for the forced convection of ambient air over the metallic external surface of the heat sink, in this way a better exchange can be ensured between the fins tip and the moving air.

This aspect of the designing of the WB can be fundamental since, with a proper design, the Safe Operating Area can be extended to higher temperature regimes. On the other hand a poor thermal management system can lead to a restriction of the utilization area of the charger.

6.2.1 Derating curve

Since it is not possible to obtain accurate information from the data sheet provided by the manufacturer on the type of power reduction that the unit performs to maintain the integrity of the components inside the WB, several observations were made in this regard.

At first only the heat sink temperature was recorded, then a second thermocouple was added to the measurement layout in order to have also the ambient temperature signal.

From the data sheet provided, there is a brief indication of the presence of a power control when the ambient temperature to which the WB is exposed exceeds 40°C.

Figure 6-20 (up) shows the temperature recorded using the thermocouple on the heat sink. Since this is a transducer that converts voltage signals into temperature, it is very sensitive to any insulation fault on the WB, when it is supplied with power.

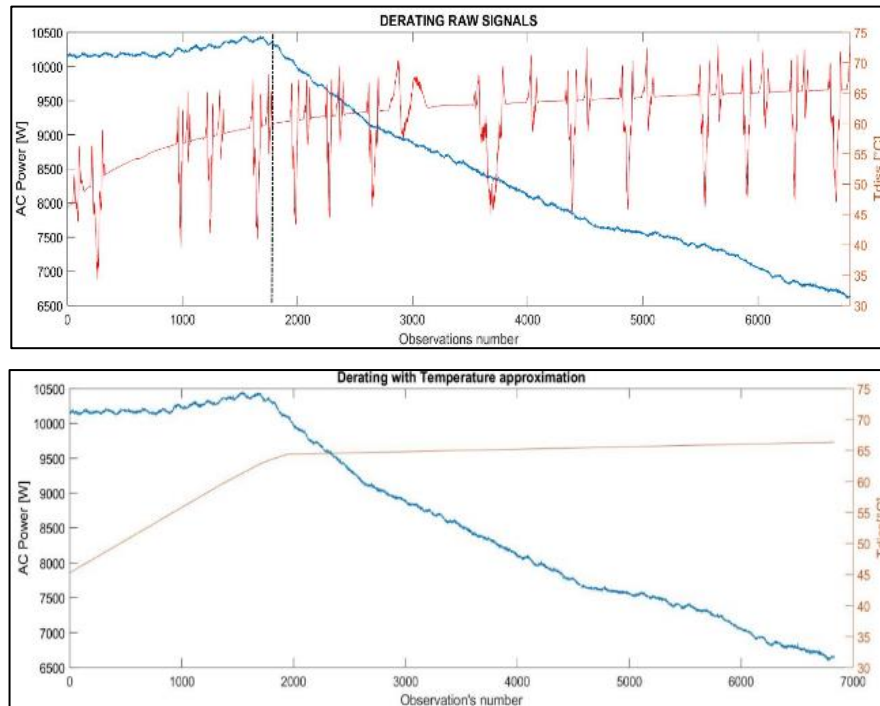


Figure 6-20 Heat sink's temperature signal approximation procedure

This led to having many instabilities in the recorded signal. One way to avoid this problem would be to use a thermal glue, which being a polymer, is also insulating. This aspect could not be implemented due to time constraints.

The solution adopted was to simplify the recorded signal using a piecewise linear function. This second aspect can be seen in *Figure 6-20* (down) shown.

This procedure is adopted for every recording, this one above is taken only as an example because it won't be introduced every time.

The first observations made were at an ambient temperature of 45°C. The thermocouple was held in position on the heat sink to record its evolution on the device. According to reference studies, power reduction is often carried out in such a way that the internal temperature is kept below a 120/150 °C range of interest [42][43]. An initial control strategy can therefore be based on recording the temperature of the component itself, so the first recordings were made in this direction.

One of these is selected to be able to describe in a non-redundant way the analysis strategies used and the conclusions that have been drawn during the development of the following experiences.

Since the efficiencies in G2V are much lower than those in V2G therefore with higher losses, as already shown, this operating mode at nominal voltage and nominal power is taken into consideration as a reference for our observations. The SoC has no influence on this device behaviour.

At the beginning of the experience, the power of the AC side fluctuates around the nominal value of 10 kW, behaving like in standard conditions. Then, a derating process begins, which is expressed with a continuous modulation of the power. The first indication that can

be derived from this is that the power derating is continuous and thus not based on discrete power values. The derating is linear and proceeds until the power reaches the range between 6800W and 7500W are reached. At these values, the power reduction stops and its value starts to fluctuate around it.

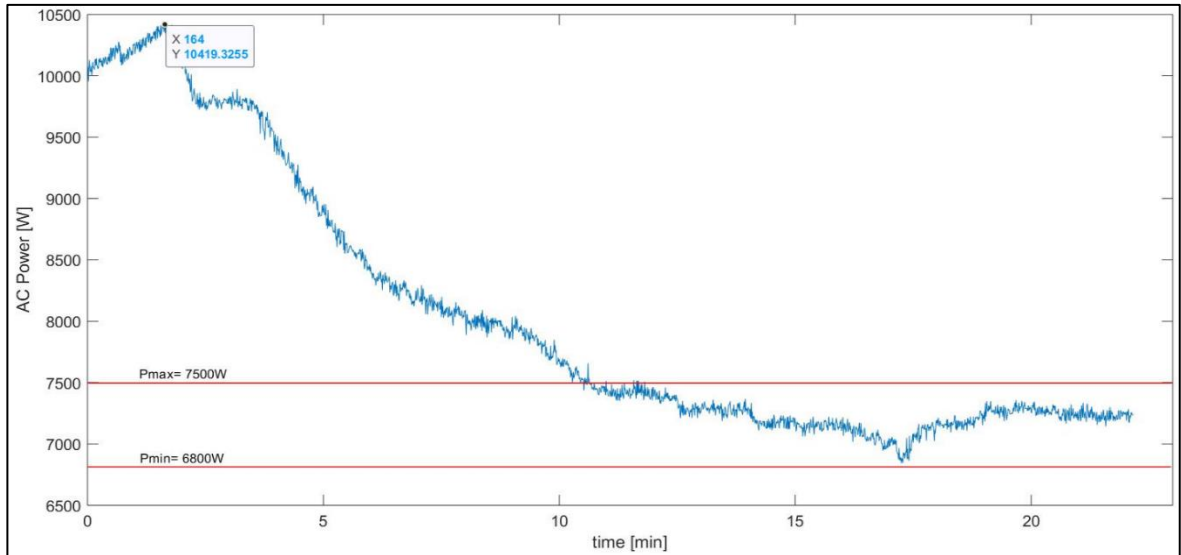


Figure 6-21 10kW derating behaviour

Another useful indication is the peak value of power that occurs just before the power reduction begins. Immediately before the linear decrease, in fact, the power reaches 10400W. A peak of active power of about 400 W is then recorded, after which the power reduction begins.

This peak can be explained by the increase in the speed of ventilation of the heat sink. The unit appears to be entering in a state of emergency where it is trying to lower the surface temperature of the heat sink by increasing the speed of the airflow flowing over it. This aspect can be checked by placing the thermocouple signal next to the recorded power signal.

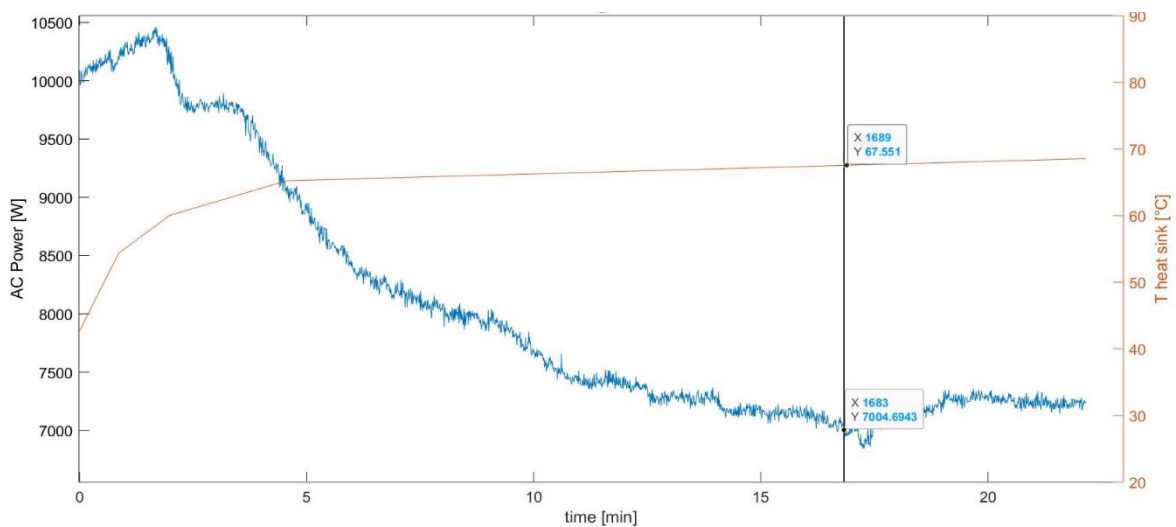


Figure 6-22 heat sink's temperature, 10kW derating

As soon as the surface temperature signal is plotted, the first impression on the peak power can be confirmed.

It can be highlighted how in correspondence (immediately after) the increase in power an abrupt change of inclination of the temperature curve on the component takes place. This is a clear signal that the heat exchange between device and environment has increased.

A different reasoning can be made with respect to the analysis on the control of derating, meaningful conclusions cannot be drawn except regarding its objective of keeping the temperature of the component below the highlighted threshold of 70°C.

In fact, it is noted that although the temperature continues to slightly increase, the power seems to settle at a stable level, furthermore the oscillations shown do not correspond with a clear variation of the temperature on the heat sink.

This casts doubts on the first hypothesis that it could be a control based on the reading of the internal temperature of the WB.

At the same time, as already discussed in the experimental layout, the thermostatic chamber having a strong dissipation inside it does not result in its ideal operating conditions. This led it to undergo a thermal conditioning from the sample inside it, corresponding to a few degrees Kelvin (about 5K) before the control of the chamber itself can act to bring the temperature back to the indicated level.

In the experimental stage, it was therefore decided to use a second thermocouple to acquire the ambient temperature and see if there is a direct correspondence between derating and ambient temperature.

For this acquisition the choice fell for convenience and timing in a second thermocouple completely equal to the first, which is therefore governed by the same characteristic equation, which after some checks has been positioned to record the temperature inside the chamber.

6.2.2 Derating's control strategy identification

This section analyses the experiences that led to the definition of the derating control method adopted by the WB. To do this, since the surface temperature of the device did not lead to significant conclusions in this sense, the ambient temperature inside the chamber is recorded.

In order to see the responsiveness of the chamber when it is subjected to a dynamic temperature change, a temperature profile must therefore be constructed and executed: the simple manual application of a temperature setpoint cannot lead to precise results in this sense. From this point of view, two temperature ramps interspersed with a stable

temperature section were chosen as the ideal for seeing the effects on the power delivered by the device:

- 2 K/min increasing temperature from 40°C to 50°C
- 15 minutes of stable temperature at 50°C
- 0.5 K/min decreasing temperature from 50°C to 40°C

The decreasing ramp is characterized by a smaller gradient as the thermal capacity of the WB needs to be considered. A fast gradient could lead to a great deviation between the controlled temperature and the one performed inside the chamber due to the dissipation of the heat from the wallbox.

A second reason lies in the need to observe with greater precision the eventual power trend in order to actually confirm or not the correspondence between derating control and ambient temperature.

The temperature profile drawn using the API of the Angelantoni chamber Winkratos 4.0 is expressed with the bold black line.

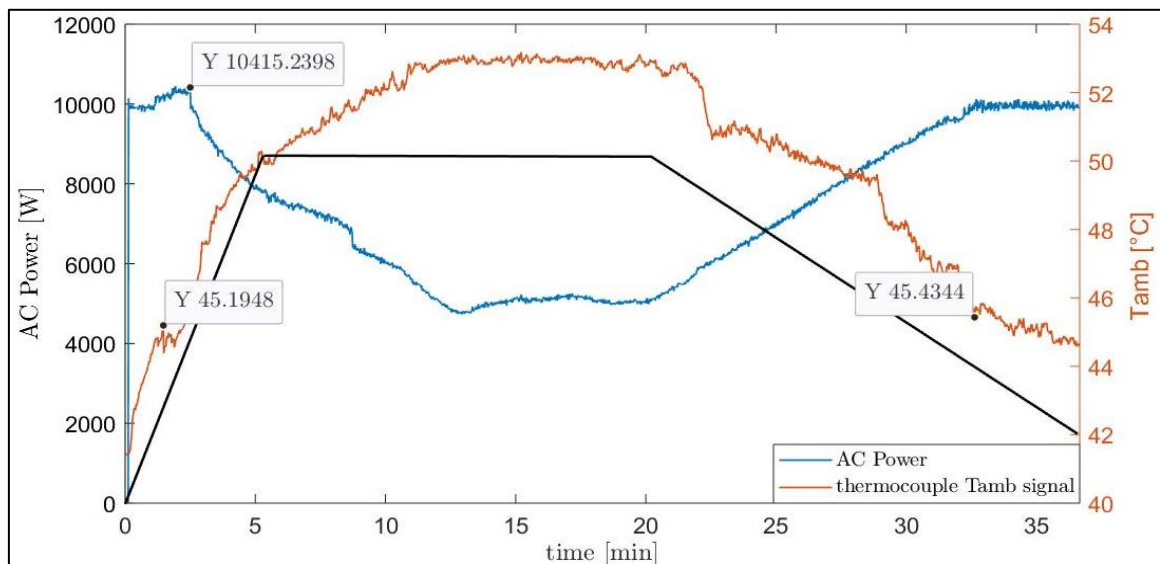


Figure 6-23 derating control strategy

The observation shown in the graph shows the dependence between the power exerted and the ambient temperature.

It can therefore be confirmed following this second set of experiences, that the two parameters are strictly connected. It was not possible to identify the location of the WB temperature control instrument, but following these observations, the interdependence of the parameters is clear.

In the previous Figure 6-23, 3 points were highlighted in this observation: The first one again reflects the power peak before the power reduction, which is about 400W even in this case.

The other two points correspond to the starting temperature of the power reduction and the temperature at which WB returns to work at nominal power. These two points correspond to 45°C, which is confirmed as the temperature at which this behaviour begins. It is then confirmed that the full power is restored as soon as the control temperature drops below the limits.

One last thing remains to be confirmed, namely the minimum limit of power modulation, if therefore there is a minimum of power exerted before any shut down occurs and it corresponds to that temperature. A series of observations like the previous one is carried out in order to build the SOA (Safe Operating Area).

6.2.3 Safe Operating Area

The safe operating area curve is a graphical representation of the power handling capability of the device under various conditions. The SOA curve takes into account the wire current carrying capability, transistor junction temperature, internal power dissipation and secondary breakdown limitations.

SOA specifications are useful to the design engineer working on power circuits such as amplifiers and power supplies as they allow quick assessment of the limits of device performance.

Safe Operating Area (SOA) should be found in device datasheets. It is a graphical representation of the devices maximum operating current and voltage at a specified temperature. on the product datasheet, however, this feature isn't indeed present. Following our observations, this characteristic of the product is reconstructed and shown in *Figure 6-24*.

We highlight how the same trend was observed in both V2G and G2V, based on the ambient temperature and not on the power dissipated by the device

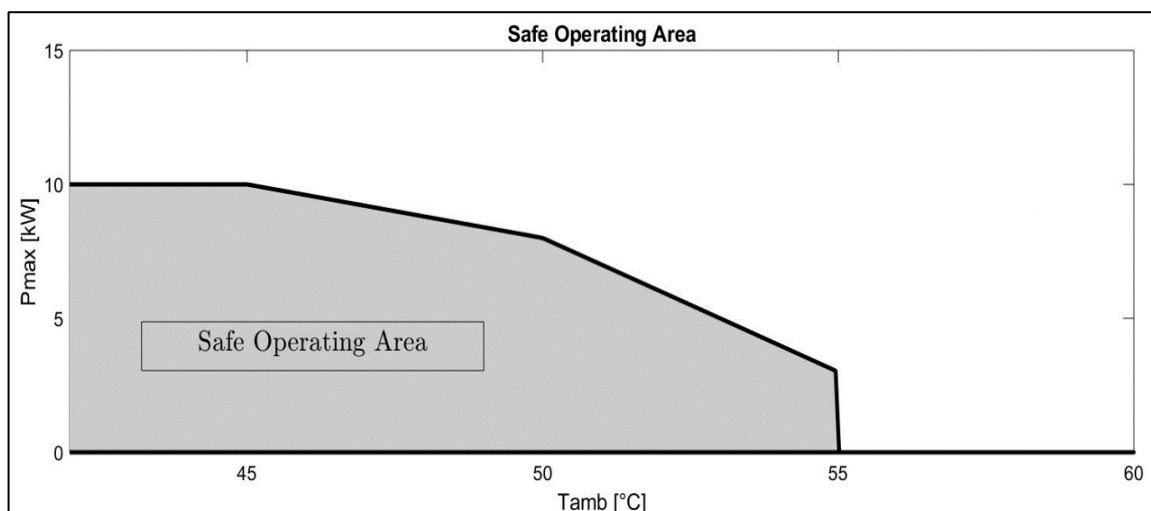


Figure 6-24 Safe Operating Area

From this study we can see how there are 4 different domains:

1. Full operability at nominal output power (10kW) at $T_{amb} < 45^{\circ}\text{C}$
2. First derating range till 8kW at $T_{amb} = 50^{\circ}\text{C}$
3. Second derating with increased slope till 3kW at $T_{amb} = 55^{\circ}\text{C}$
4. Loss of operability for $T_{amb} > 55^{\circ}\text{C}$

Loss of operability above 55°C is indicated with the WB in protection unable to leave standby mode.

If it is brought to $T > 55^{\circ}\text{C}$ when switched off, it will not leave OFF mode, which is indicated by the red LED.

On the other hand, if it is brought to this temperature while already in STAND BY and therefore marked with the blue LED stripe, it does not connect to the vehicle. When the transaction is started, there is no connection to the battery and the WB does not communicate with the cloud. It remains inoperative and also does not read the DC voltage from the battery terminals.

These kinds of measurements were made many times, both with thermal profiles with the WB switched on and operating throughout the profile. Another test was to try to enter a setpoint at nominal power when the wallbox already had temperatures above the specified threshold. In this last case, the power was directly modulated to lower values than the nominal power and this value was recorded.

This starting up value always respected the SOA described in *Figure 6-24*.

6.3 Power quality tests

The quality of electrical power, or simply the power quality, includes voltage, frequency and waveform. Good power quality can be defined as a constant supply voltage that is within the prescribed ranges, frequency that is close to the nominal value, and a uniform voltage curve (similar to a sine wave).

In general, it is useful to think of power quality as the compatibility between what comes out of a socket and the load that is connected to it. The term is used to describe the electrical power that drives an electrical load and the ability of the load to function properly. Without the proper power, an electrical device (or load) may not function properly, may fail prematurely, or may not function at all.

There are many ways in which electrical power can be of poor quality, and many more causes of such poor power quality, the main aspects analysed in this thesis are the current harmonic content and the power factor.

Given the importance of this feature for the proper functioning without damage to the entire electrical network and the loads connected to it, these tests are evaluated through specific pass-fail criteria.

These tests therefore define whether a product can be considered suitable for the electricity market or not

6.3.1 Power factor

The goal of this test is to calculate the power factor during the charging and discharging of the electric vehicle battery, under different operating conditions, and verify that the requirements are met minimums on the power factor imposed by the standard IEC 61727: 2004, previously listed.

In particular, the power factor must be greater than 0.9 for powers greater than 50% of the rated power of the inverter (5kW). The results are listed in the graphs below.

G2V

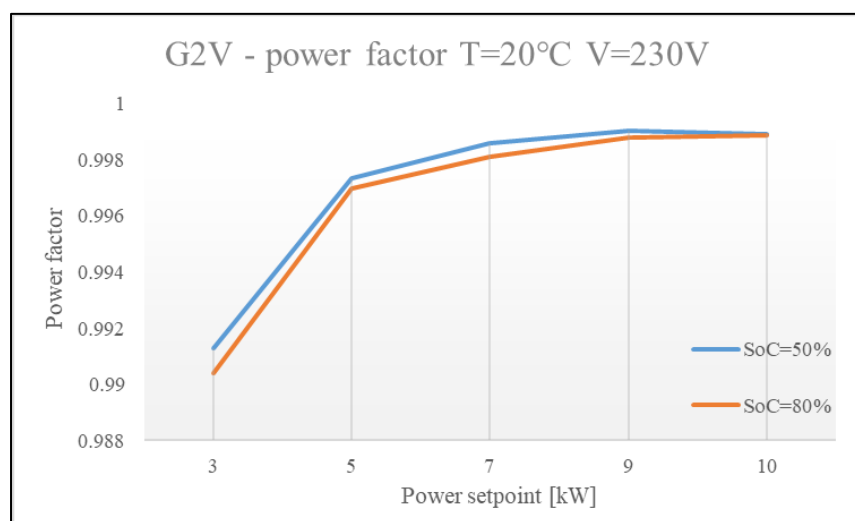
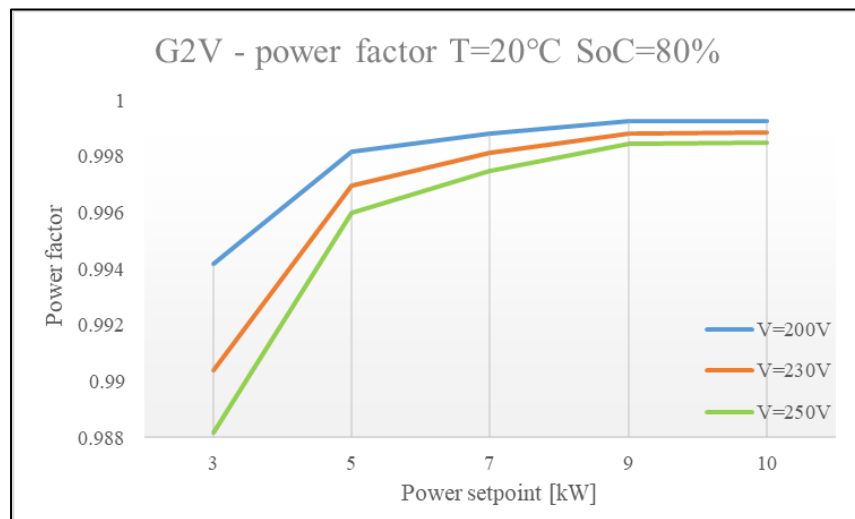
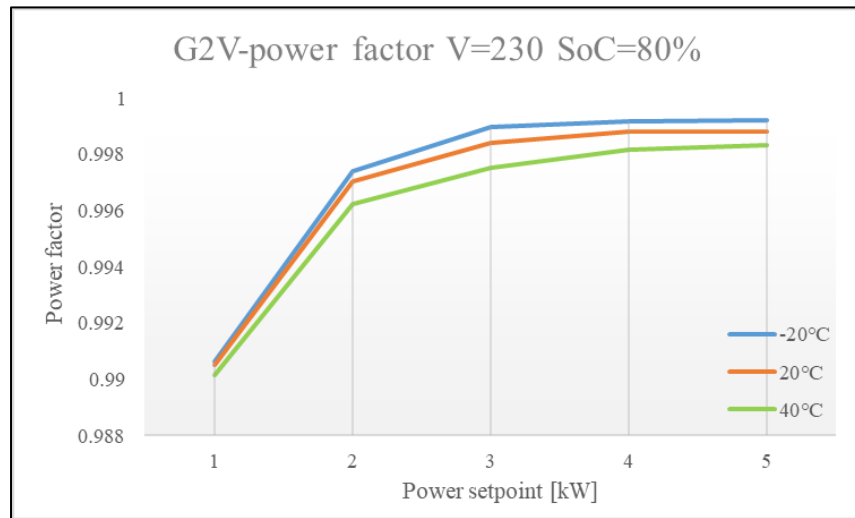


Figure 6-25 G2V power factor varying temperature (up), AC voltages (middle), SoC (down)

V2G

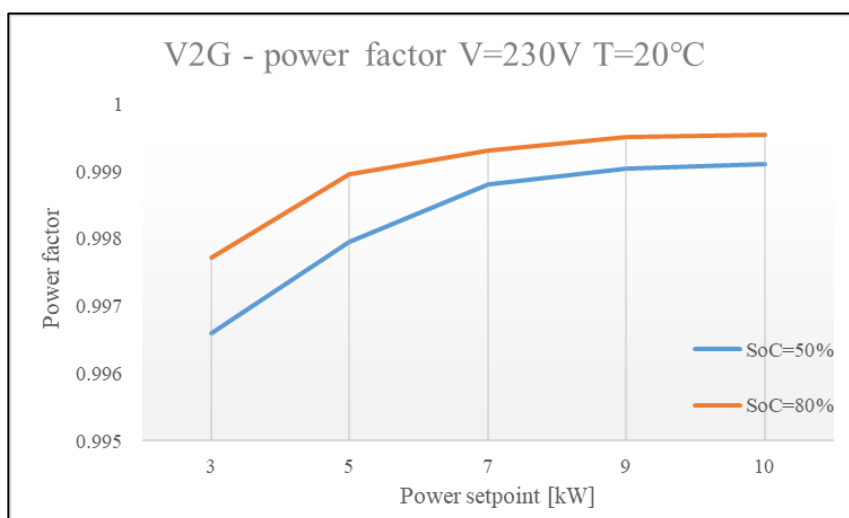
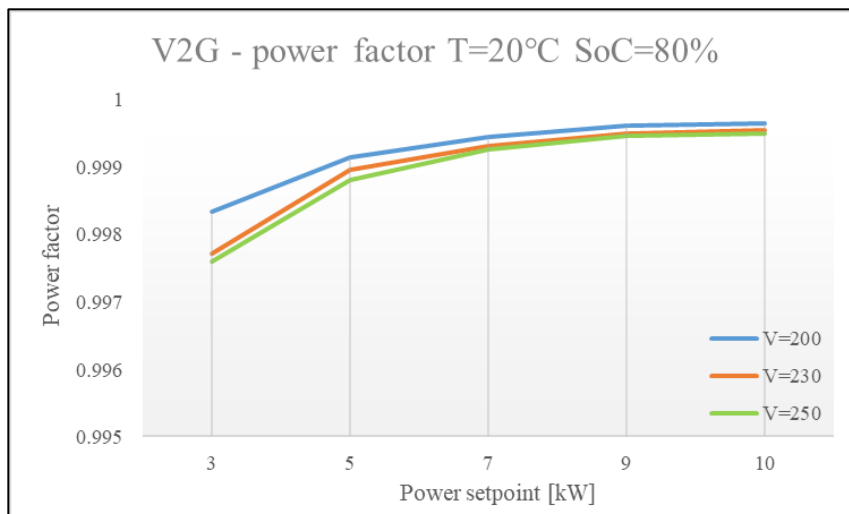
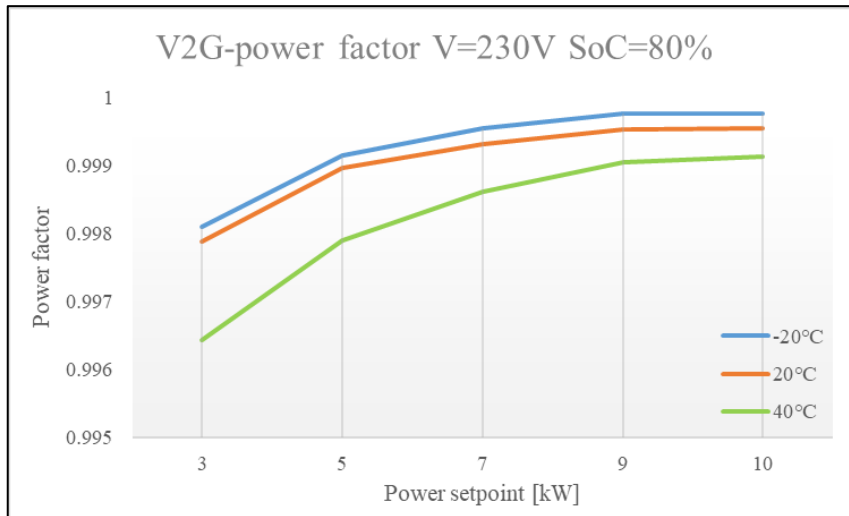


Figure 6-26 V2G power factor varying temperature (up), AC voltage (middle), SoC (down)

The test results show that the requirements of the legislation on the minimum values of the power factor are respected, therefore the test can be considered passed.

Furthermore, the power factor exceeds the minimum value of 0.9 for any power level (even less than 50%), in both operating modes (charge and discharge), at any level of mains voltage and starting from any battery SoC considered.

The lowest recorded value in the observation area is 0.990855

There wasn't highlighted any strong dependence between the operating temperature and the power factor. A small variability depending on the temperature has in fact been recorded, but nothing compromising for the functioning of the device, always falling well within the limits. Every previous figure has few sampling points and between them a linear interpolation was performed.

On the contrary, the dependence of the power factor with respect to the exchanged power is clear: in fact, for powers greater than 50% of the rated power, the power factor is much higher than the lower power values. Furthermore, even at higher powers, as the latter increase the factor of power is greater, albeit with a much less steep variation.

6.3.2 Currents harmonics THD

The power-quality issue of harmonic distortion is mainly determined by the current-harmonic emissions of power electronic components and the network impedance of the grid. These current-harmonic emissions are normally quantified in terms of magnitude.

In a linear system, i.e. a circuit with ideal resistors, capacitors and/or inductors, the voltage and current waveforms are perfectly sinusoidal. Such a system is highly unlikely and there are always some non-linearities. Certain types of loads (non-linear loads), for example, produce currents and voltages with frequencies that are whole multiples of the frequency for which the supply system is designed (50 Hz).

The objective of this test is to evaluate the harmonic content of the three-phase currents, both in charge and discharge mode, and verify that they comply with the limits indicated by the IEC 62933-2-1: 2018 [46].

Low levels of voltage and current harmonics depend upon distribution system characteristics, type of service and connected apparatus

To ensure that no adverse effects are caused to the equipment connected to the utility system, the charging station output should have low current distortions levels.

Since the voltage waveform is imposed through the simulation, is supposed to be a quasi-perfect sinewave. Thus, only the current harmonic content is measured.

The Harmonics Test aims to measure the individual current harmonics and the total-harmonic current distortion (THD) of the charging station under normal operating conditions.

$$THDi_{\%} = \frac{\sqrt{\sum_{h=2}^H I_h^2}}{I_1} * 100\%$$

where h is the harmonic order, H is the highest order of the observed harmonic categorical, I_h is the RMS value of the current h -th harmonic component, and I_1 is the current RMS value of the main frequency.

In order to prevent harmonics from affecting the utility supply, standards such as IEC-61000-3-2 sets the emission limits for equipment connected to public low-voltage systems with input current ≤ 16 A per phase. This standard can be applied in G2V.

The IEEE Std. 1547.1 has already been discussed and states the limits for V2G operation based on rules from the regulation of inverter connected PV panels with a battery storage.

To execute the test, both a charging and a discharging process were imposed to the charging station. Then, only the three AC currents were measured and saved by the DAQ. To the six samples (three for G2V, three for V2G) a Fast Fourier Transform using MATLAB environment was performed.

A fast Fourier transform (FFT) is an algorithm that computes the discrete Fourier transform (DFT) of a signal. A fast Fourier transform (FFT) is an algorithm that computes the discrete Fourier transform (DFT) of a sequence. The `fft` takes a frequency in the time domain, for example our currents signal, and divides its amplitude in the various frequencies that characterize it. The result is therefore a series of magnitudes, each one referred to its own specific frequency in which the signal of interest is reproduced.

In our case, the data samples are the AC currents and the result is a series of current RMS values, each one referred to a specific frequency. The length of the frequency series and its resolution depend on the measurement window length and the sample rate. Sampling frequency and time duration are then the two main parameters through which the characteristics of the analysis performed are defined.

The sampling frequency or sampling rate, f_s , is the number of samples obtained in one second (samples per second). This parameter is fundamental in defining the exploratory range that our analysis can obtain. In fact, for Nyquist –Shannon sampling theorem: the maximum frequency signal component that can be perfectly acquired without errors is given by half the sampling frequency at which I am measuring the starting signal. All the frequency components higher than the half of the sampling rate will be rendered with a particular non-eliminable error called Aliasing

The acquisition time, on the other hand, is responsible for the so-called frequency resolution, or rather the precision with which the frequencies of the acquired signal are divided into the "bins" of the right value. The measurements were done using a 3 s window length and a sample rate of 200 kS/sec.

The FFT was executed with a frequency resolution of 0.333 Hz, defined through the sampling rate f_s and the number of samples

$$\Delta_f = \frac{f_s}{N} = \frac{200'000 \text{ S/s}}{600'000}$$

The harmonic content is measured both in the G2V and in V2G mode for

the three AC currents. Only the intermediate results related to a phase in the two operations is presented to avoid repetitions. Subsequently a table will compare the relative values obtained with the corresponding regulatory limits.

A second section will be then devoted to the THD that will be evaluated and compared with the 5% limit that is present in the aforementioned standards. Finally, the temperature effects will be analysed.

Starting from the raw signal (*Figure 6-27*), which is the one represented in the figure, then we proceed with the Fourier analysis. The MATLAB algorithm will not be discussed. The signals of the three voltages and those of the three currents are compared. The signals both refer to the nominal power in charge and to the nominal voltage.

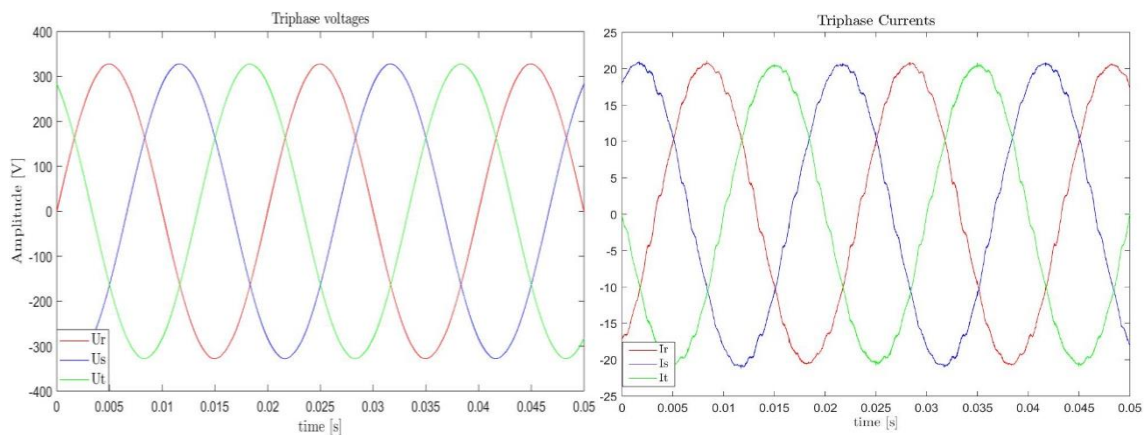


Figure 6-27 voltages from amplifier (left) currents absorbed by WB (right)

As can be clearly seen from the raw signals (*Figure 6-27*), the degree of distortion from the perfect sine wave that is present in the voltage signal is infinitesimal compared to the distortions present on the currents. Furthermore, the limits relating to the voltages are generally more permissive than the currents, since it is the latter that have a negative effect on the instrumentation, the former simply feed the generation of harmony in the latter. This brings the analysis on the distortion of the tensions negligible, as it has already been anticipated before.

The harmonic spectrum of the currents in the frequency domain can be displayed both in decimal and logarithmic scale. The harmonic spectrum of currents in the frequency domain can be displayed both in decimal and logarithmic scale. The two different representations are compared below. As already mentioned, only the second phase will be plotted, the others have been analysed in the same way.

The logarithmic spectrum of phase B was plotted as a reference. Then the limit value will be analysed and confronted with the standards.

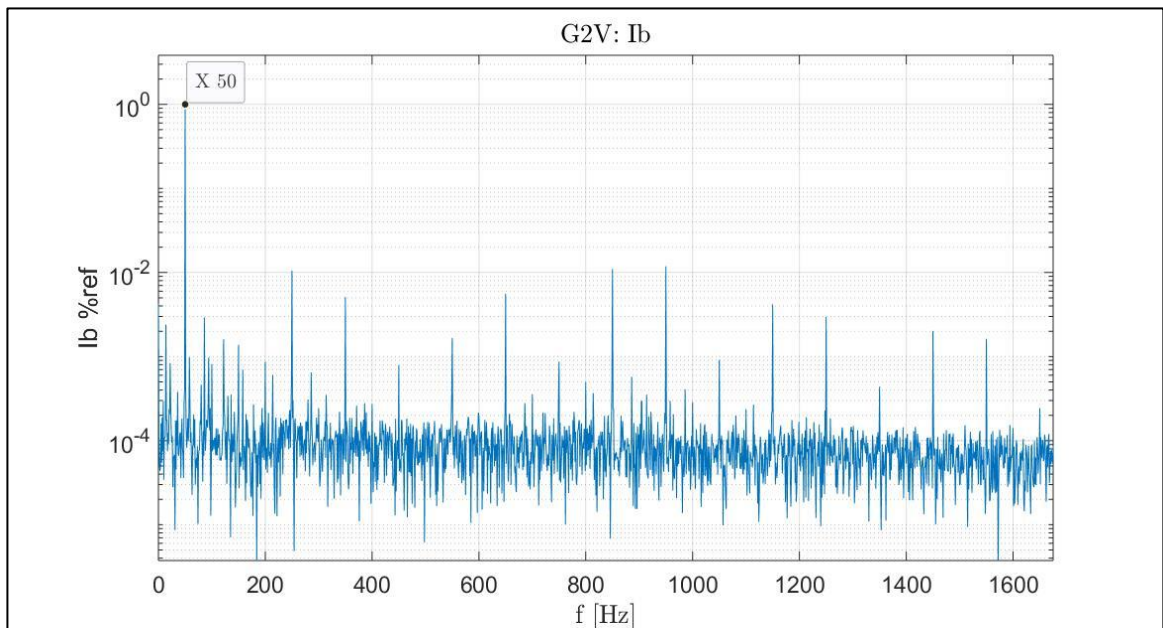


Figure 6-28 G2V 10kW frequency spectrum (fft) logarithmic scale

Subsequently, the spectrum relating to V2G operation is also presented, always under the same conditions listed above.

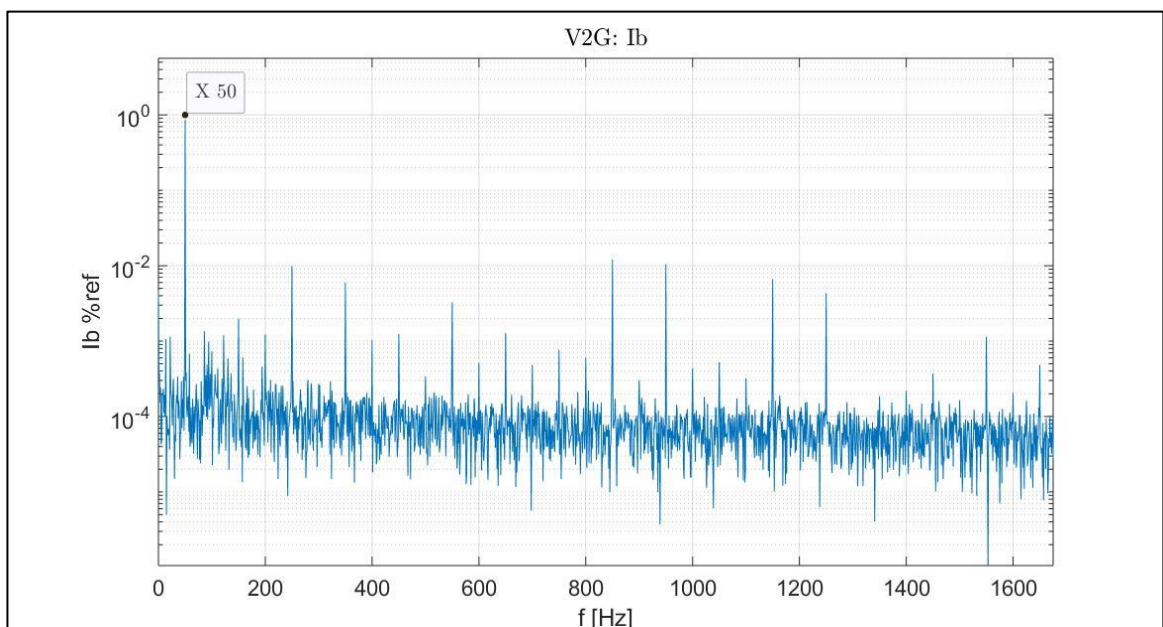


Figure 6-29 V2G 10kW frequency spectrum (fft) logarithmic scale

The fundamental component is highlighted in these plots (*Figure 6-28* and *Figure 6-29*) and corresponds to the signal that occurs exactly at 50 Hz. This is an important factor in the analysis phase when it comes to refining the frequency resolution of the harmonic spectrum.

Indeed, when the resolution is changed, the distribution of the signal components in the different frequency bins changes. With a resolution of 1 Hz, the signal at 1Hz in the first bin, this means that the fundamental will be in the 50th bin. If, on the other hand, the resolution is doubled to 0.5 Hz, the fundamental frequency is in the 100th bin. In our case, it is at the 150th bin since the resolution is 0.333 Hz.

This is not a physical effect, but a simple analytical effect resulting from the application of Fourier analysis.

As for the limits imposed by the standards, no critical issues were found for the G2V. Each of its phases lies within the prescribed limits in every condition considered. This is because the standard limits for the loads in the grid are much more permissive than for the generators that have to feed power into the grid instead. This results in the G2V having controlled and legally compliant harmonic behaviour in every working phase.

For this reason, only the full table of V2G mode is reported being the most interesting case.

Harmonic's order	Ia	Ib	Ic	LIMITS V2G
2nd	0.073292	0.096292	0.094247	1
3rd	0.170044	0.12778	0.344128	4
4th	0.173614	0.153769	0.07924	1
5th	1.090853	0.953176	0.999263	4
6th	0.070251	0.018904	0.059931	1
7th	0.657156	0.60975	0.63264	4
8th	0.136634	0.101481	0.068219	1
9th	0.119605	0.083897	0.181499	4
10th	0.057702	0.03573	0.085613	0.5
11th	0.210379	0.41895	0.15461	2
12th	0.075737	0.030308	0.108901	0.5
13th	0.239254	0.117764	0.134835	2
14th	0.071866	0.055316	0.048169	0.5
15th	0.107224	0.071929	0.189881	2
16th	0.08568	0.058103	0.026105	0.5
17th	1.193097	1.213365	1.066945	1.5
18th	0.070472	0.013221	0.076931	0.5
19th	1.233539	1.058231	1.015687	1.5
20th	0.039895	0.03863	0.058951	0.5
21st	0.031753	0.054376	0.029171	1.5
22nd	0.032036	0.020509	0.011205	0.5
23rd	0.616215	0.653811	0.592198	0.6
24th	0.076947	0.011769	0.079511	0.5
24th	0.558348	0.427807	0.498335	0.6
25th	0.035673	0.008427	0.034825	0.5
26th	0.022306	0.039424	0.057689	0.6
27th	0.025251	0.024067	0.033064	0.5
28th	0.032391	0.057865	0.053394	0.6
29th	0.019108	0.008231	0.026356	0.5
30th	0.109162	0.116315	0.082662	0.6
31st	0.032549	0.018681	0.0159	0.5
32nd	0.059152	0.04959	0.078086	0.6
33rd	0.02739	0.034017	0.009943	0.5

Table 6-3 V2G 10kW currents harmonics relative to fundamental

The 23rd order is highlighted in red, which expects the prescribed limits both in Phase A and in Phase B. Other tests varying the input conditions, led to the same result, which can be summarized in the following table, which takes the average values among those recorded in the phases. Doing more tests also the third phase turns out to be above the limits.

Harmonic order	Ph_a %	Ph.b_%	Ph.c_%
23°	0,6441	0,6601	0,639

Table 6-4 23rd harmonics, test 2

This component is above the limits at all the voltages considered. During the thesis study many different tests were carried out to verify what this high value was due to, if it was an effect of the coupling with the amplifier and if it was due to an imperfect isolation of the system.

Along with the various tests, one that led to excellent results was the recording of the 23rd harmonic at various battery charge levels.

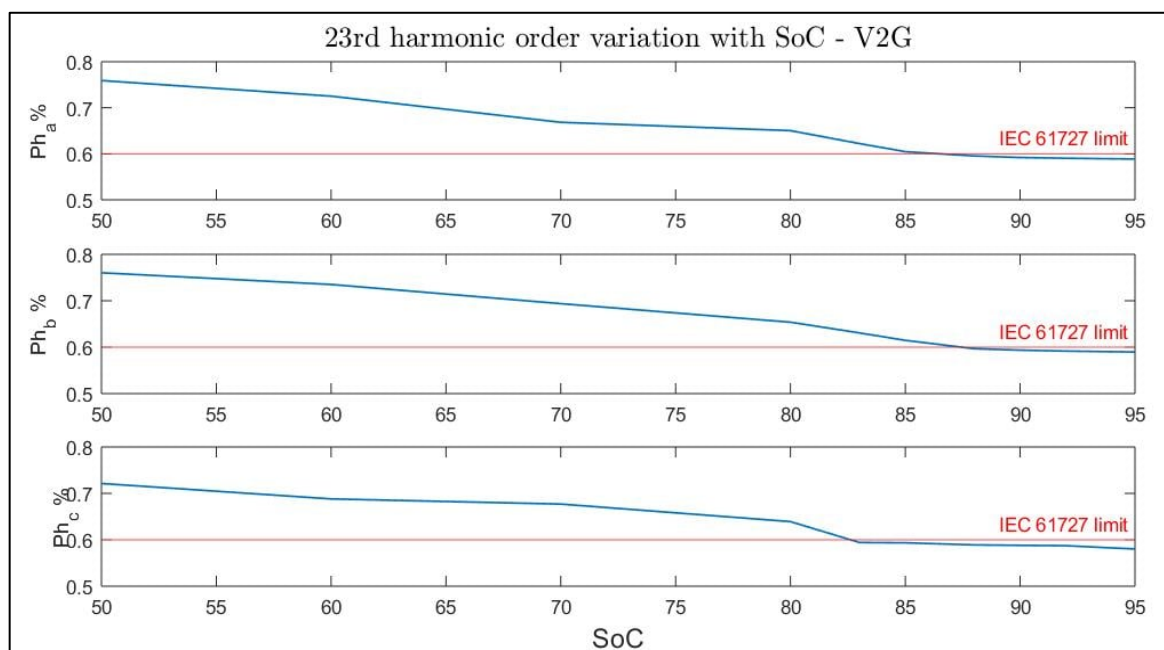


Figure 6-30 SoC effect over 23rd harmonic values

As in the figure, it turns out that the SoC unexpectedly has a major influence on the development of the harmonica in question from WB. Indeed, as soon as 85% of the SoC is exceeded, this value returns below the regulatory limits for all three phases. The limit value of 0.6% expressed by the standard is indicated with the red line in the graphs shown.

Strict regulations for its use can be derived from this result. It is therefore recommended to use it in V2G as a generator for very high SoC values of the EV battery. This, de facto, severely limits the range of use if we consider the application landscape of a fleet of vehicles connected to many WBs in parallel.

As regards the THDi, obviously this parameter registers a strong increase as the operating power decreases (due to the lower currents involved), therefore it is certainly recommended to use it at nominal power.

As for the limits, which refer to the nominal power, the value is below them. This test can therefore be considered passed. The THD compliance is respected as every value is below the 5% limit.

G2V

THD_A	2.15%
THD_B	1.89%
THD_C	2.23%

V2G

THD_A	2.19%
THD_B	2.15%
THD_C	2.29%

Table 6-5 G2V (up) and V2G (down) THDs

Now the study proceeds with the analysis and observation of the effect that the ambient temperature has on this parameter. As can be seen in *Figure 6-31* below, no effect was recorded on the harmonic content of the signal.

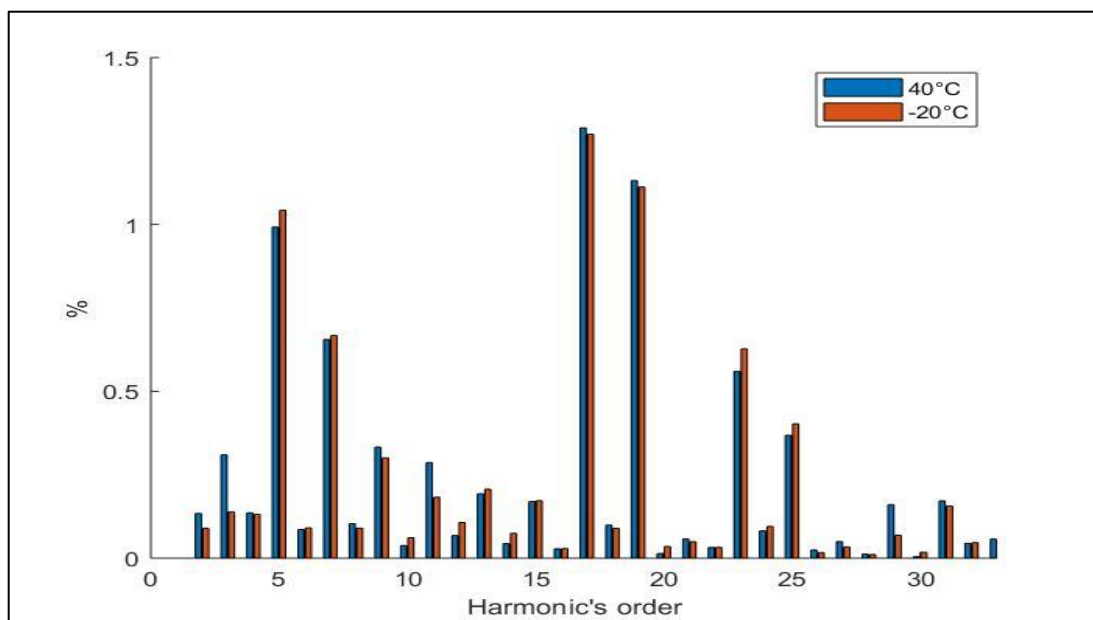


Figure 6-31 harmonics relative value at different temperatures

In the graph, the harmonics in relative terms, starting from the second order one, are represented in the bins to which they belong with a bar graph. The blue ones represent the harmonic content recorded at the maximum temperature, the orange ones at the minimum.

Also this result can be considered unexpected compared to what is presented in the literature. In fact, in the studies taken as a reference for this analysis, a dizzying increase in harmonics has always been verified, with a very evident effect on the THDi, which concerned all the components involved in simultaneous mode.

Even in this case, as for the conversion efficiency, the distinction is given by the thermal non-conditioning of the battery, which remains at room temperature. When it cools, it can draw much less current due to the increase in its internal resistance. The effect was that in those studies it could be that there was a tendency to increase in the THDi, as the temperature decreases. Citing the study in question “This could be explained by the reduction of the current being requested by the vehicle, as the temperature decreased as well thus, resulting in a direct impact decrease in the THDi”. Because by decreasing the magnitude value of the fundamental that was absorbed, the relative values become more important, leading this ratio to increase a lot.

This non-result turns out to be an important indication to bring in the design of the EVs systems. By managing to condition the vehicle battery when they approach recharging, leading to an increase in its temperature, with a small expenditure of energy present in the battery itself, the limitations imposed by the large harmonic's values could be avoided since the chargers are not involved. This study has therefore succeeded in identifying the weak link in this very common issue in the charging systems.

6.3.3 Stand by power consumption

Standby apparent power, on the other hand, refers to the electrical power consumed by a device when not in actual operation, but is only connected to a power source, is ready to be used. In this study, apparent power is presented in VA units, hence, both active and reactive powers are considered.

This consumption is given by the continuous operation of the screen, the filters, and the other internal circuits. The DUT has fans to mitigate the heat, but do not have resistances to deal with low temperatures scenarios. The fans on the WB remain on, albeit at reduced speed, even during standby, causing leaks when not in use.

The high power absorbed in standby, when prolonged over time, can lead to significant economic losses for the V2G owner or for the supplier of the car park enabled for ancillary services. In fact, these devices are often disconnected from vehicles, so limiting the power consumption when they do not need to be operational is an aspect that can result in large economic differences. In this analysis the parameter is first introduced by collecting the information from the datasheet, then the variables that affect the results obtained are introduced. Finally, there will be a comparison on the results obtained depending on the temperature exerted.

6.3.3.1 Stand by conditions

There are two main characteristics that distinguish the different STANDBY situations of the WB:

1. The WB can be online or offline from internet communication
2. The EV can be plugged or unplugged during the STANDBY

From datasheet only the Real Power consumption when the vehicle is unplugged and the WB offline is expressed. This value should then be lower than 20W.

Previous observations have noted a large increase in the power consumed deriving from the components that manage communication with the cloud, while during the operations in STAND BY with the connected vehicle, a power of about 30W could be constantly noticed at the output from the WB, therefore referred to the DC side.

For this study we considered the most frequent condition within the standby operation of the WB, ie when the vehicle is disconnected, but the WB remains online. This seems to be the most representative condition of the condition of the WB when not using the G2V or V2G. These conditions were performed to carry out a study on the effect of temperature on this parameter.

On the other hand, subsequently, single observations at room temperature were carried out in the various conditions described above to quantify the data not provided by the manufacturer and to verify what is instead is expressed.

6.3.3.2 Apparent power consumption

The apparent power S [VA] was always recorded using the three tensions of interest with the vehicle disconnected from the Wb, but with the device connected to the internet via an ethernet cable. The results obtained at the different operating temperatures are shown in Figure 6-32. The temperatures studied were, the 3 subjects of study regarding the conversion efficiencies (-20°C, 20°C, 40°C) plus an additional temperature inside the derating range (45°C).

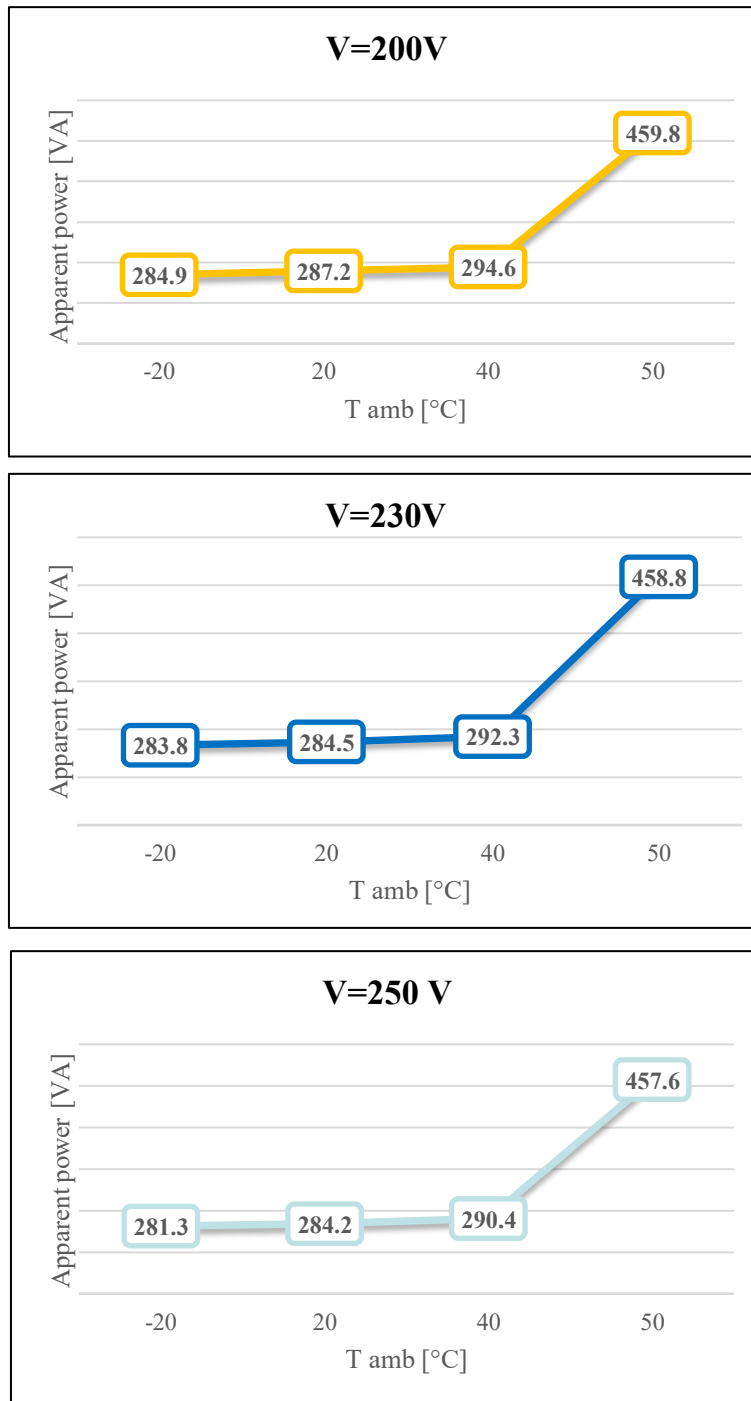


Figure 6-32 Standby power at different temperatures for different AC voltages

It is clear that the temperature has no particular effect on the apparent power consumption of the device in the normal operating range.

Reaching 45°C, however, due to the high temperature recorded by the WB, it begins to intensify the use of the external fans of the heat sink. This, as had already been observed during the experiences on derating, lead the power to express a peak of considerable importance. In terms of apparent power this in fact almost doubles in its consumption.

As regards active power consumption, an increase of 400W was recorded during derating, in line with the apparent power increase recorded.

The latest indications were taken from the behaviour of the disconnected WB, 26W were recorded, approximately 6W more than those indicated in the product data sheet.

7 Conclusions

We had set ourselves the goal of continuing an experimental activity already started in the Energy Center. As a matter of fact, the laboratory has been adapted to the new working plan. In this paper we tried to deepen the theme of Vehicle-to-Grid adopting several tests to evaluate the performances of a supplied device under test when exposed to critical ambient temperatures.

As a first step, in order to carry out an appropriate environmental testing, a development of the laboratory layout was carried out consisting in the addition of the thermostatic chamber used for temperature control capable of the device.

Subsequently, the temperature measuring instruments were calibrated, which had not yet been implemented in the laboratory. This allowed a consistent acquisition of the thermal parameters during the execution of each test considered.

Finally, it was possible to carry out the actual tests. Considering the research field concerning performance tests more promising, in the first instance, the investigation proceeded in that direction and then also some interconnection tests to verify the compliance of the instrument with European standards were carried out.

The major criticalities on the wallbox's behaviour were found at high temperatures, both as regards the conversion efficiency and the derating logic adopted by the instrument. With regard to this second point, it is emphasized that greater attention to the control logics of heat dissipation on these devices can greatly expand their application ranges, which can be severely limited in their use in some particularly hot climatic areas.

Tests at low temperatures did not show great results, but these too drew important indications through bibliographic comparison. It has been highlighted that the greatest limitations in the harshest environments are due to the behavior of the battery rather than the charging devices. This represents the main bottleneck for an industry that will also have to develop at high latitudes.

Upcoming studies may be of interest accompanied by battery conditioning. While the horizon of the effects on power quality remains unexplored as a result of multiple similar or different devices connected to the same point of common coupling of the distribution. This field of application could give very interesting results in the face of a very scarce study of these effects on bidirectional V2G systems.

8 Bibliography and Webography

- [1] “United Nations Framework Convention on Climate Change”, Nazioni Unite, 1992
- [2] Rifkin, Jeremy. *The Third Industrial Revolution : How Lateral Power Is Transforming Energy, the Economy, and the World*. New York, Palgrave Macmillan, 2013.
- [3] Directorate-General for Mobility and Transport. “Commission Publishes Strategy for Low-Emission Mobility.” *Transport.ec.europa.eu*, 22 Sept. 2016, transport.ec.europa.eu/news/commission-publishes-strategy-low-emission-mobility-2016-09-22_mt.
- [4] <https://www.ge.com/digital/lp/industry-insights-v2g-revolution>
- [5] ERTRAC, EPoSS and ETIP SNET. *European Roadmap Electrification of Road Transport Status: Final for Publication*. June 2017.
- [6] Contributor, Guest. “EVs on the Grid - Challenges and Opportunities.” *Smart Energy International*, 7 Aug. 2019, www.smart-energy.com/industry-sectors/electric-vehicles/evs-on-the-grid-challenges-and-opportunities/. Accessed 3 Jan. 2022.
- [7] Lang, Scott. “Electric Vehicles and the Smart Grid: Charging Forward! - Special Electric Vehicle Section.” *Electric Energy Online*, Nov. 2010, electricenergyonline.com/energy/magazine/542/article/Electric-Vehicles-and-the-Smart-Grid-Charging-Forward-.htm#:~:text=The%20Smart%20Grid%20is%20the%20key%20to%20smart. Accessed 15 Mar. 2022.
- [8] U.S. Department of Energy. “What Is the Smart Grid?” *Smartgrid.gov*, 2019, www.smartgrid.gov/the_smart_grid/smart_grid.html.
- [9] Balamurugan, and Sujithkumar. *Smart Grid: How Reliable It Is*. 2019.
- [10] Kaur, Inderpreet. “Chapter 29 - Metering Architecture of Smart Grid.” *ScienceDirect, Academic Press*, 1 Jan. 2021, www.sciencedirect.com/science/article/pii/B9780128245552000307. Accessed 15 Mar. 2022.
- [11] Khan, Ahsan Raza, et al. “Load Forecasting, Dynamic Pricing and DSM in Smart Grid: A Review.” *Renewable and Sustainable Energy Reviews*, vol. 54, Feb. 2016, pp. 1311–1322, www.sciencedirect.com/science/article/pii/S136403211501196X, 10.1016/j.rser.2015.10.117.
- [12] Fraunhofer-Gesellschaft. “Seamless E-Vehicle/Smart Grid Connectivity through Intelligent Communication.” *Www.nanowerk.com*, 12 Feb. 2014, www.nanowerk.com/news2/green/newsid=34373.php. Accessed 15 Mar. 2022.
- [13] Datta, Ujjwal, et al. *The Strategies of EV Charge/ Discharge Management in Smart Grid Vehicle-To-Everything (V2X) Communication Networks*.
- [14] Jones, Laura, et al. *The a to Z of V2G a Comprehensive Analysis of Vehicle-To-Grid Technology Worldwide*. 2021.

- [15] Ravi, Sai Sudharshan, and Muhammad Aziz. "Utilization of Electric Vehicles for Vehicle-To-Grid Services: Progress and Perspectives." *Energies*, vol. 15, no. 2, 14 Jan. 2022, p. 589, 10.3390/en15020589. Accessed 15 Mar. 2022.
- [16] ARERA, «Delibera 583/2017/R/eel - Approvazione del regolamento, predisposto da Terna ai sensi della delibera 300/2017/R/eel, relativo al progetto pilota per la partecipazione della generazione distribuita, come UVAP, al MSD,» 03 Agosto 2017. [Online]. Available: <https://download.terna.it/terna/0000/1051/81.PDF>
- [17] Franzò, Simone. "UVAM: Un Asset Strategico per Il Sistema Elettrico Nazionale?" *Energy Saving*, 11 Apr. 2019, www.energysaving.it/uvam-un-asset-strategico-per-il-sistema-elettrico-nazionale/. Accessed 15 Mar. 2022.
- [18] Plett, G.L. Extended Kalman filtering for battery management systems of LiPB-based HEV battery packs—Part 2. Modeling and identification. *J. Power Sources* 2004, 134, 262–276.
- [19] Bullis, K. Electric Vehicles out in the Cold. *MIT Technology Review*. Available online: <https://www.technologyreview.com/s/522496/electric-vehicles-out-in-the-cold/>.
- [20] M.baath, Jaydeep. "Effect of Temperature on Battery Life and Performance in Electric Vehicle - Current Issue - IJSR." *Www.worldwidejournals.com*, Oct. 2013, [www.worldwidejournals.com/international-journal-of-scientific-research-\(IJSR\)/fileview.php?val=October_2013_1493280454_43.pdf](http://www.worldwidejournals.com/international-journal-of-scientific-research-(IJSR)/fileview.php?val=October_2013_1493280454_43.pdf).
- [21] Ma, Shuai, et al. "Temperature Effect and Thermal Impact in Lithium-Ion Batteries: A Review." *Progress in Natural Science: Materials International*, vol. 28, no. 6, Dec. 2018, pp. 653–666, 10.1016/j.pnsc.2018.11.002. Accessed 15 Mar. 2022.
- [22] Lucas, Alexandre, et al. "Power Quality Performance of Fast-Charging under Extreme Temperature Conditions." *Energies*, vol. 11, no. 10, 2 Oct. 2018, p. 2635, 10.3390/en11102635. Accessed 15 Mar. 2022.
- [23] Carter, R, et al. *EVS International Battery, Hybrid and Fuel Cell Electric Vehicle Symposium Impacts of Harmonic Distortion from Charging Electric Vehicles on Low Voltage Networks*. 2012.
- [24] BS EN 60068-1-2007 "Environmental testing: general guidance"
- [25] BS EN 60068-2-2007 "Environmental testing: tests"
- [26] S. Chakraborty, W. Kramer, B. Kroposki, "Interim Test Procedures for Evaluating Electrical Performance and Grid Integration of Vehicle-to-Grid Applications", NREL, 2011
- [27] R. Singh and A. Singh, "Energy loss due to harmonics in residential campus — A case study," *45th International Universities Power Engineering Conference UPEC2010*, 2010, pp. 1-6.
- [28] Jaisiva, S, et al. "HARMONIC ANALYSIS in NON -LINEAR LOADS of POWER SYSTEM." *IRJET*, May 2016.
- [29] SPHEREA Puissance Plus - Documentation Guide. 4Q POWER AMPLIFIER with different options - User Manual.url:(Partial_Source)%20https://www.puissanceplus.com/assets/produitpdf/Amplifier

- %204Q%20AC%20DC%20Three%20phases%203x7kVA%20limited%20absorption%20V7.pdf.
- [30] Department of Mechanical and Aerospace Engineering Buffalo. Laboratory 1 Static and Dynamic Calibration of Thermocouples.
- [31] CFI Education Inc. "R-Squared - Definition, Interpretation, and How to Calculate." Corporate Finance Institute, 2018, corporatefinanceinstitute.com/resources/knowledge/other/r-squared/.
- [32] Trentadue, Germana, et al. Evaluation of Fast Charging Efficiency under Extreme Temperatures. 25 July 2018, 10.3390/en11071937. Accessed 15 Mar. 2022.
- [33] World Meteorological Organization—Temperatures and Extreme Weather Conditions. Available online: <https://public.wmo.int/en/media/news/high-temperatures-and-extreme-weather-continue>.
- [34] F. Musavi, M. Edington, W. Eberle, and W. G. Dunford, Evaluation and Efficiency Comparison of Front End AC-DC Plug-in Hybrid Charger Topologies. 2012, pp. 413-421.
- [35] F. Musavi, W. Eberle, and W. G. Dunford, "A High-Performance Single-Phase Bridgeless Interleaved PFC Converter for Plug-in Hybrid Electric Vehicle Battery Chargers," IEEE Transactions on Industry Applications, vol. 47, no. 4, pp. 1833-1843, 2011.
- [36] S. S. Williamson, A. K. Rathore, and F. Musavi, "Industrial Electronics for Electric Transportation: Current State
- [37] Lee, J.H., and B.H. Cho. "Large Time-Scale Electro-Thermal Simulation for Loss and Thermal Management of Power MOSFET." IEEE 34th Annual Conference on Power Electronics Specialist, 2003. PESC '03., July 2003, 10.1109/pesc.2003.1218282. Accessed 15 Mar. 2022.
- [38] Jose, Jitty, et al. "Study of Temperature Dependency on MOSFET Parameter Using MATLAB." IRJET, July 2016.
- [39] Lakkas, George. Enterprise Systems Analog Applications Journal MOSFET Power Losses and How They Affect Power-Supply Efficiency.
- [40] Graovac, Dr. Dušan, et al. "MOSFET Power Losses Calculation Using the Datasheet Parameter." Digchip.com, 2022, application-notes.digchip.com/070/70-41484.pdf.
- [41] Application Notes: DC/DC Converter Thermal Management.
- [42] De León-Aldaco, S.E., et al. "Experimental Assessment of Derating Guidelines Applied to Power Electronics Converters." Journal of Applied Research and Technology, vol. 11, no. 1, Feb. 2013, pp. 103–114, www.scielo.org.mx/pdf/jart/v11n1/v11n1a9.pdf, 10.1016/s1665-6423(13)71519-0. Accessed 15 Mar. 2022.
- [43] Stupar, A., et al. "Advanced Setup for Thermal Cycling of Power Modules Following Definable Junction Temperature Profiles." The 2010 International Power Electronics Conference - ECCE ASIA -, 2010, www.academia.edu/73652165/Advanced_setup_for_thermal_cycling_of_power_modules_following_definable_junction_temperature_profiles. Accessed 15 Mar. 2022

- [44] International Electrotechnical Commission (IEC). Photovoltaic (PV) systems – Characteristics of the utility interface. (CEI/IEC 61727- 2004).
- [45] IEC 61000-1 Part 4-7: Testing and measurement techniques – General guide on harmonics and interharmonics measurements and instrumentation, for power supply systems and equipment connected to
- [46] International Electrotechnical Commission (IEC). Bidirectional grid connected power converters - Part 1: General requirements. (IEC 62909-1:2017)
- [47] International Electrotechnical Commission (IEC) 61000. Electromagnetic compatibility (EMC) – Part 3-2: Limits – Limits for harmonic current emissions (equipment input current ≤ 16 A per phase)
- [48] Rashmi. “Estimation of Internal Resistance of Lithium Ion Battery.” IRJET, 8 Aug 2021.